Aus dem Walther-Straub Institut für Pharmakologie und Toxikologie der Ludwig-Maximilians-Universität München

Vorstand: Prof. Dr. Thomas Gudermann

Domain-specific role of the channel-kinase TRPM7 in cell signaling

Dissertation
zum Erwerb des Doktorgrades der Naturwissenschaften
an der Medizinischen Fakultät der
Ludwig-Maximilians-Universität zu München

Vorgelegt von

Sarah Hampe

aus

Berlin

Im Jahre

2019

Mit Genehmigung der Medizinischen Fakultät
Der Universität München

Betreuerin:	Prof. Dr. Ingrid Boekhoff
Zweitgutachter:	Prof. Dr. Alexander Faußner
Dekan:	Prof. Dr. med. dent. Reinhard Hickel
Tag der mündlichen Prüfung:	18.12.2019

Für meinen Vater

Prof. Dr. Andreas Hampe

genialer Wissenschaftler und liebevoller Daddy

‚Was man tief in seinem Herzen besitzt, kann man nicht durch den Tod verlieren.' (Goethe)

Table of contents

1 Summary

TRPM7 is an essential, ubiquitously expressed protein which combines the function of a non-selective ion channel together with a serine- and threonine-phosphorylating alpha-kinase. While the channel domain and the role of TRPM7 for cellular Mg^{2+} and Ca^{2+} homeostasis and Zn^{2+} uptake and release has been intensively studied, function of TRPM7's phosphotransferase activity is less well understood; among other reasons, this is mainly due to the fact that the so far few identified substrates do not show any similarity in the consensus sequence, aggravating determination of a universal substrate recognition motif.

Regarding its importance for physiological functions, TRPM7 has been shown to regulate different basic cellular processes such as proliferation, differentiation, migration and apoptosis, wherefore it is also implicated in the pathogenesis of different diseases such as inflammation, cancer development and progression. More recent studies suggest that this regulation occurs through the control of different cell signaling pathways which then lead to the induction of specific gene transcription; thus, TRPM7 has been shown to affect the activation of the PI3K/Akt, MAPK/ERK, JAK/STAT3 and TGF-β/SMAD2 pathway by controlling Akt, ERK1/2, STAT3 and SMAD2 phosphorylation. However, the so far published results are partially contradictory, rendering it impossible to draw final conclusions regarding the exact function of TRPM7 in these signaling cascades.

In this respect, purpose of the present study was to clarify the role of TRPM7 in cellular signaling events and closer illuminate how either the channel or kinase unit participate in the regulation of TRPM7-affected pathways. Therefore, I utilized two different TRPM7 models generated in a haploid chronic myeloid leukemia cell line (HAP1): The HAP1 TRPM7 KO cell clone lacking expression of the full-length protein and the HAP1 TRPM7 KI cell clone carrying a functional channel, but an inactivated kinase domain. In each experiment, the TRPM7 mutants were compared to their respective parental wild-type (WT) clone expressing an intact TRPM7 protein, which were carried along as controls.

The first part of my studies focused on the validation of the effective genetic manipulation of the two HAP1 TRPM7 cell models. Western Blot analysis using an antibody targeting the autophosphorylation site Ser1511 of the TRPM7 kinase confirmed inactivation of TRPM7's phosphotransferase in the TRPM7 KI clone. Electrophysiological measurements of both clones demonstrated that, while the TRPM7 KO clone lacks the typical TRPM7-like current and thus confirms functional depletion of the channel-kinase, inactivation of the kinase domain does not significantly alter TRPM7 current amplitude and its kinetics.

After successfully validating the generation of the two TRPM7 cell models, I specifically investigated the impact of TRPM7 on the above-mentioned cell signaling cascades regulating gene transcription.

Most importantly, the present work discovers TRPM7 to function in gene expression and catalytic activity of the immunologically relevant enzyme COX-2. Thus, real-time quantitative polymerase chain reaction (RT-qPCR) experiments in resting and with the adenylyl cyclase activator forskolin stimulated HAP1 TRPM7 KO cells illustrated that TRPM7 promotes constitutive as well as inducible *COX-2* gene expression. Moreover, analysis of the HAP1 TRPM7 KI showed that, while constitutive *COX-2* gene expression is primarily regulated by TRPM7 kinase activity, the induction of *COX-2* transcription necessitates both a functional TRPM7 channel and kinase domain. In addition, performing a COX activity assay demonstrated that TRPM7 augments enzymatic activity of COX-2, as knockout of TRPM7 in the HAP1 cells results in diminished COX-2-mediated prostaglandin (PG) synthesis. Yet, the experimental setup is not eligible to tell if the observed TRPM7-dependent increase in COX-2 activity is due to enhanced *COX-2* gene respectively protein expression or if TRPM7 facilitates substrate conversion by directly affecting COX-2.

To address the question which pathway(s) are involved in the observed TRPM7-dependent regulation of *COX-2* gene expression in the HAP1 cells, I performed Western Blot experiments using phospho-specific antibodies targeting different signaling molecules being part of the pathways introduced above. Comparison of the phosphorylation status of the cell signaling kinases Akt (Ser473) and GSK3β (Ser9) in the HAP1 TRPM7 WT and KO cells demonstrated that TRPM7 augments both Akt and GSK3β phosphorylation. This is accompanied by nuclear accumulation of the transcription factor NFAT, which is known to function in *COX-2* gene expression and induction. Thus, I hypothesize that TRPM7 regulates *COX-2* gene expression through an Akt – GSK3β – NFAT signaling axis in the HAP1 cells. However, further evaluating the impact of the TRPM7 kinase activity on these signaling molecules revealed that, although the kinase is required for Akt Ser473 phosphorylation, it is redundant for GSK3β Ser9 phosphorylation and NFAT nuclear localization. Hence, the TRPM7 kinase-dependent regulation of *COX-2* gene expression must occur through the activation of a different TRPM7-affected pathway. Linking my results to the current literature, one might speculate that the kinase unit potentially enhances *COX-2* gene expression by initiating an Akt – NFκB /CREB cascade.

In order to substantiate the hypothesized domain-specific role of TRPM7 in *COX-2* gene expression which was drawn from the results summarized above, I analyzed the effect of pharmacological inhibition of TRPM7 respectively its kinase domain in primary humane immune cells. RT-qPCR experiments showed that blockade of TRPM7 with NS8593 in neutrophils significantly attenuates lipopolysaccharide (LPS)-induced *COX-2* gene expression. Likewise, administration of the TRPM7 kinase inhibitor TG100-115 significantly decreases *COX-2* gene expression in LPS-stimulated cells. In the light of COX-2 being the central target molecule when it comes to treatment of numerous diseases – such as various types of cancer, neurodegenerative diseases and autoimmune disorders –

but administration of common unselective COX-1 and COX-2 inhibitors showing severe adverse effects (e.g. risk elevation of gastrointestinal injuries and cardiovascular diseases), my results uncover that TRPM7 might represent a promising alternative target for the therapy of COX-2-mediated diseases in the future.

2 Zusammenfassung

TRPM7 ist ein essentielles, ubiquitär exprimiertes Fusionsprotein, das sich aus einem nicht-selektiven Ionenkanal und einer Serine und Threonine phosphorylierenden Alpha-Kinase-Einheit zusammensetzt. Während die Kanaldomäne und die Bedeutung des TRPM7 für die zelluläre Homöostase von Mg^{2+} und Ca^{2+} und die Aufnahme und Freisetzung von Zn^{2+} recht gut erforscht ist, ist die Funktion der Kinasedomäne weitaus weniger gut verstanden, was u. a. daran liegt, dass sich bezüglich der Konsensussequenz der Kinaseinheit in den bisher identifizierten wenigen Substraten kein eindeutiges und übereinstimmendes Motiv erkennen lässt.

Hinsichtlich seiner physiologischen Funktion haben Studien der letzten zwei Dekaden gezeigt, das TRPM7 maßgeblich an der Regulation einer Reihe elementarer Zellfunktionen wie der Proliferation, der Migration, der Differenzierung und der Apoptose beteiligt ist. Die sich daraus ableitende Relevanz des TRPM7 für die Pathogenese einer Vielzahl von Erkrankungen, wie die Entstehung und das Voranschreiten von Entzündungsreaktionen oder Tumoren, konnte ebenfalls bestätigt werden. Aktuellere Arbeiten deuten darauf hin, dass die Regulation dieser zellulären Prozesse durch die Kontrolle unterschiedlichster Signaltransduktionswege vermittelt wird, die final die Transkription bestimmter Zielgene beeinflussen: So spielt TRPM7 z. B. eine Rolle bei der Weiterleitung von Signalen durch die Kaskaden PI3K/Akt, MAPK/ERK, JAK/STAT3 und TGF-β/SMAD2, in dem es die Phosphorylierung der zwischengeschalteten Regulatorproteine Akt, ERK1/2, STAT3 und SMAD2 beeinflusst. Eine endgültige Aussage hinsichtlich der Regulation dieser Signalkaskaden durch TRPM7 ist gegenwärtig jedoch nicht möglich, da einige der bisher hierzu publizierten Befunde sich teilweise widersprechen.

Ziel dieser Arbeit war es daher, den Effekt von TRPM7 auf die genannten Signalwege zu überprüfen und dabei explizit zwischen dem Einfluss der Kanal- und der Kinaseeinheit zu unterscheiden. Dazu wurden zwei unterschiedliche Klone in einer haploiden, chronisch-myeloiden Leukämiezelllinie (HAP1) generiert: Der HAP1 TRPM7 KO Klon, in dem kein funktionelles TRPM7 Protein exprimiert wird und der HAP1 TRPM7 KI Klon, der zwar eine intakte Kanaleinheit aber eine inaktivierte Kinase aufweist. Diese wurden in allen Experimenten mit ihrem jeweiligen parentalen Wildtyp (WT) Klon mit einem intakten TRPM7 Protein verglichen, welche als Kontrollzelllinien mitgeführt wurden.

Zunächst wurden beide TRPM7 Zellmodelle bezüglich ihrer erfolgreichen genetischen Manipulation untersucht. Western Blot Analysen mit einem Antikörper, der die Autophosphorylierungsstelle Ser1511 der TRPM7-Kinase erkennt, bestätigten die erfolgreiche Inaktivierung der Kinase in dem TRPM7 KI Klon. Weiterführende ‚Patch Clamp' Experimente zur Erfassung der Kanalaktivität zeigten, dass der typische, durch TRPM7 vermittelte Ioneneinstrom in den HAP1 TRPM7 KO

Zellen fehlt, was als Bestätigung für die erfolgreiche funktionelle Deletion des Proteins gewertet werden kann; die Ausschaltung der Phosphotransferase-Aktivität hat hingegen keinerlei Auswirkungen auf die Amplitude und die Kinetik des TRPM7-vermittelten Ionenflusses.

Nach der erfolgreichen Validierung der Herstellung der TRPM7-Zellmodelle wurden anschließend gezielte Analysen zur Bedeutung des TRPM7 bzw. dessen Kinase Domäne für die Regulation der oben erwähnten Signalwege zur Stimulation von Transkriptionsprozessen durchgeführt. Dabei konnte ich im Rahmen dieser Arbeit feststellen, dass TRPM7 einen bedeutenden Einfluss auf die Genexpression und die Aktivität der immunologisch relevanten Cyclooxygenase-2 (COX-2) hat. Im Detail haben quantitative Polymerase-Kettenreaktions-Experimente (RT-qPCR) an ‚ruhenden' und an mit dem Adenylylcyclase Aktivator Forskolin stimulierten HAP1 TRPM7 KO Zellen gezeigt, das TRPM7 sowohl die Genexpression der konstitutiven, aber auch die der induzierbaren *COX-2* positiv beeinflusst. Parallel durchgeführte Analysen an Zellen des HAP1 TRPM7 KI Klons ergaben weiter, dass die Stimulation der konstitutiven *COX-2* Genexpression im Wesentlichen auf die Aktivität der TRPM7 Kinase zurückzuführen ist, während für die Erhöhung der Genexpression der induzierbaren *COX-2* die Aktivität beider TRPM7 Domänen erforderlich ist. Ein mit HAP1 TRPM7 KO Zellen durchgeführter COX Aktivitätsassay lieferte zudem den Hinweis, dass TRPM7 auch die Aktivität der COX-2 begünstigt. Ob die registrierte erhöhte Substratumsetzung der COX-2 allerdings lediglich auf die gesteigerte Expression des Enzyms zurückzuführen ist oder ob der TRPM7 die Enzymaktivität möglicherweise durch eine direkte Interaktion oder auch Modifikation erhöht, konnte nicht abschließend geklärt werden.

Bezüglich der Frage, welche Signalkaskade(n) an der Stimulation der TRPM7-vermittelten *COX-2* Genexpression in den HAP1 Zellen beteiligt ist, wurden zusätzliche Western Blot Analysen mit phosphospezifischen Antikörpern gegen verschiedene Regulatorproteine der oben eingeführten Signalwege durchgeführt. Ein Vergleich des Phosphorylierungsgrades von Akt (Ser473) und GSK3β (Ser9) zwischen HAP1 TRPM7 WT und KO Zellen ergab, dass TRPM7 offenbar die Phosphorylierung von Akt und GSK3β verstärkt; gleichzeitig wurde eine TRPM7-vermittelte Akkumulation des Transkriptionsfaktors NFAT im Zellkern beobachtet. Da bekannt ist, dass NFAT die Transkription von *COX-2* induziert, liegt es nahe, dass TRPM7 die *COX-2* Genexpression durch die Initiierung einer Akt – GSK3β – NFAT Signalkaskade stimuliert. Weiterführende Studien mit Kinase-inaktivierten Zellen ergaben jedoch, dass die Enzymeinheit zwar an der Phosphorylierung von Akt beteiligt ist, aber keinen Einfluss auf die GSK3β Phosphorylierung und die nukleare Akkumulation von NFAT hat. Dies lässt vermuten, dass der beobachtete Effekt der TRPM7 Kinase auf die *COX-2* Genexpression durch die Aktivierung eines anderen durch TRPM7 beeinflussten Signalweges hervorgerufen wird. So wäre es anhand meiner Ergebnisse und in Anlehnung an die bis

dato publizierte Literatur vorstellbar, dass die TRPM7 Phosphotransferase die *COX-2* Genexpression zusätzlich durch eine Akt – NFκB /CREB Kaskade induziert.

Um die sich aus den bisherigen Befunden abzuleitende Hypothese zu überprüfen, ob die beiden funktionellen Einheiten des TRPM7 tatsächlich an der Genexpression der *COX-2* beteiligt sind, wurden pharmakologische Blockierungsexperimente an primären humanen Immunzellen durchgeführt. Dabei zeigten RT-qPCR Versuche, dass die Inhibition des TRPM7 in Neutrophilen mittels NS8593 zu einer signifikanten Reduktion der durch Lipopolysaccharide (LPS)-induzierten *COX-2* Genexpression führt. Ein ähnlicher Effekt konnte beobachtet werden, wenn die LPS-stimulierten Zellen stattdessen zuvor mit dem TRPM7 Kinase Inhibitor TG100-115 behandelt wurden. Betrachtet man diese Ergebnisse vor dem Hintergrund, dass die COX-2 eine zentrale therapeutische Zielstruktur für die Behandlung einer Vielzahl von Erkrankungen, wie z. B. Krebs, neurodegenerative oder Autoimmunerkrankungen darstellt, die Gabe der häufig zur therapeutischen Anwendung kommenden unspezifischen COX-1 und COX-2 Blocker aber mit dem bekannten unerwünschten Nebenwirkungsprofil (Erhöhung des Risikos für gastrointestinale Schäden/Verletzungen, kardiovaskuläre Erkrankungen etc.) einhergeht, könnten die hier gesammelten Befunde einen neuen, TRPM7-vermittelten Therapieansatz zur selektiven Inhibition der COX-2 darstellen.

3 Introduction

3.1 TRP channels

In 1989, Craig Montell and Gerald Rubin proposed that the eye-specific Drosophila *trp* gene might encode for a channel or transporter within the photosensitive rhabdomeral membrane of photoreceptor cells [3]. Although studies on this gene go further back in time, this was the first time it was assumed that *trp* might be coding for a light sensitive ion channel affecting the intracellular calcium (Ca^{2+}) levels. This hypothesis was confirmed in 1992 by another study from Hardie and Minke, showing that 'transient receptor potential' (TRP) was indeed a Ca^{2+} conducting channel activated by light [4]. Three years later, the first mammalian TRP homologue, TRPC1, was discovered [5, 6]. This laid the foundation for the subsequently following, fast expanding research area on TRP channels.

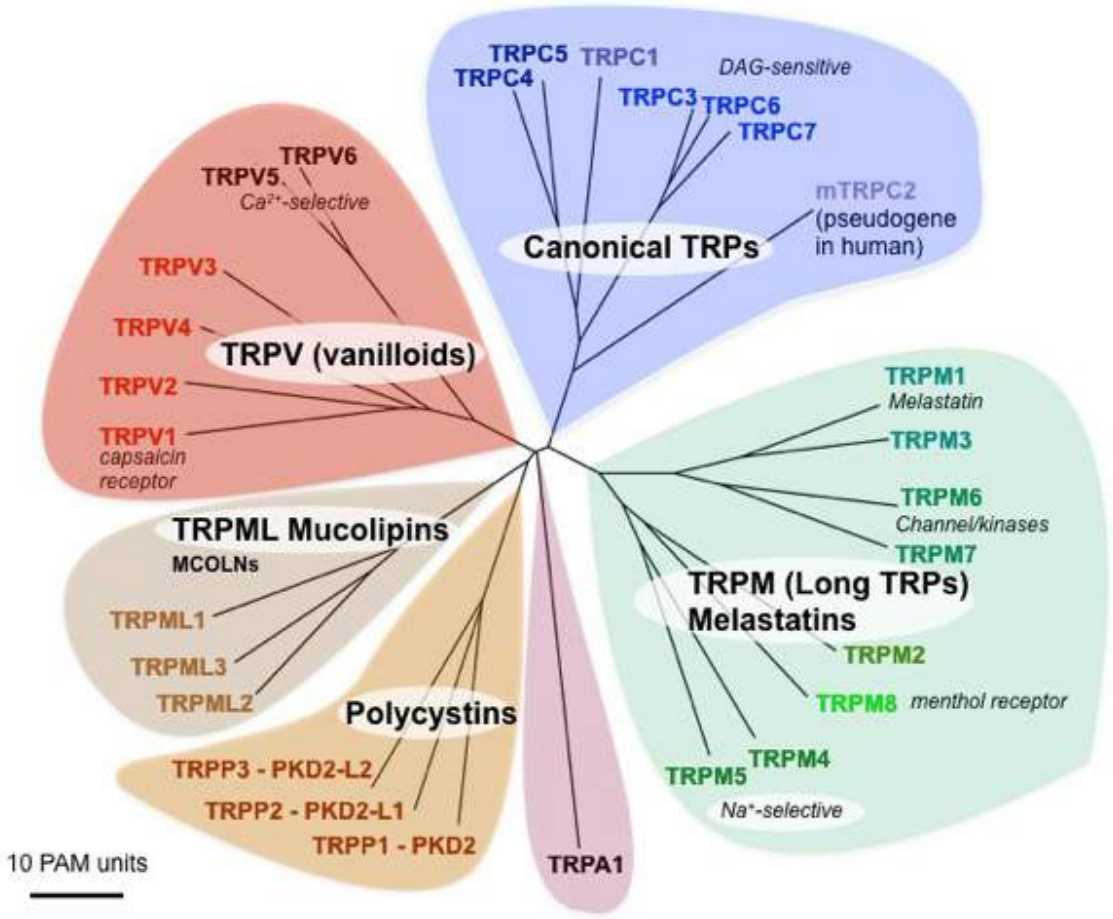

Figure 3.1 Phylogenetic tree of mammalian TRP channels. Due to great similarity in their primary protein structure, the 28 TRP channels are divided into 6 different subfamilies – named TRPC, TRPM, TRPA, TRPP, TRPML and TRPV – according to their amino acid (AA) composition. Each group (except TRPA) further splits up into the even closer related family members numbered 1 through maximum 8. The point accepted mutation (PAM) index (see left corner for scale bar) reveals how comparatively small the difference between the respective TRP channels is. One PAM denotes mutation of one AA of the protein. Modified from [1].

Over the last two decades, intensive exploration led to the knowledge of 28 mammalian TRP channels, which can be classified into six different subfamilies due to their sequence similarity: TRPA (ankyrin), TRPC (canonical), TRPM (melastatin-like), TRPML (mucolipin), TRPP (polycystin) and TRPV (vanilloid) [1, 7]. This classification differs from the usual, as ion channels normally are categorized by their activation mechanism and ion specificity. But as ligand binding and function are so differing between the TRP channels and in some cases are still unknown, TRP channels were grouped by their similarity in amino acid (AA) composition (Figure 3.1) [1].

3.1.1 Classification, structure and function of TRP channels

Comparison of all TRP channels among each other reveals only 20 % shared sequence identity [1], with the best conserved region being the channel pore region [8]. Nevertheless, they all comprise the basic architecture of an intracellular located N- and C-terminus flanking six transmembrane (TM) domains, with the channel pore being located between the fifth and sixth segment. The subfamilies are again summarized into two groups: Group 1 includes TRPA, TRPC, TRPM, TRPV and TRPN channels (TRPN is not existent in mammals though), while group 2 is represented by TRPML and TRPP (Figure 3.2) [9]. All members of group 1 except TRPM channels carry several N-terminal ankyrin repeat domains, which are, in case of TRPCs, directly followed by a coiled-coil domain. TRPC, TRPM and TRPN additionally contain the typical TRP domain – composed of the conserved TRP boxes 1 and 2 – positioned right behind the last membrane-crossing segment within the C-terminus [9]. Another element occurring in at least three of the TRP subfamilies, TRPC, TRPM and TRPV, are calmodulin (CaM) binding sites, in some cases overlapping with inositol 1,4,5-triphosphat-receptor (IP_3R) binding sites, domains by which the channels can be modulated [10]. Such sites are often found in ion channels, and CaM's strong interaction with channels even led Saimi and Kung to the concept of CaM being an 'ion channel subunit' [11, 12]. Furthermore, an extraordinary feature can be found within the TRPM subfamily: Member 2, 6 and 7 carry an enzymatic domain attached C-terminal to the TM region, wherefore they are also called 'chanzyme's (channel-enzyme) [13].
Representing the ancient TRP channels, the group 2 members TRPP and TRPML display high sequence homology within their TM region and enclose a C-terminal endoplasmatic reticulum (ER) retention signal (Figure 3.2) [9]. Almost all TRPs assemble in tetramers to form functional channels, either with themselves (except TRPC1) or other members of the same subfamily [14, 15]. But also heterotetramers between different subfamilies have been observed [14]. The resulting functional channels conduct mono- and divalent cations, with Ca^{2+}, magnesium (Mg^{2+}) and sodium (Na^{2+}) being the most important players. In general, all TRP channels are non-selective, except for TRPM4 and 5 (permeability (P) ratio $P_{Ca}/P_{Na}>0.05$), which solely conduct monovalent ions, and TRPV5 and 6 that only conduct divalent ions ($P_{Ca}/P_{Na}>100$) [1].

Regarding their expression profile, most members of the family are ubiquitously expressed, while some show a more restricted distribution. Additionally, multiple TRPs are not only located in the plasma membrane, but can also be found in membranes of intracellular compartments [16, 17]. There, they impact vesicle trafficking as well as biosynthetic, autophagic, endocytotic and exocytotic events [16].

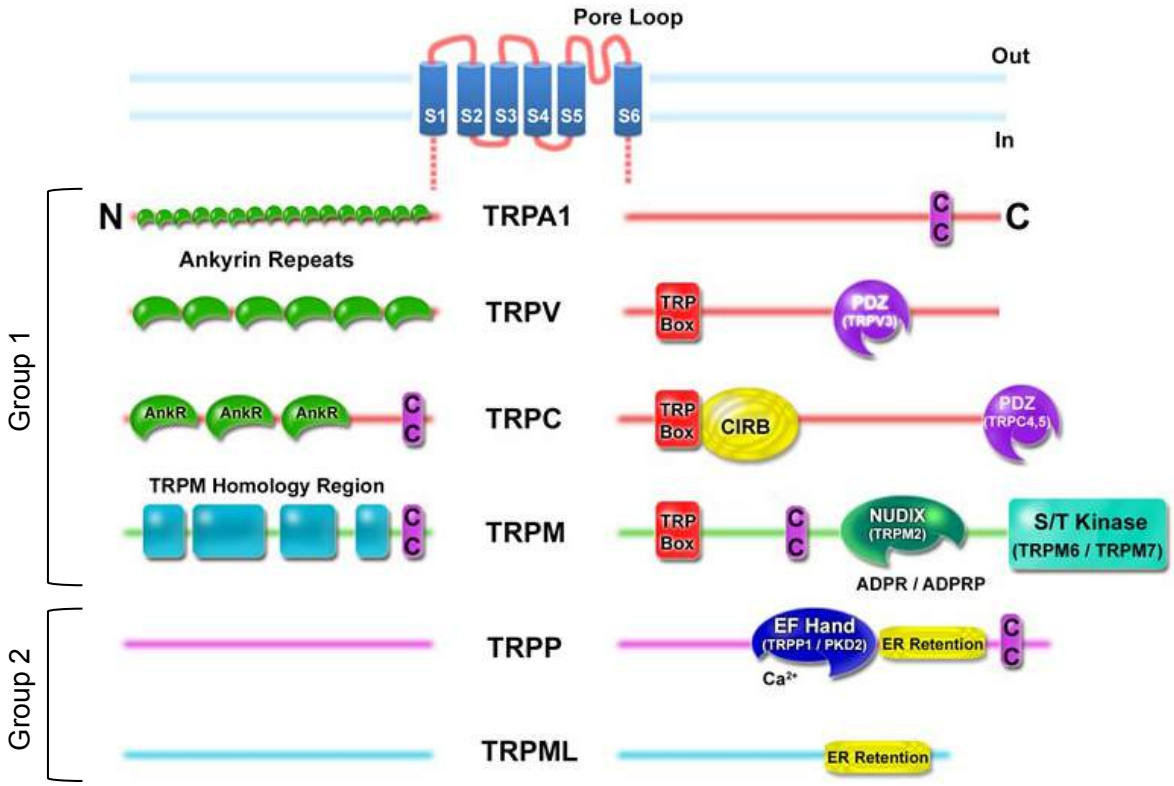

Figure 3.2 Topology of the TRP channel subfamilies. All TRP channels comprise one or more conserved domains carrying specific functions. Domains being shared among TRP group 1 members are the N-terminal ankyrin repeat domain (AnkR; TRPMA, TRPV, TRPC), a coiled-coil domain (CC; TRPC and TRPM) and the TRP domain located C-terminal of the transmembrane (TM) region (TRP box; TRPV, TRPC, TRPM). In addition, members of the TRPC, TRPM and TRPV subfamily reveal calmodulin (CaM) binding sites (not shown) and TRPM2, 6 and 7 exhibit the special feature of a C-terminally located enzymatic domain [Ser/Thr (S/T) Kinase in case of TRPM6 and 7]. The small TRP group 2 on the other hand is united by an endoplasmatic reticulum (ER) retention signal domain (TRPP and TRPML). Modified from [1]

Taken together, TRPs are not only important for systemic and cellular ion homeostasis, but are also involved in ion flux required for processes such as cell growth, proliferation, migration, differentiation and cell death. Hence, they also reveal a strong pathophysiological background, as mutations in TRP proteins often cause organ-specific or systemic malfunctioning and severe diseases such as cancer, tumor progression and heart diseases such as hypertrophy, ischemic cardiomyopathy, arrhythmogenesis and cardiac fibrosis (also see 3.2.5) [7, 18, 19].

3.1.2 TRP channels in ion homeostasis

3.1.2.1 TRP channels in Ca^{2+} homeostasis

One of the main attributes of TRP channels is their impact on Ca^{2+} homeostasis. Many studies revealed that there are three different ways of how TRP channels influence the intracellular (cytosolic as well as compartimental) Ca^{2+} concentrations: (a) as direct Ca^{2+} entry pore, (b) by plasma membrane induced depolarization or (c) by orchestrating Ca^{2+} release from intracellular stores [20].

(a) As described in 3.1.1, almost all TRP channels are Ca^{2+} permeable and thereby significantly contribute to ion homeostasis by directly mediating Ca^{2+} influx. Nevertheless, Ca^{2+} conductivity largely differs among the individual TRP channel subtypes due to their large variance in selectivity and permeability. But also other factors, such as activators and/or associating proteins, influence the magnitude of Ca^{2+} influx by changing pore dilation and thereby permeability, which is usually expressed by P_{Ca2+}/P_{Na+} (according to the Goldman-Hodgkin-Katz theory, see [21] for a short overview). Additionally, variable experimental conditions including temperature, pH or extracellular Mg^{2+} or Ca^{2+} concentrations also influence ion conductance [22, 23].

(b) Because inward-directed, fractional Ca^{2+} currents of some TRP channels are relatively small, the question arose if TRP channels might exert their (Ca^{2+}-related) functions by additional mechanisms. In excitable cells, activated TRP channels cause a slight rise of the cytosolic Ca^{2+} concentration ($[Ca^{2+}]_{i/cyt}$) which induces a shift in the membrane potential that results in the opening of voltage-dependent Ca^{2+} channels (VDCCs) [24-27] (for overview see [20]). This TRP-dependent regulatory mechanism also applies for other ion channels, predominantly in non-excitable cells, where TRP-induced de- or hyperpolarization either causes opening or closing of Ca^{2+}-dependent potassium (K^+) or Na^+ channels [28-30]. Furthermore, many of the TRP channels are regulated by Ca^{2+} themselves, not only through Ca^{2+}- and CaM-binding sites, but also via molecules and events involved in Ca^{2+} signaling, such as phospholipase C (PLC) -modulation or protein kinase C (PKC) -activation [20, 31, 32].

(c) As mentioned before, TRP channels are not exclusively found in the plasma membrane, but also inserted in the lipid bilayer of intracellular compartments. Basically, intracellular organelles are divided into two groups: Group 1 encloses the endoycytotic, secretory and autophagic compartments (with the ER and Golgi apparatus, secretory vesicles, endosomes, autophagosomes, and lysosomes), while group 2 comprises the mitochondria, peroxisomes and the nucleus. Despite their diverse functions, most of them serve as intracellular Ca^{2+}- stores, and the luminal Ca^{2+} concentrations ($[Ca^{2+}]_{lumen}$) are much higher than the resting $[Ca^{2+}]_{i/cyt}$ ($[Ca^{2+}]_{lumen}$ = μM to mM, $[Ca^{2+}]_{i/cyt}$ ~ 100 nM) [16]. By now, several studies strengthened the view that the

intracellular located TRP channels participate in the release of Ca^{2+} from the stores into the cytosol (for overview see [16]).

3.1.2.2 TRP channel in magnesium (Mg^{2+}) homeostasis

While nearly all TRP channels conduct Ca^{2+}, the number of Mg^{2+} permeable ones is more limited. Nevertheless, representatives are found within the TRPA (TRPA1), TRPV (TRPV2 and 4), TRPP (TRPP2 and 3), TRPML (TRPM1 and 3) as well as TRPM (TRPM1-3 and 6-7) subfamily [33]. For nearly all of those, their Mg^{2+}-associated function(s) remain unclear, whereas the impact of TRPM6 and 7 on Mg^{2+} homeostasis and Mg^{2+}-affected processes has been intensively studied. Both of them essentially contribute to the cellular Mg^{2+} household, as manifold conditional and full knockout studies showed [34-37].

TRPM6 was originally identified as central player in Mg^{2+} uptake and intercellular transport in patients displaying hypomagnesemia with secondary hypocalcemia [38, 39]. It is predominantly but not exclusively expressed in the kidney and the intestine, two organs that are both important for Mg^{2+} reabsorption [38, 40-42]. Nevertheless, Chubanov et al. found that nephric TRPM6, other than intestinal, is dispensable for maintenance of systemic Mg^{2+} [42]. Furthermore, TRPM6 indirectly affects embryonic development, as channel function is required for proper maternal Mg^{2+} supply to the embryo [42]. TRPM7 on the other hand shows a more ubiquitous expression pattern and is primarily responsible for cellular Mg^{2+} balance [41]. Nonetheless, it also participates in systemic Mg^{2+} homeostasis and facilitates reabsorption by forming heteromeric channels with TRPM6 [35, 36, 42-44]. Thus, it's not surprising that mutations or disruption of those channels can cause severe malignancies or even lead to early embryonic lethality [35, 45].

3.2 TRPM7

The TRPM (sub)family encompasses eight members named after its founding member, TRPM1, and numbered consecutively through 8 [46, 47]. Due to shared sequence similarities endowing them with group-specific functions, they are paired into four groups: TRPM1/3, TRPM2/8, TRPM4/5 and TRPM6/7 [48].

Regarding the homolog proteins TRPM6 and TRPM7, both ion channels were found to share two features to be highlighted: They (a) are essential for Mg^{2+} homeostasis (see 3.1.2.2) and (b) contain a unique C-terminally located atypical alpha-kinase domain (Figure 3.3).

3.2.1 The TRPM7 channel

3.2.1.1 Function of the TRPM7 channel unit

As mentioned in chapter 3.1.2.2, TRPM7 represents a ubiquitously expressed protein important not only for Ca^{2+}, but also essential for Mg^{2+} uptake [49]. The first investigations regarding TRPM7 in the chicken-derived DT-40 B cells [50] aimed at its role in Mg^{2+} homeostasis and demonstrated its significance for fundamental cell functions and survival [34]. Since then, requirement of both channel and kinase domain for viability and development has been confirmed in many different cell types as well as in *in vivo* experiments [35, 36]. However, some studies claim that the necessity of TRPM7 is independent from its function in Mg^{2+} uptake [45]. Hence, TRPM7's function as a modulator of intracellular Mg^{2+} levels remains controversial. But the rescue of TRPM7 depletion-caused phenotypes by either additional supplementation of Mg^{2+} to the growth media or overexpression of the plasma-membrane Mg^{2+} transporter solute carrier family 41 member 2 (SLC41A2) supports the original idea of it being essential for Mg^{2+} homeostasis [36].

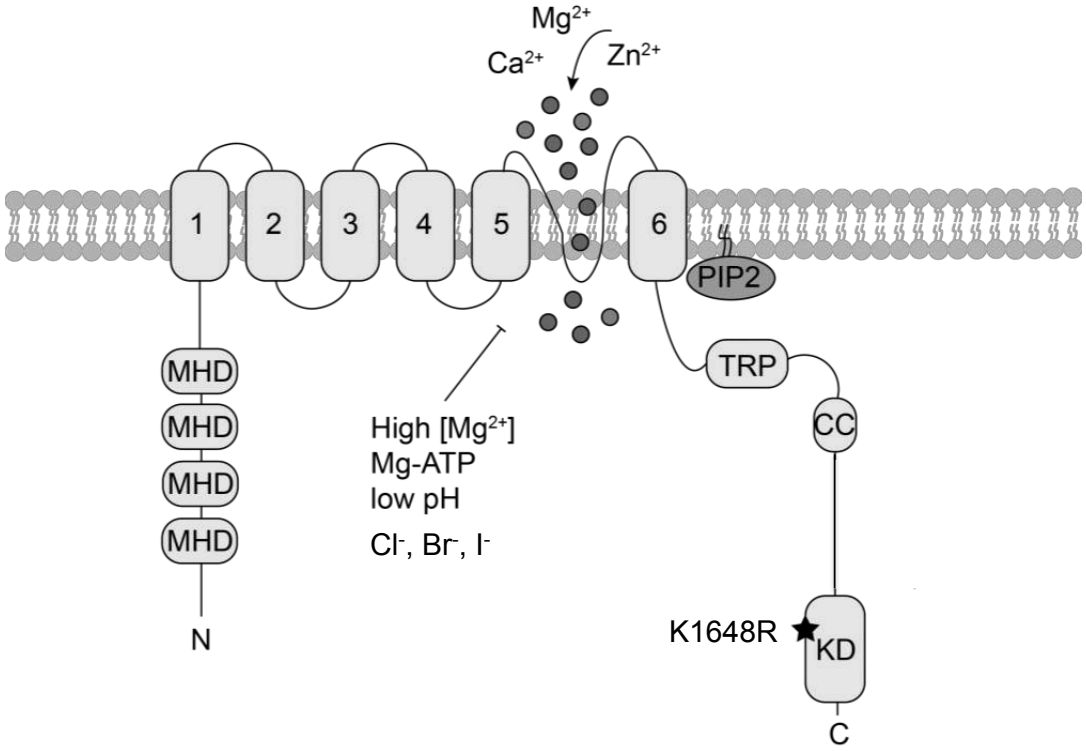

Figure 3.3 TRPM7 structure. TRPM7 is composed of a cytosolic N-terminus, 6 transmembrane (TM) domains and a cytosolic C-terminal tail. Its channel pore is formed between the 5th and 6th TM-spanning segment and conducts mono-, but primarily divalent cations such as Ca^{2+}, Mg^{2+} and Zn^{2+}. The channel function is physiologically modulated by intracellular Mg^{2+} concentration and Mg-ATP (but also other Mg-conjugated nucleotides), pH and the halide anions chloride (Cl^-), bromide (Br^-) and iodide (I^-). While the N-terminus contains 4 name-explaining melastatin homology domains (MHD), the C-terminus encloses the TRP, the coiled-coil (CC) and the atypical alpha-kinase domain (KD). This Ser/Thr kinase can be inactivated by mutation of lysine (K) to arginine (R) at the active site of the enzyme (K1648R). Modified from [2]

Besides its importance for Mg^{2+} and Ca^{2+} uptake, TRPM7's permeation profile shows that other monovalent and divalent cations can pass the channel as well, with some [in particular zinc (Zn^{2+}) and nickel (Ni^{2+})] exhibiting a driving force even four times higher than Ca^{2+} [51]. More recent studies reveal a possible implication in Zn^{2+} homeostasis, as TRPM7 is not only relevant for Zn^{2+} uptake through the plasma membrane, but also controls its release from intracellular stores [52-54]. Furthermore, protons enter through the pore into the cell and compete with metal ions for entry [55].

3.2.1.2 Regulation of channel activity via physiological mediators

The channel can be regulated by various factors, including intracellular cations, nucleotides, halide anions and low pH (Figure 3.3). Mg^{2+}-bound adenosine triphosphate (Mg-ATP) and guanosine triphosphate (Mg-GTP) suppress channel function in concentration-dependent manner when applied in millimolar concentrations [34]. Testing the effect of free intracellular Mg^{2+} demonstrated a complete channel block at 3 mM, which is above physiological free Mg^{2+} levels in the cell under normal conditions (100 - 900 μM) [56]. Thus, it was postulated that Mg-ATP is the main regulator of TRPM7, since cytosolic ATP levels are up to five-fold higher than other nucleoside triphosphates such as GTP (ATP: 1 - 10 mM, GTP: 0.2 - 0.5 mM) [57-59]. These findings led to the predominant opinion of Mg^{2+} and Mg-ATP working together in modulating channel opening, which is also reflected in the definition of the TRPM7 current: MagNuM (magnesium nucleotide-regulated metal ion) and MIC (magnesium-inhibited cation) [60]. Interestingly, the response of TRPM7 to its feedback regulators Mg^{2+} and Mg-ATP is fine-tuned by the heteromerization with TRPM6 in transporting epithelia: By complex formation of TRPM6 and 7 into functional heteromeric channels (TRPM6/7), TRPM6 reduces TRPM7's sensitivity to Mg-ATP, while *vice versa* TRPM7 lowers TRPM6's susceptibility to free internal Mg^{2+} [44, 61]. Consequently, TRPM6/7 channels are constitutively active at physiological cytosolic Mg^{2+} and Mg-ATP levels. While probably expendable in resting cells, this mechanism of desensitization of TRPM6 and TRPM7 homomers to their internal natural blockers most likely is required in cells with high metabolic activity or organs that mediate transcellular uptake of Mg^{2+}. Accordingly, such TRPM6/7 heteromers have been detected in epithelial cells in the intestine, the kidney and the placenta and are possibly being formed in other TRPM6-expressing tissues as well [42, 44, 62]. In terms of halide anions, both chloride (Cl^-) and bromide (Br^-) block the channel in synergy with Mg^{2+}, while the inhibition through iodide (I^-) is Mg^{2+}-independent [63].

Another parameter regulating the channel is the proton concentration. Cytosolic acidification blocks the channel, which might be due to shielding negatively charged phosphorylheadgroups from lipids involved in channel gating [64]. These findings are particularly of interest, as they connect the pH-dependence of the channel with current-amplifying effects of the phospholipid phosphatidylinositol-4,5-bisphosphate (PIP_2) [65].

3.2.2 The TRPM7 kinase

3.2.2.1 Structure of the TRPM7 kinase

The TRPM7 protein is not only characterized by its channel domain essentially contributing to ion homeostasis, but also is defined through its unique direct fusion to an atypical kinase domain. This C-terminally located kinase belongs to a class of protein kinases operating in a before unknown mode of substrate recognition that was first introduced by Ryazanov et al. in 1999 [66]. Other than conventional protein kinases (CPKs), which phosphorylate their targets usually within loops, β-turns or irregular structures, the alpha-kinases phosphorylate AAs located in α-helical conformations [67, 68]. As there are only six mammalian alpha-kinases existent, TRPM7 and TRPM6 are even more exceptional in that their alpha-kinases are fused to membrane-spanning channels [34, 69].

Despite differences in its AA sequence, the crystal structure of the TRPM7 alpha-kinase displays similarities to CPKs: It contains a nucleotide binding P-loop (e.g. present in protein kinase A (PKA)) and a region promoting protein dimerization, supposedly separable into "activation sequence" (1553-1562) and "dimerization sequence" (1563-1570) [70]. Both of these elements are essential for kinase activity, while the latter additionally facilitates homo- as well as heterodimerization with TRPM6 [43, 71]. Due to TRPM6's distinct distribution and ion conductivity, it has been suggested that this interaction primarily supports transcellular Mg^{2+} transport in corresponding tissues (see chapter 3.2.1.2) [44]. A similar conclusion was drawn from TRPM6 expression in embryonic stem cells (ESCs), which require high amounts of Mg^{2+} for rapid cell division [35].

The zinc-binding module within the TRPM7 C-terminus upstream of the coiled-coil and alpha-kinase domain stabilizes the kinase domain [72]. TRPM6 and 7 kinase share features such as requirement of manganese (Mn^{2+}) or Mg^{2+} for activity and the use of mainly ATP for phosphorylation [73]. This refers to substrate- as well as autophosphorylation, the latter occurring at so far 14 discovered phosphorylation sites *in vitro* which are all located within the C-terminus of TRPM7 (serine (Ser)/threonine (Thr) ratio = 12/2). Seven of those are found within a Ser/Thr-rich domain, and addition of phosphoryl groups to positions Ser1386, Ser1404, Ser1565 and Ser1567 in this sequence has been reported to be involved in regulation of the alpha-kinase activity [74, 75]. This finding was validated by another *in vitro* study, which revealed that autophosphorylation within the Ser/Thr-rich domain is not only important for subsequent substrate phosphorylation, but also increases the rate of substrate recognition[75]. Remarkably, TRPM6 is able to cross-phosphorylate TRPM7 within those regulatory sites and thereby modulates its subcellular localization and – in absence of Mg^{2+} – its impact on cell growth [76, 77]. More recent analysis of TRPM7 phosphorylation *in vivo* via liquid chromatography-mass spectrometry/mass spectrometry (LC-MS/MS) suggests 15 residues to be autophosphorylated; however, only a few of those concide with the *in vitro* acquired data[77].

Nevertheless, congruent to the *in vitro* studies, phosphorylation is able to control kinase activity, as mutagenesis experiments show [77].

3.2.2.2 Function of the TRPM7 kinase: Substrate phosphorylation

As being a phosphoryl group-transferring enzyme, the apparent main feature of the TRPM7 kinase is the mechanistic control of cellular processes through target phosphorylation. In 2010, Zhang et al. performed TRPM7-polypeptide interaction studies and defined certain regions to be critical for substrate binding and recognition via computational analysis [78]. However, TRPM7's exact target phosphorylation motif remains unknown, making it difficult to predict potential TRPM7 kinase substrates. Thus, it's not surprising that, to date, only a few proteins have been identified to be phosphorylated by TRPM7. Yet, these substrates and their downstream effectors give a hint how widespread TRPM7 kinase function supposedly is. So far, *in vitro* studies elucidated TRPM7 kinase-dependent phosphorylation of the immunological relevant molecule annexin A1 (ANXA1), the myosin II A heavy chain (MIIA heavy chain) which is implicated in cell structure remodelling and the cell signalling triggering molecule PLCγ2 (PLCγ2) [79-82]. In context of another study, we were recently able to show that the kinase also directly phosphorylates the transcription factor Mothers against decapentaplegic homolog 2 (SMAD2) *in vitro* and *in vivo* [83]. An exception among the already known substrates is the nuclear protein histone H3, which is phosphorylated upon release and nuclear translocation of the TRPM7 kinase domain [84].

ANXA1 (also referred to as lipocortin 1, 37 kDa) is a glucocorticoid-affected and -regulated protein predominantly present in immune cells and counteracting inflammation. Cell activation initiates ANXA1's immediate translocation to the membrane and subsequent secretion [85-88]. In accordance, it is involved in granule fusion, exo- and phagocytosis, all processes which are able to resolve inflammation [85, 87, 89, 90]. By phosphorylating ANXA1 within its N-terminus at Ser5, TRPM7 directly affects its activation and therewith membrane translocation [91]. Conversely, structural interaction analysis showed that the negative charge of the phosphoryl group attached to Ser5 counteracts membrane binding by hindering the N-terminal tail to form an amphipathic α-helix [92]. Together these data suggest that, by phosphorylation at Ser5, TRPM7 participates in the tight regulation of ANXA1 membrane localization and interaction. Moreover, the TRPM7 kinase-dependent Ser5 phosphorylation promotes ANXA1 nuclear translocation inducing apoptosis in neurons [93]. Therefore, TRPM7's catalytic domain seems to control ANXA1 cellular transport in general.

The motor protein myosin II is a hexamer comprising two heavy, two essential light and two regulatory chains, all together regulating cell events required for cytoskeletal contraction [94]. Processes such as adhesion, migration and cytokinesis as well as regulation of the cell shape in general require bipolar filament assembly, which is inhibited by myosin phosphorylation, e.g. through

TRPM7 [81, 95]. The TRPM7 kinase domain was shown to phosphorylate MIIA heavy chain phosphorylation at Ser1943 and thereby controls tumor migration in breast cancer cells [96].

PLCγ2 triggers the conversion of PIP_2 into the second messengers diacylglycerol (DAG) and inositol-1,4,5-trisphosphate (IP_3). Thereby, the enzyme contributes to intracellular Ca^{2+} increase and signaling events resulting in PKC- and thus immune cell activation (PLCγ2/Ca^{2+}/PKC pathway) [97]. Under hypomagnesaemic conditions, TRPM7-directed PLCγ2 phosphorylation at the two target sites Ser1645 and Thr1045 supports B cell receptor (BCR) -mediated Ca^{2+} signaling in B cells [80].

Studying murine T cells, we discovered SMAD2 as a direct target of the TRPM7 kinase (results are published in Romagnani et al., 2017, and are not presented within this thesis) [83]. Mutagenesis-caused TRPM7 kinase-inactivation in mice reduced the phosphorylation of SMAD2 at Ser465/467 and thereby decreased transforming growth factor β (TGF-β) -dependent signaling important for T cell differentiation [83]. Subsequent *in vitro* analysis confirmed a direct interaction of TRPM7 and SMAD2.

A whole new aspect regarding the function of TRPM7 was first brought up when Desai et al. discovered that TRPM7's kinase is released by proteolytic cleavage [98]. The truncated C-terminal fragment comprising the kinase domain enters the nucleus where it phosphorylates multiple sides of histone H3 (Ser10, Ser28) *in vitro* [84]. The kinase-dependent histone modifications help to control chromatin remodelling, DNA repair and facilitate gene transcription [84]. Despite the preceding domain separation, the TRPM7 channel contributes to this process, as the nuclear accumulation of the kinase domain relies on Zn^{2+}. In particular, increase in cytosolic Zn^{2+}, which is partly conducted through TRPM7 the channel, facilitates binding of the kinase domain to zinc-finger containing transcription factors or chromatin remodeling complexes and thus promotes its nuclear transport [84] (also see 3.2.6 for more details).

3.2.3 Pharmacological TRPM7 inhibition

The TRPM7 channel can be inhibited by a broad spectrum of natural and synthetic molecules. Most frequently used is the non-specific blocker 2-aminoethyl diphenylborinate (2-APB, IC_{50}=174 μM), although it simultaneously blocks numerous other channels and transporters such as IP_3Rs, store-operated Ca^{2+} channels (SOCCs), sarco/endoplasmic reticulum Ca^{2+}-ATPase (SERCA), TRP channels and potassium channels [99-110]. The compounds NS8593 and waixenicin A on the other hand are not only more specific for TRPM7, but also display lower IC_{50} values (1.6 μM and 16 nM, respectively) [101]. NS8593, originally identified as a K^+ channel inhibitor [111], reversibly suppresses channel activity in dependence of internal [Mg^{2+}] and the kinase domain [112]. Likewise, waixenicin A works in synergy with intracellular Mg^{2+} and inhibits TRPM7 in a kinase-dependent manner; yet, its inhibition is irreversible [113]. Other candidates are found in the analogs sphingosine (IC_{50}=0.6 μM)

and FTY720 (IC_{50}=0.7 μM), which display even higher binding affinities for TRPM7 than NS8593 and waixenicin A [114]. A novelty amongst TRPM7 inhibitors was discovered in 2017, when Song et al. showed that the known phosphoinositide 3-kinase (PI3K) inhibitor TG100-115 blocks TRPM7 kinase activity with an IC_{50} of 1.07 μM [115]. Yet, the same group also demonstrated the TRPM7 channel activity to be suppressed by TG100-115 in a dose-dependent manner, which lowered the chance of the drug being a TRPM7 kinase-specific inhibitor. However, application of 20 μM TG100-115 in our own measurements (Nadolni et al., in preparation) did not significantly affect channel activity, thus demonstrating that TG100-115 is more potent to block the kinase than the channel. Hence, the undesired side effect of TRPM7 channel inhibition by TG100-115 can be bypassed by reducing the concentration of the drug, and thus, we assume that TG100-115 is the first inhibitor discovered blocking TRPM7 kinase, but not channel activity.

3.2.4 TRPM7 channel and kinase crosstalk

The unusual conjunction of a channel and a kinase raises the question if those two domains affect one another. Most of the mechanisms regulating the channel (described in 3.2.1.2) occur through binding of the modulators to the intracellular C-terminus. Hence, one focus of interest is if the kinase domain respectively its activity is required for channel function. *In vitro* experiments revealed that HEK-293 cells overexpressing the TRPM7 kinase-lacking mutant TRPM7-ΔK (truncated at AA1569) develop WT-like currents, but are more sensitive to Mg^{2+}- or Mg-ATP-caused block [36]. These findings are in line with results acquired for mast cells and ESCs derived from heterozygote TRPM7-ΔK mice analyzed *ex vivo*, which likewise displayed reduced channel activity [35]. In contrast, Desai et al. showed that natural occurring Fas-induced cleavage of TRPM7 at the position D1510 by the caspases 8 and 3 yields in higher TRPM7 current amplitudes under normal physiologic conditions [98]. Taken together, these results indicate that the site of truncation of TRPM7 is crucial for channel properties [98].

The kinase inactivating point mutations, K1648R and G1799D, left TRPM7 currents unaltered, but reduced sensitivity to inhibition by cellular Mg^{2+} and Mg-ATP [36, 68]. Similar experiments with a corresponding murine construct, K1646R, did not show changes in sensitivity to Mg^{2+} and Mg-ATP [116]. In agreement, mice carrying the point mutation revealed normal current progression and regulation under physiological conditions ($[Mg^{2+}]_{cyt}$=100-900 μM) [83, 117, 118].

The impact of the channel on the kinase domain is far less understood. One indication for the channel also controlling the kinase activity is the fact that the kinase requires divalent cations (such as Mg^{2+}, Mn^{2+} and Zn^{2+}) for its function [73, 84]. Indeed, pharmaceutical inhibition of the channel by the synthetic compound NS8593 significantly decreased TRPM7 autophosphorylation in HEK-293 cells by about 40 % [119]. Furthermore, ion influx through the channel also seems to control kinase

interactions, as binding of the cleaved kinase domain to zinc-finger containing transcription factors in the nucleus relies on Zn^{2+}, which in turn is conducted trough the TRPM7 channel [84]. Overall, these findings strongly substantiate an interdependence of the TRPM7 channel and kinase domain.

3.2.5 TRPM7's physiological relevance in diseases

Numerous studies emphasize the importance of TRPM7 for fundamental cellular functions such as survival, growth, proliferation, but also differentiation and migration in almost all cell types [120]. Thus, the channel-kinase has been shown to be associated with a lot of different pathologies, as malfunctioning of these processes often contributes to disease development and progression. Besides cancer, TRPM7 is involved in ischemic stroke, neurodegenerative and cardiovascular diseases [121].

TRPM7's involvement in cancer has manifested over the last decade. Being aberrantly overexpressed in many carcinoma subtypes, it promotes tumor progression and metastasis by regulating proliferation, survival, migration and invasion in malignant cells [120, 122-124]. Furthermore, polymorphisms of the protein have been discovered in colon, breast or ovarian cancer [125-127]. Interestingly, one of these somatic mutations of TRPM7, T1482I, was originally found in patients with the Guamanian form of amyotrophic lateral sclerosis (ALS-G) and Parkinsonism dementia (PD-G) [128]. In the neuronal system, TRPM7's role seems to be more complex and depends on the availability of oxygen. Although it is initially required for brain development in embryonic mice, it showed to be dispensable after day 10.5 [129]. Nevertheless, latter studies documented that it participates in and preserves synaptic signaling via release of neurotransmitters and fosters neuronal survival and growth under normal conditions [130-134]. Under pathological conditions, which are characterized by anoxia or hypoxia, respectively, TRPM7 operates towards the opposite direction. In an environment low in oxygen, for example following ischemic stroke, the channel-kinase promotes neuronal cell death and thus impairs cognitive function [135-137]. Furthermore, a recent study detected TRPM7's kinase activity to promote ischemic disease by facilitating thrombocyte aggregation [138].

TRPM7 was also found to regulate Mg^{2+} homeostasis, vessel size and other essential cell functions in vascular smooth muscle cells (VSMCs) and cardiac fibroblasts (CFs) [139-141]. Despite its indispensability for heart development and cardiac function, more and more indices accumulated linking TRPM7 to diseases regarding the cardiovascular system [142, 143]. In 2016, Antunes et al. brought evidence that TRPM7 is involved in hypertension through its kinase domain [144]. Another study revealed that interleukin 18 (IL-18) induced vascular calcification, a common predictor of coronary heart disease, necessitates the chanzyme [145]. Additionally, TRPM7 also contributes to cardiac diseases such as fibrillation and fibrosis by its Ca^{2+} and Mg^{2+} conductance [141, 146, 147].

In summary, the channel-kinase comprises large therapeutic potential for a spectrum of diseases, which could be treated through pharmacological modulation of specific TRPM7 functions (channel and/or kinase activity). To exclude side effects, it is necessary to investigate TRPM7's operation mode and identify pathways activated downstream.

3.2.6 TRPM7 in cell signaling

With proceeding understanding of the TRPM7 channel and kinase functions and its implications in health and disease, more focus was put on the downstream effects of ion flux and substrate phosphorylation. Indeed, in terms of cell signaling, TRPM7 has been shown to function in Ca^{2+}-dependent as well as -independent signaling pathways (see Figure 3.4). Importantly, these TRPM7-controlled signaling cascades not only coordinate general cellular functions but also contribute to proliferation and propagation of malignant cells which will be outlined below.

The PI3K/protein kinase B (Akt) pathway is classically activated by ligand-induced cell surface receptors. Activated PI3K generates the second messenger phosphatidylinositol-3,4,5-trisphosphate (PIP_3) by phosphorylating PIP_2. PIP_3 recruits pleckstrin homology (PH) domain-containing proteins to the membrane, such as phosphoinositide-dependent kinase-1 (PDK1) and Akt. In turn, Akt is activated by two phosphorylations occurring in the activation loop (Thr308 by PDK1) as well as in the C-terminal region (Ser473 by PDK2). Akt itself has several downstream phosphorylation targets, modulating many proteins involved in cell cycle progression, cell survival and proliferation [148]. These modulatory effects are either inhibitory [e.g. inhibition of glycogen synthase kinase 3 (GSK3) activity] or activating [initiating survival gene transcription by 3',5'-cyclic adenosine monophosphate (cAMP) response element-binding protein (CREB) and other transcription factors] [148-150]. In 2008, Sahni et al. published that TRPM7-deficient lymphocytes display impaired phosphorylation of PI3K and downstream kinases such as Akt and mechanistic target of rapamycin (mTOR) in a Mg^{2+}-dependent manner [151]. A TRPM7-dependent PI3K pathway regulation was later reconfirmed in osteoblasts, hepatic stellate cells (HSCs), chondrocytes and oncogenic cell types and in many cases facilitates disease progression [152-159]. In glioblastoma, prostate and bladder cancer cells, for example, TRPM7 induces tumor cell proliferation and migration by increasing Akt phosphorylation [155, 157]. The PI3K downstream kinase is also relevant for hepatic fibrosis triggered by TRPM7, but dispensable for TRPM7-dependent breast cancer migration [154, 160].

Another TRPM7 affected signaling cascade is the mitogen-activated protein kinase/extracellular signal-regulated kinase (MAPK/ERK) pathway typically involved in proliferation and apoptosis [161, 162]. Free Ca^{2+} entering the cell binds to and thereby activates CaM, and together they activate members of the Ca^{2+}/CaM-dependent kinase family (CaMKs) [163-166]. This initiates a phosphorylation cascade of more protein kinases (from MAPKKKs to MAPKs) resulting in the

activation of the Ser/Thr kinase ERK1/2, which further phosphorylates members of the MAPK-activated protein kinase (MAPKAPK) family (MNKs and RSKs) and is directly as well as indirectly involved in regulation of cell proliferation and cell cycle progression [149, 167, 168]. In breast cancer cells, TRPM7 promotes invasion via the (MAPK/ERK) pathway by phosphorylation of ERK1/2 (alias MAPK3), c-Jun terminal kinase (JNK) and p38 [160]. A TRPM7-dependent control of the MAPK/ERK pathway has also been observed for other cancer cell types, VSMCs and astrocytes, but TRPM7's impact on ERK phosphorylation seems to be ambiguous. While several groups detected a reduction in ERK phosphorylation upon TRPM7 deletion, other experiments displayed an increase [155, 169-172].

Moreover, murine knockout studies suggested a role for TRPM7 in the phosphorylation of signal transducer and activator of transcription 3 (STAT3) [45]. This protein belongs to the Ca^{2+}-inducible transcription factor family STAT [173, 174]. Typically activated by the Janus kinase (JAK), STAT proteins homo- respectively heterodimerize upon phosphorylation, translocate to the nucleus and eventually stimulate specific gene transcription. All seven family members have been shown to be important (in some cases even essential, STAT3) regulators of development, cell proliferation and - due to their cytokine responsiveness - immunity [175, 176]. Further analysis of TRPM7-dependent STAT3 phosphorylation in *in vitro* experiments showed that TRPM7 promotes tumorigenesis of different carcinoma subtypes by activation of JAK/STAT3 signaling [174, 177, 178]. *Vice versa*, TRPM7 inward current can be inhibited through the IL-6/JAK2/STAT3 pathway independently of Ca^{2+} or the kinase domain, as Liu et al. demonstrated [179]. A positive feedback loop on the other hand was observed for TGF-β-dependent TRPM7 regulation. Through binding to its receptor TGF-β type II, TGF-β induces phosphorylation of the TGF-β type I receptor, thereby initiating subsequent phosphorylation of the receptor-regulated SMADs (R-SMADs) of which two of those are SMAD2 and 3 [180, 181]. Together with the collaborating SMAD4, SMAD2 and 3 translocate into the nucleus were they activate gene transcription [180, 181]. The TGF-β/SMAD signaling axis has been associated with processes such as cell proliferation and differentiation, cytoskeletal remodeling and – as being a cytokine – regulation of immune reactions [182, 183]. In HSCs, TGF-β elicits TRPM7 expression via the SMAD pathway, which in turn enhances SMAD2 and SMAD3 phosphorylation [184]. Very recently, members of our group discovered that SMAD2 represents a direct target of the TRPM7 α-kinase in $CD4^+$ T cells, where the channel-kinase aids TGF-β-mediated signaling (also see 3.2.2.2) [83].

Next to its impact as an upstream activator of many signaling cascades in the cytosol, the channel-kinase is also able to modify gene transcription by directly targeting proteins located in the nucleus. Happening *in vitro* and *in vivo,* the before mentioned cleavage of TRPM7 results in the separation of the channel and kinase domain (also see 3.2.2.2). Upon their release, C-terminal fragments comprising

the kinase domain migrate into the nucleus were they bind to nuclear components [84]. Computational analysis revealed that this nuclear translocation could occur through a putative nuclear localization sequence within the C-terminus of TRPM7 (AAs 1780-1807). Nevertheless, Krapivinsky et al. hypothesized that nuclear transport of the kinase domain could also be facilitated by the interaction with nuclear proteins itself. Once in the nucleus, the kinase associates with numerous transcription factors respectively subunits of chromatin-remodeling complexes, such as Yin Yang 1 (YY1), Ring1 and YY1 binding protein (RYBP) or enhancer of zeste homolog 2 (EZH2). Valid for those proteins containing a zinc-finger motif, binding of the kinase domain to these molecules is Zn^{2+}-dependent; hence, the TRPM7 channel most likely aids these interactions through its Zn^{2+} conductance. Furthermore, kinase inactivation in some cases prevents or augments binding to the nuclear proteins, indicating that kinase activity defines its own selectivity regarding potential interaction partners. The active kinase also participates in histone phosphorylation. Overexpression experiments in TRPM7-deficient mouse ESCs (mESC) illustrate a TRPM7 kinase-dependent phosphorylation of histone H3 at Ser10, Ser28 and Thr3, and an *in vitro* kinase assay strongly suggest that both Ser10 and Ser28 are directly phosphorylated by the enzyme. Together with the TRPM7-promoted histone H3 acetylation at Lys9 and Lys27, these modifications correlate with increased expression of genes important for early developmental processes and cell differentiation. Thus, both the TRPM7 channel and kinase are proposed to differentially contribute to gene expression essential for embryonic development for example [84]. More recently, the same group demonstrated that TRPM7's close related family member, TRPM6, likewise is cleaved, modulates gene transcription and phosphorylates histones via its C-terminally located kinase domain [185].

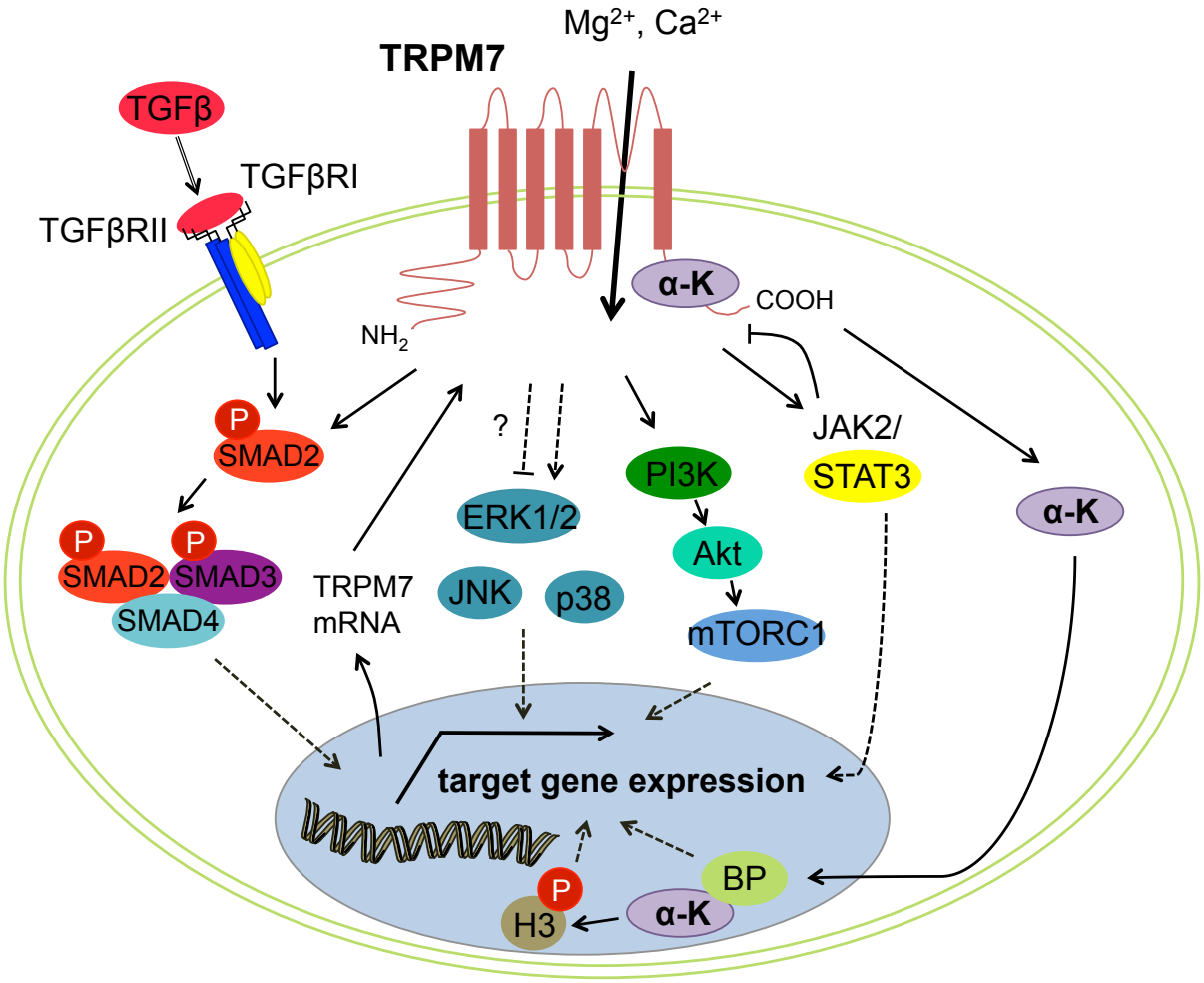

Figure 3.4 TRPM7 in cell signaling. Both JAK/STAT and PI3K/Akt signal transduction followed by target gene expression have been shown to be facilitated by TRPM7. In addition, TRPM7 was demonstrated to affect the MAPK/ERK pathway by targeting the cells signaling kinases ERK1/2, JNK and p38; yet, its impact on ERK1/2 activation is still not clear and most likely is cell type specific. Besides, the TRPM7 kinase promotes TGF-β-induced signaling through SMAD2, 3 and 4 by directly phosphorylating SMAD2 at Thr465/467. Moreover, the TRPM7 kinase domain also regulates gene expression by directly targeting nuclear located proteins. Thus, the TRPM7 C-terminus enclosing the kinase unit is truncated and translocates into the nucleus where it interacts with different binding partners (BP) and facilitates histone H3 phosphorylation, thereby inducing specific gene transcription.

α-K – alpha-kinase domain, Akt – protein kinase B (PKB), BP – binding partners, COOH – C-terminus, ERK – extracellular signal-regulated kinase, H3 – histone H3, JAK – Janus kinase, JNK – c-Jun terminal kinase, mTORC - mechanistic target of rapamycin complex, NH_2 – N-terminus, PI3K – phosphoinositide 3-kinase, SMAD – Mothers against decapentaplegic homolog, STAT – signal transducer and activator of transcription, TGF-β – transforming growth factor β, TRPM – transient receptor potential, melastatin-like

3.3 The HAP1 cells

In 1999, a subclone of the heterogeneous human chronic myelogenous leukemia (CML) cell line KBM-7 initiated the beginning of a new cell line [186, 187]. At this time, these cells presented haploidy for almost all chromosomes except for the chromosome 8 and, in some cases, 15 (dependent on the subclone) and retained their karyotypes in cell culture for up to 12 weeks [187]. In general, haploid cells represent an exceptional tool for studying protein-specific effects by target modification and genetic screens, as they lack the second set of chromosomes which normally covers introduced mutations [188, 189].

Thus, in the following years, researchers focused on elimination of the one respectively two remaining chromosome copies (8 and 15) existent in the above-mentioned KBM-7 subclone to generate a fully haploid cell line. First experiments lead to the extinction of the second copy of chromosome 8, and about five years later, application of the new futuristic technology CRISPR/Cas9 [190, 191] finally resulted in full haploidy, wherefore the cells were named HAP (haploid) 1 [192, 193]. Since then, it turns out that HAP1 cells present an extremely valuable cellular knockout system to study the molecular function of a respective target protein, which was also already applied for investigations regarding TRPM7 function [189, 193-195].

3.4 Aim of the work

Different experimental approaches within the last two decades impressively document the fundamental role of TRPM7 for a vast variety of physiological processes including embryonic development, cell growth, proliferation and differentiation as well as adhesion and migration. In many cases, the impact of TRPM7 on these essential (cell) functions is mediated by regulation of various cell signaling pathways. However, with the exception of two papers [78, 79], all of the so far published work refers to the TRPM7 full-length protein, thus lacking differentiation between the action of the ion channel and the kinase domain.

Yet, to get a better understanding of the TRPM7 channel-kinase, it is more than important to discriminate between TRPM7-mediated ion influx and its phosphotransferase activity.

Given these aspects, overall aim of this work was to first confirm and expand the knowledge about TRPM7's functional role in already identified signaling pathways in HAP1 cells and secondary to unravel the impact of the TRPM7 kinase domain on particular mediators of these signaling cascades.

To accomplish this goal, I will utilize two different HAP1 cell lines mutated for TRPM7: One lacks TRPM7 full-length protein expression (abbreviated TRPM7 KO), whereas the other mutated variant carries a point mutation within the kinase domain that leads to the loss of phosphotransferase activity (abbreviated TRPM7 KI). This enables me to at first decipher the role of full-length TRPM7 for distinct cellular signal transduction as well as gene transcription processes and secondly to relate TRPM7-directed actions directly to TRPM7`s kinase activity.

In particular, the following procedure is scheduled:

With use of DNA-based genetic sequencing, I will first verify the correct insertion of the two mutations (TRPM7 KO, TRPM7 KI) in the HAP1 cell line. These experiments will be completed by whole-cell patch clamp measurements: By a systematic comparison of currents typically displayed by TRPM7, the results not only allow confirming a successful deletion of TRPM7 but additionally enable me to detect current alterations which can be attributed to an inactivated TRPM7 kinase domain. In respect to TRPM7's function in ion homeostasis, impact of TRPM7 respectively its kinase activity on intracellular ion concentrations will be reviewed using inductively coupled plasma mass spectrometry (ICP-MS).

In a next step, I plan to investigate the phosphorylation state of signaling molecules which already have been identified to be part of TRPM7-controlled cascades, such as Akt and GSK3β (PI3K/Akt pathway), ERK1/2 (MAPK/ERK pathway), STAT3 (JAK/STAT pathway) and SMAD2 (TGF-β /SMAD pathway). Phosphorylation of these target proteins will be determined using phospho-specific antibodies in Western Blot analysis. In the event of indeed discovering a TRPM7-respectively kinase activity-controlled phosphorylation of one of the examined signaling molecules, I

next want to check for potential alterations of downstream effectors such as transcription factors. Employment of a luciferase-based reporter gene assay will help to clarify domain-specific function of TRPM7 in transcriptional activity of potentially affected transcription factors. Furthermore, TRPM7 respectively kinase activity-dependent regulation of gene expression will subsequently be examined with the sensitive real-time quantitative polymerase chain reaction (RT-qPCR) technique which allows the simultaneous analysis of multiple genes. By directly comparing the results obtained for the TRPM7 KO and the KI clone, respectively, this strategy makes it possible to precisely differentiate between TRPM7 full-length protein and kinase-directed actions on distinct signaling molecules.

To finally verify results obtained by the genetic manipulations of TRPM7, I plan to selectively inhibit either TRPM7 or its kinase domain in primary cells. With the myeloid origin of the HAP1 cells in mind, I intend to utilize primary human neutrophils, which are developed from myeloid progenitor cells and can easily be isolated from blood samples. The results of such an experimental approach should permit the conclusion if identified target proteins of TRPM7 and/or its kinase domain in HAP1 cells are identical to the ones in primary cells.

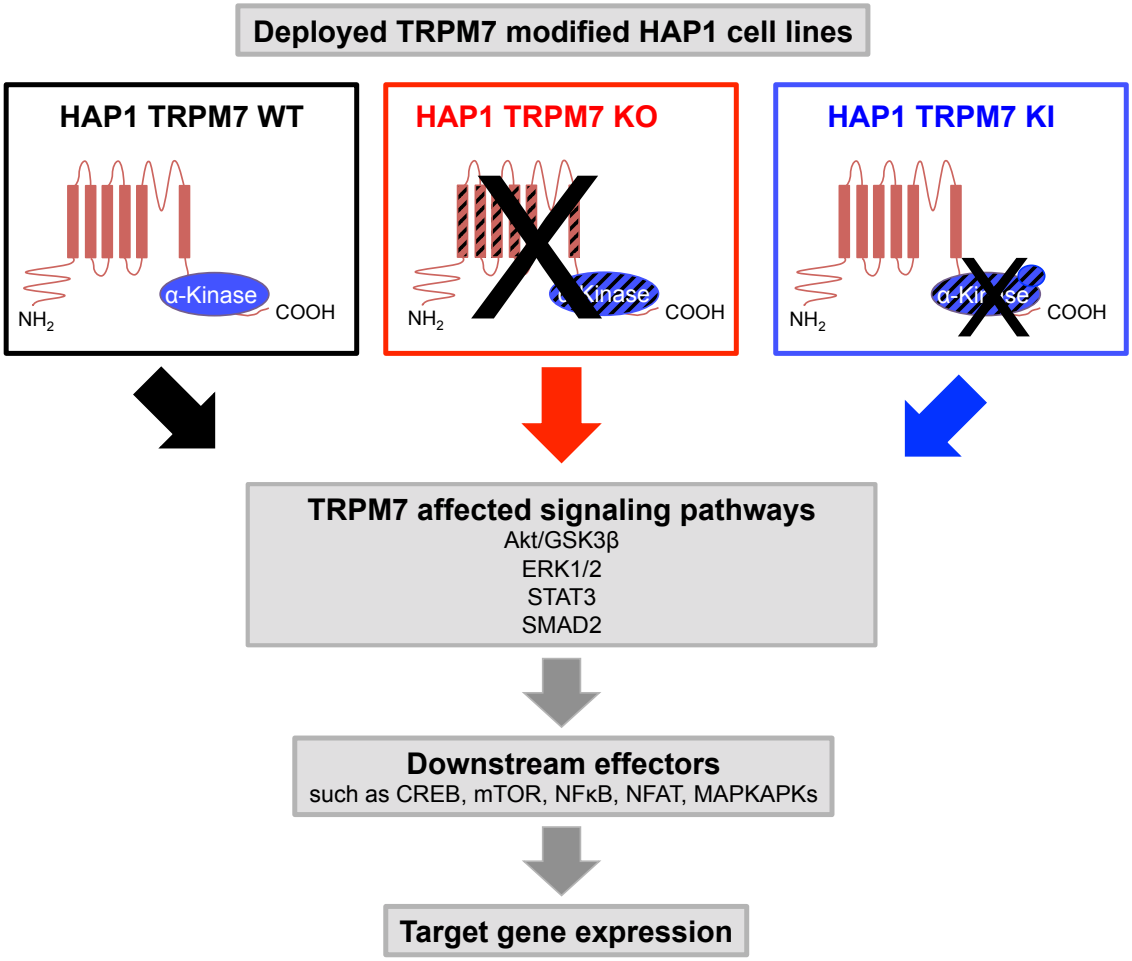

Figure 3.5 Scientific working strategy to study TRPM7 protein respectively TRPM7 kinase-specific function in cell signaling.
TRPM7 has been shown to modify various components of different cell signaling cascades such as the kinases Akt and ERK1/2 as well as the transcription factors STAT3 and SMAD2. However, whether the effect of TRPM7 is mediated by an ion flux through its channel pore and/or is catalyzed by a phosphorylation of target proteins by the fused kinase domain is currently not clear. To elucidate the exact role of the two TRPM7 domains in cell signaling, different HAP1 cell models modified for TRPM7 will be utilized and compared to a HAP1 TRPM7 wild-type (WT) model (black). First is the HAP1 TRPM7 knockout (KO) clone (red) lacking expression of the correct full-length protein, which enables one to study TRPM7-specific function(s) in general. Secondly, the HAP1 TRPM7 knock-in (KI) clone (blue), which carries a point mutation within the TRPM7 kinase domain inactivating its phosphotransferase activity, will be utilized to uncover the impact of the TRPM7 kinase unit.
Initially, each HAP1 cell model will be employed to assess the domain-specific effect of TRPM7 on the phosphorylation of Akt and GSK3β, ERK1/2, STAT3 and SMAD2. If indeed discovering a TRPM7 or kinase activity-dependent phosphorylation of these proteins, I will next focus on potential alterations regarding downstream effectors of the affected signaling pathway(s), such as further downstream located kinases or transcription factors. Finally, attempts will be made to depict the effect of TRPM7 and/or its kinase activity on specific target gene expression.

Akt – protein kinase B (PKB), COOH – C-terminus, CREB – cAMP response element-binding protein, ERK – extracellular signal-regulated kinase, GSK3β – glycogen synthase kinase 3 β, MAPKAPK – mitogen-activated protein kinase-activated protein kinase, mTOR – mechanistic target of rapamycin, NFAT – nuclear factor of activated T cells, NFκB – nuclear factor kappa-light-chain-enhancer of activated B cells, NH2 – N-terminus, SMAD – Mothers against decapentaplegic homolog, STAT – signal transducer and activator of transcription, TRPM – transient receptor potential, melastatin-like.

4 Material

4.1 Devices and laboratory equipment

Device	Supplier
Agarosegelelectrophoresis system model 40-1214	PeqLab, Erlangen (Germany)
CCD AxioCam MRm camera	Zeiss, Jena (Germany)
Chemiluminescence detection system Chemi-Smart™-5100	Peqlab, Erlangen (Germany)
Cell incubator New Brunswick™ Galaxy 170 S	Eppendorf, Hamburg (Germany)
Centrifuge 5424 R	Eppendorf, Hamburg (Germany)
Centrifuge 5804 R	Eppendorf, Hamburg (Germany)
Centrifuge HERAEUS Biofuge Stratos	Thermo Fisher Scientific, Waltham (USA)
Centrifuge HERAEUS Pico 17	Thermo Fisher Scientific, Waltham (USA)
Cytostatic safety cabinet FlowSafe® C-[MAXPro]^3-190	Berner, Elmshorn (Germany)
Easypet® 2	Eppendorf, Hamburg (Germany)
Faraday cage	HEKA, Lambrecht (Germany)
FlexCycler^2 PCR Thermal Cycler	Analytik Jena, Jena (Germany)
Flow cytometer Guava® easyCyte 5	Merck Millipore, Billerica (USA)
Fluorescence Light Source	Olympus, Hamburg (Germany)
Fluorescence Micropscope Olympus IX70	Olympus, Hamburg (Germany)
Fluostar Omega	BMG Labtech, Ortenberg (Germany)
Freezer -80°C	Eppendorf, Hamburg (Germany)
Heating block HX1	PeqLab, Erlangen (Germany)
Hematocytometer (Neubauer chamber)	Brand, Wertheim (Germany)
Inverted microscope system IX71	Olympus, Hamburg (Germany)
Inverted microscope Axio Vert.A1	Zeiss, Jena (Germany)
LED light source for fluorescence Colibri 2	Zeiss, Jena (Germany)
LightCycler® 480	Roche, Rotkreuz (Austria)
Light microscope Axiovert 35 M	Zeiss, Jena (Germany)
Magnetic stirrer C-MAG HS7	IKA, Staufen (Germany)
Micromanipulator PatchStar	ΨScientifica, Uckfield (UK)
Micro scale	Sartorius, Göttingen (Germany)
Microwave	Daewoo Electronics, Frankfurt (Germany)

Device	Supplier
Monochromator Polychrom V	Till Photonics, München (Germany)
Monochrome camera X10	Olympus, Hamburg (Germany)
Mini-Protean® Tetra Handcast Systems	Bio-Rad, Hercules (USA)
Mini Trans-Blot® Cell	Bio-Rad, Hercules (USA)
Osmometer VAPRO 5600	Wescor, Logan (USA)
Patch clamp Amplifier EPC-10	HEKA, Lambrecht (Germany)
pH meter FiveEasy Plus	Mettler Toledo, Columbus (USA)
Platform shaker Duomax 1030	Heidolph, Kehlheim (Germany)
PowerPac™ Basic Power Supply	Bio-Rad, Hercules (USA)
PowerPac™ HC High-Current Power Supply	Bio-Rad, Hercules (USA)
Puller DMZ-Universal Puller	Zeitz, Martinsried (Germany)
Rocking shaker Duomax 1030	Heidolph Instruments, Schwabach (Germany)
Spectrophotometer BioPhotometer plus UV-Visible	Eppendorf, Hamburg (Germany)
Thermomixer® Compact	Eppendorf, Hamburg (Germany)
Tube rotator	Workshop of the Walther-Straub-Institut, LMU Munich, Munich (Germany)
UV-gel documentation system Infinity 3026	Peqlab, Erlangen (Germany)
Vibration isolation table	TMC, Peabody (USA)
Vortex mixer MS 3 basic	IKA, Staufen (Germany)

4.2 Consumables

All consumables (sterile cell culture equipment, pipettes and pipette tips, reaction tubes etc.) were sourced from Sarstedt, Nürmbrecht if not stated otherwise. General glassware (glass bottles, Erlenmeyer flasks, beakers etc.) was purchased from Carl Roth, Karlsruhe.

Item	Product Number	Supplier
Blotting Paper	BP0035860	Hahnemühle, Dassel (Germany)
Borosilicate glass with firepolished ends with filament	GB150TF-8P	Science products, Hofheim (Germany)
Corning® cell strainers, 40 µM/100 µM	CLS431750/ CLS431752	Sigma-Aldrich, Deisenhofen (Germany)
Glass Coverslips, diameter of 12 mm	P231.1	Carl Roth, Karlsruhe (Germany)

Item	Product Number	Supplier
Glass Coverslips, diameter of 24 mm	1-6290	NeoLab,Heidelberg (Germany)
Corning® 96 well solid polystyrene microplate	CLS3917	Sigma-Aldrich, Deisenhofen (Germany)
Nitrocellulose membrane Amersham Protran 0.45 µM	10600002	GE Healthcare, Buckinghamshire (UK)
Parafilm M	PM992	Pechiney Plastic Packaging, Chicago (USA)
Pasteur pipettes	4522	Carl Roth, Karlsruhe (Germany)

4.3 Chemicals and reagents

Substance	Product Number	Supplier
4-(2-hydroxyethyl)piperazine-1-ethanesulfonic acid (HEPES)	H3375	Sigma-Aldrich, Deisenhofen (Germany)
2-Propanol	0733	Carl Roth, Karlsruhe (Germany)
2-Mercaptoethanol	M6250	Sigma-Aldrich, Deisenhofen (Germany)
Acetic acid	3738	Carl Roth, Karlsruhe (Germany)
Agarose	3810	Carl Roth, Karlsruhe (Germany)
Albumin fraction V (BSA)	8076	Carl Roth, Karlsruhe (Germany)
Ammonium peroxydisulfate (APS)	9592	Carl Roth, Karlsruhe (Germany)
Bromophenol blue	B0126	Sigma-Aldrich, Deisenhofen (Germany)
Calcium chloride dihydrate ($CaCl_2$)	HN04	Carl Roth, Karlsruhe (Germany)
Cesium hydroxide solution (CsOH)	232068	Sigma-Aldrich, Deisenhofen (Germany)
cOmplete™, Mini, EDTA-free Protease Inhibitor Cocktail (Tablets)	04693159001	Sigma-Aldrich, Deisenhofen (Germany)

Substance	Product Number	Supplier
D-(+)-Glucose	G8270	Sigma-Aldrich, Deisenhofen (Germany)
Diethyl pyrocarbonate (DEPC)-treated H_2O	95284	Sigma-Aldrich, Deisenhofen (Germany)
Dimethyl sulfoxid (DMSO)	D4540	Sigma-Aldrich, Deisenhofen (Germany)
Dithiothreitol (DTT)	6908	Carl Roth, Karlsruhe (Germany)
Deoxynucleostide triphosphate (dNTP) mix (10 mM)	R0192	Thermo Fisher Scientific, Waltham (USA)
Ethanol ≥ 99,8 %	9065	Carl Roth, Karlsruhe (Germany)
Ethylenediaminetetraacetic acid (EDTA)	E6758	Sigma-Aldrich, Deisenhofen (Germany)
Ethylene glycol-bis (β-aminoethyl ether)- N,N,N',N'-tetraacetic acid (EGTA)	3045	Carl Roth, Karlsruhe (Germany)
FastAP Thermosensitive alkaline phosphatase (1 U/µl)	EF0654	Thermo Fisher Scientific, Waltham (USA)
Fura-2 acetomethyl (AM) ester	47989	Sigma-Aldrich, Deisenhofen (Germany)
Glycine	0079	Carl Roth, Karlsruhe (Germany)
Guava ViaCount®	4000-0040	EMD Millipore Coop., Billerica (USA)
LightCycler® 480 SYBR Green I Master	04707516001	Roche, Rotkreuz (Austria)
Lipofectamin® 2000 Transfection Reagent	12566014	Thermo Fisher Scientific, Waltham (USA)
Lipopolysaccharide (LPS)	L4391	Sigma-Aldrich, Deisenhofen (Germany)
L-Glutamic acid	G1252	Sigma Aldrich, Deisenhofen (Germany)
Luminol	A8511	Sigma-Aldrich, Deisenhofen (Germany)

Substance	Product Number	Supplier
Dual-Glo® Luciferase Assay System	E2940	Promega, Mannheim (Germany)
Magnesium chloride hexahydrate ($MgCl_2$)	HN03	Carl Roth, Karlsruhe (Germany)
p-Coumaric acid	C9008	Sigma-Aldrich, Deisenhofen (Germany)
PhosSTOP™	PHOSS-RO	Sigma-Aldrich, Deisenhofen (Germany)
Pluronic® F-127	P2443	Sigma-Aldrich, Deisenhofen (Germany)
PolymorphPrep™	1114683	Progen, Heidelberg (Germany)
Poly-D-lysine (PDL) hydrobromide	P7280	Sigma-Aldrich, Deisenhofen (Germany)
Ponceau S	P3504	Sigma-Aldrich, Deisenhofen (Germany)
Potassium chloride (KCl)	HN02	Carl Roth, Karlsruhe (Germany)
Potassium hydroxide (KOH)	7986	Carl Roth, Karlsruhe (Germany)
$Oligo(dT)_{12-18}$	Costum order	Metabion, Planegg (Germany)
Sodium chloride (NaCl)	HN00	Carl Roth, Karlsruhe (Germany)
Sodium dodecylsulfate (SDS)	0183	Carl Roth, Karlsruhe (Germany)
Spectra™ Multicolor Broad Range Protein Ladder	26634	Thermo Fisher Scientific, Waltham (USA)
Sucrose	84097	Sigma-Aldrich, Deisenhofen (Germany)
SuperScript® II Reverse Transcriptase	18064-014	Thermo Fisher Scientific, Waltham (USA)
RIPA buffer	R0278	Sigma-Aldrich, Deisenhofen (Germany)
Roti® GelStain	3865	Carl Roth, Karlsruhe (Germany)
Rotiphorese® Gel 30 (acrylamide/bisacrylamide solution)	3029	Carl Roth, Karlsruhe (Germany)

Substance	Product Number	Supplier
N,N,N',N'-Tetramethylethylendiamin (TEMED)	8142	Carl Roth, Karlsruhe (Germany)
Thapsigargin	T9033	Sigma-Aldrich, Deisenhofen (Germany)
Trichlorol®	43546	Lysoform, Berlin (Germany)
Tris	4855	Carl Roth, Karlsruhe (Germany)
Tris/HCl	9090	Carl Roth, Karlsruhe (Germany)
Trizol	15596	Thermo Fisher Scientific, Waltham (USA)
Trypan blue solution	T8154	Sigma-Aldrich, Deisenhofen (Germany)
TurboFect™ Transfection Reagent	R0533	Thermo Fisher Scientific, Waltham (USA)
Tween® 20	P9416	Sigma-Aldrich, Deisenhofen (Germany)
Zeocin™ Selection Reagent	R25001	Thermo Fisher Scientific, Waltham (USA)

4.4 Cell culture media and supplements

Substance	Product Number	Supplier
Dulbecco's modified eagle medium (DMEM)	61965026	Thermo Fisher Scientific, Waltham (USA)
Dulbecco's modified eagle medium (DMEM), no phenol red	21063029	Thermo Fisher Scientific, Waltham (USA)
Dulbecco's phosphate buffered saline (DPBS)	D8537	Sigma-Aldrich, Deisenhofen (Germany)
Fetal bovine serum (FBS)	10270	Thermo Fisher Scientific, Waltham (USA)
Hanks' balanced salt solution (HBSS)	H6648	Sigma-Aldrich, Deisenhofen (Germany)
Iscove's modified Dulbecco's medium (IMDM)	31980030	Thermo Fisher Scientific, Waltham (USA)

Substance	Product Number	Supplier
Penicillin-Streptomycin	P4333	Sigma-Aldrich, Deisenhofen (Germany)
Trypsin-EDTA solution	T4049	Sigma-Aldrich, Deisenhofen (Germany)

4.5 Kits and assays

Kits	Product Number	Supplier
Cyclooxygenase Activity Assay Kit (Fluorometric),	ab204699	Abcam, Cambridge (UK)
MyTaq™ Extract-PCR Kit	21126	Bioline Reagents, London (UK)
MyTaq™ HS Red Mix	25047	Bioline Reagents, London (UK)
GeneJET Gel Extraction Kit	K0691	Thermo Fisher Scientific, Waltham (USA)
Nuclear Extract Kit	40010	Active motif, Carlsbad (USA)

4.6 Inhibitors and activators

Name	Activator of	Product Number	Supplier
Forskolin	adenylyl cyclase	S2449	Selleckchem, Munich (Germany)

Name	Inhibitor of	Product Number	Supplier
IPI-549	PI3K-γ	S8330	Selleckchem, Munich (Germany)
Nemirasilib/ GSK2269557	PI3K-δ	S7937	Selleckchem, Munich (Germany)
NS8593	TRPM7 and $K_{Ca}2$ channels	N-196	Alomone Labs, Jerusalem (Israel)
TG100-115	TRPM7 kinase and PI3K	S1352	Selleckchem, Munich (Germany)

4.7 cDNA expression constructs

Plasmid	Product Number	Supplier
Control vector pcDNA™ 3.1	V79020	Thermo Fisher Scientific, Waltham (USA)
Control vector pcDNA™ 4	V102020	Thermo Fisher Scientific, Waltham (USA)
NFAT reporter gene pGL4.30 [luc2P/NFAT-RE/Hygro] Vector	E8481	Promega, Mannheim (Germany)
pRL Renilla Luciferase Control Reporter Vector	E2261	Promega, Mannheim (Germany)

Plasmid	Vector backbone	Protein expressed	Source/Reference
G5α	pEGFP-C1	GFP-Aequorin fusion protein	Dr. Breit, Walther-Straub-Institute, LMU Munich [196]
TRPM7 WT	pIRES-eGFP	WT mouse TRPM7 protein	Dr. Chubanov, Walther-Straub-Institute, LMU Munich [197]
TRPM7 KI (K1646R)	pIRES-eGFP	kinase-dead variant of mouse TRPM7	Dr. Chubanov, Walther-Straub-Institute, LMU Munich [197]

4.8 Solutions

4.8.1 Buffers for electrophysiology and Fura-2 AM based Ca^{2+} imaging

Buffer/Solution	Components
External solution for patch clamp measurements	140 mM NaCl 2.8 mM KCl 10 mM HEPES-KOH 0.2 % (w/v) Glucose 3 mM $CaCl_2$ (pH 7.20, ~285 mM mOsm/kg)
Internal solution for patch clamp measurements	140 mM Cs-glutamate (pH 7.2) 8 mM NaCl 10 mM HEPES-CsOH

Buffer/Solution	Components
	5 mM EDTA 10 mM EGTA (pH 7.20, ~300 mM mOsm/kg
External solution for Fura-2 AM based Ca^{2+} imaging experiments	140 mM NaCl 2.8 mM KCl 10 mM HEPES-KOH 0.2 % (w/v) Glucose 2 mM $CaCl_2$ 1 mM $MgCl_2$ (pH 7.20, ~285 mM mOsm/kg)
Fura-2 AM staining solution	140 mM NaCl 2.8 mM KCl 10 mM HEPES-KOH 0.2 % (w/v) Glucose 2 mM $CaCl_2$ 1 mM $MgCl_2$ 0.02 % Pluronic® F-127 0.1 % BSA 2 μM Fura-2 AM (pH 7.20, ~285 mM mOsm/kg)

4.8.2 Buffers for agarose gelelectrophoresis

Buffer/solution	Components
TAE buffer	40 mM Tris 20 mM acetic acid 1 mM EDTA

4.8.3 Buffers for protein analysis (via SDS-PAGE and Western Blot)

Buffer/solution	Components
4 x Laemmli buffer (SDS-sample buffer)	62.5 mM Tris/HCl 20 % (v/v) Glycerol 5 % (v/v) β-Mercaptoethanol

Buffer/solution	**Components**
	4 % (w/v) SDS
	0.1 % (w/v) Bromophenol blue
SDS separation gel	8 % respectively 10 % acrylamide/bisacrylamide
	375 mM Tris/HCl (pH 8.8)
	0.1 % SDS
	0.1 % APS
	0.1 % TEMED
SDS stacking gel	3% acrylamide/bisacrylamide
	125 mM Tris/HCl (pH 6.8)
	0.1 % SDS
	0.1 % APS
	0.1 % TEMED
SDS running buffer	192 mM Glycine
	25 mM Tris/HCl
	1 % (w/v) SDS
Transfer buffer	25 mM Tris/HCl
	192 mM Glycine
Ponceau S Solution	0.1 % Ponceau S (v/v)
	5 % acetic acid (v/v)
TBST	50 mM Tris/HCl
	150 mM NaCl
	0.1 % (v/v) Tween-20
Enhanced chemiluminescence (ECL) solution 1	100 mM Tris/HCl
	1% (v/v) Luminol
	0.44 (v/v) p-Coumaric acid
	pH 8,5
ECL solution 2	100 mM Tris/HCl
	0.6 % (v/v) H_2O_2
	pH 8,5

4.8.4 Buffer for dual-luciferase reporter gene assay

Buffer/solution	Components
Lysis Buffer	25 mM Tris/HCl (pH 8,5) 4 mM EGTA 8 mM $MgCl_2$ 1 mM DTT 1 % (v/v) Triton X pH 7,4

4.9 Antibodies

4.9.1 Primary antibodies

Name	Host	Dilution	Product Number	Supplier
pAKT (Ser473)	Rabbit	1:600	9271	Cell Signaling Technology, Cambridge (UK)
pERK (Tyr204)	Mouse	1:2500	sc-7383	Santa Cruz Biotechnology, Heidelberg (Germany)
pGSK3β (Ser9)	Rabbit	1:1000	sc-11757-R	Santa Cruz Biotechnology, Heidelberg (Germany)
pSMAD2 (Ser465/467)	Rabbit	1:200	3101	Cell Signaling Technology, Cambridge (UK)
pSTAT3 (Tyr705)	Rabbit	1:2500	9131	Cell Signaling Technology, Cambridge (UK)
GAPDH	Rabbit	1:2500	PA5-85074	Thermo Fisher Scientific, Waltham (USA)
NFATc1	Rabbit	1:600	sc-13033	Santa Cruz Biotechnology, Heidelberg (Germany)
NFATc2	Rabbit	1:1000	sc-13034	Santa Cruz Biotechnology, Heidelberg (Germany)
NFATc3	Rabbit	1:1000	sc-8321	Santa Cruz Biotechnology, Heidelberg (Germany)
NFATc4	Rabbit	1:1000	sc-13036	Santa Cruz Biotechnology, Heidelberg (Germany)

Name	Host	Dilution	Product Number	Supplier
LaminB1	Rabbit	1:10000	PA-519468	Thermo Fisher Scientific, Waltham (USA)
TRPM7 pSer1511	Rabbit	1:300	self-made	Dr. Chubanov, Walther-Straub-Institute, LMU Munich

4.9.2 Secondary antibodies

Name	Host	Dilution	Product Number	Supplier
Goat anti-mouse horse radish peroxidase (HRP) conjugate	Goat	1:4000	1706516	BioRad, Hercules (USA)
Goat anti-rabbit HRP conjugate	Goat	1:5000	1706515	BioRad, Hercules (USA)

4.10 Primers

4.10.1 Sequencing primers

The genomic human TRPM7 primers were designed according to the primers published by Chubanov et al. [195]. Primers for the human TRPM7 cDNA were designed using the software Primer-Blast by the National Center for Biotechnology Information (NCBI).

Name	PubMed entry	5' → 3' Sequence
TRPM7 knockout	NC_000015.10	(+) 5' – TAT TTG TAT GCA CCT TTG TA – 3' (–) 5' – TGT TTT AAT CTC ACC TTT TT– 3'
TRPM7 knock-in	NM_017672.6	(+) 5' – TCA CTT CTC CAT TTA AGC CAG C – 3' (–) 5' – ACT GTC CTG CTG AAT GGC AA – 3'

4.10.2 RT-qPCR primers

All primers listed below were designed with the Universal ProbeLibrary from Roche (Rotkreuz, Germany) using the corresponding PubMed entry. In some cases, the resulting primers were found to match primers which have already been published (sources indicated below).

Gene	PubMed entry	5' → 3' Sequence
HPRT1	NM_000194.2	(+) 5' – AAG CTT GCT GGT GAA AAG GA – 3' [198]
		(−) 5' – AAG CAG ATG GCC ACA GAA CT – 3' [199]
COX-2	NM_000963.3	(+) 5' – TGT ATG TAT GAG TGT GGG ATT TGA C – 3'
		(−) 5' – GAT CAT CTC TGC CTG AGT ATC TTT G – 3'
IL-2	NM_000586.3	(+) 5' – GTC ACA AAC AGT GCA CCT AC – 3' [200]
		(-) 5' – CCC TGG GTC TTA AGT GAA AG – 3' [200]
Myc	NM_002467.4	(+) 5' – AAT GAA AAG GCC CCC AAG GTA GTT ATC C – 3' [201]
		(−) 5' – GTC GTT TCC GCA ACA AGT CCT CTT C – 3' [201]
RCAN3	NM_001251977.1	(+) 5' – TAT TTT GCA CAG GTG CAG ATG TCC – 3'
		(−) 5' – CAG AGT CTC ACC TAT GCT GTT CG – 3'

4.11 Cell lines

Name	Feature/Mutation	Source/Reference
HAP1 TRPM7 WT	wild-type	Dr. Chubanov, Walther-Straub-Institute, LMU Munich [195]
HAP1 TRPM7 KO	Lacks TRPM7 protein expression	Dr. Chubanov, Walther-Straub-Institute, LMU Munich [195]
HAP1 TRPM7 KI	Carries a TRPM7 kinase inactivating point mutation (K1648R)	Generated by HorizonGenomics via CRISPR/Cas9 technology
HEK-293 WT	wild-type	Dr. Breit, Walther-Straub-Institute, LMU Munich
HEK-NFAT	Stable expression of an NFAT luciferase reporter	Generated from the HEK-293 WT cell line as part of this project
HEK-G5α	Expresses the Ca^{2+} sensor apoaequorin fused to GFP	Dr. Breit, Walther-Straub-Institute, LMU Munich [196, 202]

4.12 Software

Software	Version	Supplier
Chemi-Capt 5000	15.02	Vilber, Eberhardzell (Germany)

Software	Version	Supplier
FitMaster	2x53	HEKA, Lambrecht (Germany)
GraphPad PRISM	7	GraphPad Software, Inc., San Diego (USA)
Igor Pro	6.2.2.2	Wavemetrics, Portland (USA)
ImageJ	1.51h	Wayne Rasband (NIH)
Infinity-Capt	14.2	Vilber, Eberhardzell (Germany)
LightCycler® Software	Version 1.5.0.39	Roche, Rotkreuz (Austria)
MARS data analysis software	2.10	BMG Labtech, Ortenberg (Germany)
Microsoft® Excel®	14.7.7	Microsoft Cooperation, Washington (USA)
PatchMaster	2x69	HEKA, Lambrecht (Germany)
Primer Blast		NCBI, Bethesda (USA)
TillVision	V4.5.60	TillPhotonics, Graefeling (Germany)
ZEN 2 Pro	2.0.0.0	Zeiss, Jena (Germany)

5 Methods

5.1 Cell lines and primary cells

5.1.1 HAP1 cells

As described in the introduction (see 3.3), the HAP1 cell line originates from the CML cell line KBM-7 which was genetically modified via the CRISPR/Cas9 technology to become fully haploid [186, 187, 192, 193]. Due to their haploidy, HAP1 cells present a convenient tool to study protein-specific functions as they lack the second set of chromosomes which usually masks particular effects caused by genetic deletion, inactivation or mutation of the respective target (for more details, see 3.3).

5.1.1.1 HAP1 TRPM7 models

To study TRPM7 function, two different HAP1 TRPM7 cell models were applied: The HAP1 TRPM7 knockout (TRPM7 KO) model lacking the full.-length protein and thus presenting a suitable tool to study the function of the entire dual-function protein TRPM7 and the kinase-dead HAP1 TRPM7 K1648R clone (TRPM7 KI) carrying an inactivated kinase domain and therefore allowing precise distinction of specific TRPM7 kinase-related functions. Both clones were manufactured by HorizonGenomis, Vienna, Austria using the CRISPR/Cas9 technology [190, 191]. The knockout of TRPM7 was generated by depletion of 17 nucleotides within exon 4 of the TRPM7 gene which leads to a frame shift that causes ablation of TRPM7 function (also see 6.1.1) [194, 195]. The kinase inactivating point mutation on the other hand was inserted by replacing three nucleotides within the TRPM7 gene (AAA to CGG) changing the genetic code for the AA position 1648 from lysine (K) to arginine (R) (K1648R) (also see 6.2.1). For the experiments, each of these two cell lines was compared to their corresponding parental clone, which is - for facilitation of data interpretation - not to be further distinguished and simply named HAP1 TRPM7 WT.

5.1.2 HEK-293 cells

The human embryonic kidney cell line 293 (HEK-293), first introduced 1977, is still one of the most common cell lines used nowadays. Back then, the post-doctoral researcher Frank Graham successfully transformed human embryonic kidney cells with the human adenovirus type 5 - supposedly in his 293rd experiment explaining the name HEK-293 [203]. Despite the initial origin and the comprehensive view, a more recent large-scale genetic analysis and comparison to five other cell types revealed that the 'kidney' cells rather show analogies to adrenal than to kidney cells [204]. Nevertheless, they resemble a nice tool for a broad spectrum of functional studies, as they proliferate fast and are easy to transfect.

5.1.2.1 HEK-293 NFAT reporter (HEK-NFAT) cell line

For investigations regarding TRPM7's impact on NFAT transcriptional activity, the HEK-293 cells were used to create clones stably expressing an NFAT-luciferase reporter (named HEK-NFAT). For the exact generation protocol, see chapter 5.10.1

5.1.2.2 Aequorin HEK-293 (HEK-G5α) cell line

To examine Ca^{2+} concentrations in HEK-293 cells, HEK cells having the vector G5α inserted were used [196, 202]. By stably expressing the biological Ca^{2+} sensor apoaequorin N-teminally fused to the green fluorescent protein (GFP), these cells represent a suitable system to measure internal Ca^{2+} levels with a high accuracy and independently of fluorescent markers or additional excitation. For more detail, also see 6.1.6.

5.1.3 Primary human neutrophils

Neutrophils are a type of immune cells that originates from multipotential hematopoietic stem cells. These hematopoietic stem cells develop into myeloid progenitor cells that represent the direct precursors of neutrophils [205]. Thus, human neutrophils and HAP1 cells share the same myeloid background, which increases the chance of the acquired results being transferable from one cell type to another. Accordingly, freshly isolated primary neutrophils of human origin were applied to test if pharmacological inhibition of TRPM7 respectively its kinase activity affects *COX-2* gene expression.

5.2 Cell culture

5.2.1 HAP1 cells

5.2.1.1 Maintenance and splitting

HAP TRPM7 WT and KI cells were cultivated in IMDM supplemented with 10 % FBS ('HAP WT medium'), while the medium for the TRPM7 KO cells additionally contained 10 mM $MgCl_2$ for proliferation (otherwise the cells tend to go into growth arrest due to magnesium deficiency) [195]. All reagents used for splitting were prewarmed to 25°C. At a confluence of ~70-80 %, cells were washed once with 5 ml DPBS, incubated with 0.5 ml trypsin-EDTA solution for 3-5 min at 37°C and subsequently the reaction was stopped with 5.5 ml medium. Dependent on the next time of usage, an appropriate fraction (between a 1:10-1:30 ratio) of the cell suspension was then transferred into a new flask already filled with medium for further cultivation and incubated in the cell incubator at 37°C, 5 % CO_2.

5.2.1.2 Seeding

For experiments, cells were washed, treated with trypsin-EDTA solution and then the reaction was stopped equivalent to splitting (see 5.2.1.1). Then, 10 µl of the cell suspension was diluted with 10 µl trypan blue (1:1 ratio) and subsequently, cell number was manually counted using a Neubauer chamber [206]. The cell number per ml was calculated with the following equation:

$$concentration\ of\ cell\ suspension\ \left[\frac{cells}{ml}\right] = \frac{number\ of\ cells * dilution\ factor}{volume\ of\ chamber\ square\ [ml]} = \frac{(number\ of\ cells * 2 * 25 * 10^4)}{ml}$$

Dependent on the experiments, the required cell number was then transferred into therefore suitable well plates or dishes already prepared with the corresponding medium. Note that for all experiments except the characterization of the HAP1 cell clones, the medium of the HAP KO cells was changed to IMDM + 10 % FBS without additional magnesium in the afternoon of the day prior to the experiment. All cells were incubated overnight at 37°C, 5 % CO_2.

5.2.1.3 Starvation

To starve the cells (e.g. for Western Blot analysis), cells were incubated with IMDM without FBS 3 h prior to the experiment. This step was introduced as FBS contains a plethora of growth factors and other proteins which can affect signaling molecules and thus distort the respective experimental results [207].

5.2.1.4 Stimulation of the HAP1 cell with forskolin

For stimulation with the adenylyl cyclcase activator forskolin, medium of the cells was changed to fresh IMDM + 10 % FBS and cells were subsequently treated with 50 µM forskolin for 1 h at 37°C, 5 % CO_2. Reactions were stopped by placing the cells on ice and washing the cells with cold DPBS.

5.2.2 HEK-293 cell lines

5.2.2.1 Maintenance and splitting

All HEK-293 cell lineages were cultured in high glucose DMEM supplemented with 10 % FBS and 1 % Penicillin-Streptomycin solution. All reagents used for splitting were prewarmed to 25°C. At a confluence of ~80-90 %, cells were carefully washed once with 5 ml DPBS and detached by incubation at 37°C for 3-5 min with another 0.5 ml of DPBS. The reaction was stopped with 5.5 ml medium, and, dependent on the next time of usage, an appropriate fraction (between a 1:10-1:30 ratio) of the cell suspension was then transferred into a new flask already filled with medium for further cultivation and incubated in the cell incubator at 37°C, 5 % CO_2.

5.2.2.2 Seeding

For experiments, cells were washed, detached and the reaction was stopped equivalent to splitting (see 5.2.2.1). Then, 10 µl of the cell suspension was diluted with 10 µl trypan blue and manually counted using a Neubauer chamber. The cell number per ml was calculated with the following equation:

$$concentration\ of\ cell\ suspension\ \left[\frac{cells}{ml}\right] = \frac{number\ of\ cells * dilution\ factor}{volume\ of\ chamber\ square\ [ml]} = \frac{(number\ of\ cells * 2 * 25 * 10^4)}{ml}$$

Dependent on the experiments, the required cell number was then transferred into therefore suitable well plates or dishes already prepared with fresh medium.

5.2.2.3 Starvation

To starve the cells for dual-luciferase reporter gene assay, cells were incubated with DMEM without supplements 4 h prior to the experiment. Also here this step was introduced as FBS contains a plethora of growth factors and other proteins which can affect the investigated NFAT-dependent gene expression and thus distort the experimental results [207].

5.2.3 Primary human neutrophils

5.2.3.1 Isolation and separation

The neutrophils were isolated from fresh human blood samples (50-100 ml). The blood was carefully layered over the room temperature (RT)-warm density gradient media PolymorphPrep™ (1:1 ratio) in 50 ml reaction tube and centrifuged at 600 rcf for 35 min. After carefully removing the two topmost layers (blood plasma and mononuclear cells), the intermediate layer containing the polymorphonuclear leucocytes (PMNs) was harvested and transferred into a new 50 ml reaction tube. PMNs, also called granulocytes, include three immune cell types: Neutrophils, basophils and eosinophils. However, the amount of basophils and eosinophils is comparably low in contrast to neutrophils [208, 209], wherefore the abbreviation 'PMN' often exclusively stands for polymorphonuclear neutrophils [210]. Hence, as it is commonly accepted [210], the obtained fraction can be referred to as human neutrophils. Further following up the protocol, the neutrophils were washed once with 40 ml DPBS, centrifuged at 300 rcf for 10 min and, after removing the supernatant, resuspended in 10 ml HBSS buffer and counted with the Guava® easyCyte Flow Cytometer (Merck Millipore, USA) following the manufacturer's instructions. According to the acquired cell number, the cell suspension was adjusted with HBSS buffer to ≤ 2 x10^6 cells/ml.

5.2.3.2 Treatment of the neutrophils with TRPM7- and PI3K-inhibitors followed by LPS stimulation for RT-qPCR

To investigate the effect of TRPM7 inhibition respectively the inhibition of its kinase activity on *COX-2* gene expression in the neutrophils, the immune cells were first incubated with either NS8593 (30 μM), TG100-115 (20 μM) or – due to the side effects of TG100-115 on different PI3K isoforms [211, 212] – a combination of the PI3K inhibitors IPI-549 (160 nm) and GSK2292767 (100 nM) for 30 min at 37°C. In addition, two additional samples serving as controls were left untreated (ø) respectively exposed to 0.1 % DMSO (concentration matching the highest DMSO concentration used to dilute the applied drugs). Subsequent to incubation with the inhibitors, *COX-2* gene expression was induced by addition of 10 ng/ml LPS to each sample [213]. According to Cadieux et al., LPS significantly increases COX-2 mRNA production as early as one hour after drug administration [214]. After two hours of incubation at 37° and 5 % CO_2, the cells were pelleted by centrifugation at 300 rcf for 5 min, the supernatant was removed and cells were further processed for RT-qPCR experiments.

5.3 Genotyping of the HAP1 cell clones

To validate the genetic mutations of the HAP1 TRPM7 KO and KI cell clones, the respective modified DNA-sequence was analyzed and compared to the individual parental clones (HAP1 TRPM7 WT). For HAP1 TRPM7 WT and KO, DNA was extracted and amplified using the MyTaq™ HS Red Mix (Bioline, UK) according to the manufacturer's instructions. Alternatively, HAP1 TRPM7 WT and KI RNA was extracted, translated into cDNA (for detailed description, see 5.7.1 respectively 5.7.2) and then amplified with the MyTaq™ HS Red Mix (Bioline, UK) according to the manufacturer's instructions. The approaches for the two clones differed as the primer pairs for sequencing were once designed for the genomic sequence (TRPM7 KO cells) and once designed for the spliced mRNA (TRPM7 KI cells). The amplified products were separated by gel electrophoresis using 1 % agarose gels (150 ml TAE-buffer, 1.5 g agarose, 20 μl Roti® GelStain), visualized via the gel documentation software Infinity-Capt (Vilber, Germany) and extracted using the GeneJet Gel Extraction Kit (Thermo Fisher Scientific, USA) according to the manufacturer's instructions. The purified samples were sequenced by Eurofins Genomics, Munich, Germany.

5.4 Electrophysiology

To assess TRPM7 currents in the HAP1 cell clones, the whole-cell patch clamp technique was applied [34, 83]. Therefore, cells were trypsinized and seeded onto PDL-coated glass coverslips (12 mm) 30-60 min prior to the measurements. The artificially produced PDL is able to fixate the cells to

the coverslip, as the positively charged homopolymer and the negatively charged cell membrane(s) form an ionic bond [215]. After incubating the samples at 37°C and 5 % CO_2, the coverslips were transferred into culture dishes (35 mm) and covered with external solution. All measurements were recorded with the EPC10 patch-clamp amplifier controlled by the PatchMaster software (HEKA, Germany). Cells were patched with borosilicate glass pipettes, which were pulled to an opening size of 2-3 MΩ resistance with a pipette puller (Zeitz, Germany) and filled with the corresponding internal solution. Because of the different ionic components of the solutions applied, the voltage was corrected by a liquid potential of +10 mV prior to the measurements [216]. TRPM7 currents were elicited by a voltage ramp ranging from -100 to +100 mV run within 50 milliseconds (ms), measured with a frequency of 0.5 Hz and a holding potential of 0 mV. Both the capacitance currents and the series resistance were determined and corrected before each ramp via the automated capacitance compensation of the software. For illustrations, data were further processed and analyzed via the FitMaster (HEKA Lambrecht, Germany) and Igor Pro software (Wavemetrics, USA). TRPM7 inward and outward current amplitudes at -80 mV respectively +80 mV were extracted, normalized to the individually measured capacitances (current density, pA/pF) and plotted *vs.* the time (s). Furthermore, representing traces were extracted at 150 s and plotted as current-voltage relationships (I/V-curve).

5.5 ICP-MS

To determine the internal Mg^{2+}, Ca^{2+}, Zn^{2+} and Cu^{2+} concentrations in the HAP1 TRPM7 cell clones, element concentrations were analyzed via ICP-MS. Therefore, cells were cultivated overnight to a confluence of ~80 %. The next day, cells were washed once with DPBS, scraped off from the dish with 11 ml fresh DPBS and cell suspension was transferred into 50 ml reaction tubes. After centrifuging at 1.500 rpm for 5 min, the supernatant was discarded and cells were resuspended in 1.5 ml fresh DPBS and transferred into 2 ml reaction tubes. The centrifugation step was repeated, and after removing the supernatant, the cells were incubated at 70°C overnight to dry the cell pellet. On the next day, the dried cell pellets were weighed and subsequently sent of to ALS Scandinavia, Luleå, Sweden on dry ice for analysis.

5.6 Ca^{2+} imaging

Internal Ca^{2+} concentrations in the HAP1 TRPM7 cell clones were additionally analyzed using the Fura-2 AM based Ca^{2+} imaging technique [217]. Therefore, the cells were seeded onto PDL-coated glass coverslips (24 mm) 2 h prior to the experiment. Subsequently, cells were stained with the Fura-2 AM containing staining solution for 30 min in the dark. The incubation was stopped by washing the cells twice with external solution containing 2 mM $CaCl_2$. Afterwards, the coverslips were fixated into

a Ca^{2+} imaging chamber, washed another time with the 2 mM $CaCl_2$ external solution and eventually covered with the same solution for the measurement. Initially, cells were visualized and encircled as regions of interest (ROIs) at an excitation wavelength of 360 nm. To assess the cytosolic Ca^{2+} concentration, cells were alternatingly excited at 340 nm respectively 380 nm (exposure time of 10 ms) and emission was measured at 510 nm for 2 min using the software TillVision (TillPhotonics, Germany) [217]. Potential background signals were acquired by simultaneously measuring the emission of a small, cell-free region, and were subsequently subtracted of the actual values for correction. The basal Ca^{2+} concentration was determined by calculating the mean of 15 consecutive measurements of each cell.

5.7 Molecular biological methods

5.7.1 RNA Isolation

Treated or untreated cells were washed twice with DPBS and lysed by resuspension in 1 ml trizol followed by a 5 min incubation at RT [218, 219]. Then, 200 µl chloroform was added to each sample, the tube was shaken for 15 s and incubated for another 3 min at RT. For separation of the aqueous and the organic phase, samples were centrifuged at 12 000 rpm for 15 min at 4°C and the RNA-containing aqueous phase was subsequently transferred into a new 2 ml reaction tube. By addition of 500 µl Isopropanol to each sample and incubating the solution for 10 min at RT, RNA was precipitated. Another centrifugation at 12 000 rpm for 10 min at 4°C served to pellet the RNA, which was subsequently washed with 1 ml 75 % ethanol and centrifuged again at 7 500 rpm for 5 min at 4°C. After removal of the supernatant, the pellet was air-dried at RT, dissolved in 10-20 µl DEPC-treated H_2O (dependent on pellet size) and heated to 55°C for 10 min. Concentrations and purity were determined by measurement of the absorbance at 260 nm respectively 280 nm and calculating the 260/280 nm ratio using a spectrophotometer [220] and, corresponding to the individual concentrations, samples were aliquoted and stored at -80°C until usage.

5.7.2 cDNA synthesis

For further analysis via normal or quantitative PCR, RNA was converted into cDNA via reverse transcription. Therefore, 2-5 µg of RNA were mixed with 0.5 µg $Oligo(dT)_{12-18}$ and 0.5 mM dNTPs, filled up to 12 µl with DEPC-treated H_2O and incubated for 5 min at 65°C. Samples were chilled on ice for a few seconds, shortly centrifuged and mixed with 1x first strand buffer (provided with the Superscript II Reverse Transcriptase) and 5 mM DTT. After incubation for 2 min at 42°C, the Superscript II Reverse Transcriptase was added and the samples were incubated for another 50 min

at 42°C. Subsequently, the reaction mix was inactivated by heating to 70°C for 15 min. Samples were either stored at -20°C or directly used.

5.7.3 PCR

To test primers designed for RT-qPCR, the corresponding primer pairs for the gene to be tested (forward and reverse primer, end concentration of 0.4 µM each) were mixed together with the 2 x MyTaq™ Mix (Bioline, UK) and diluted with DEPC-treated H_2O (see Table 5.1 for example):

Table 5.1 Mastermix composition for conventional PCR using the RT-qPCR primers

Mastermix

Substance	Concentration	Volume [µl]
Forward primer	10 µM	1
Reverse primer	10 µM	1
MyTaq™ Mix	2x	12.5
DEPC-treated H_2O		9,5
Total Volume		24 µl

Then, 1 µl (0.5-2 µg) of cDNA template was added and the following PCR protocol was applied for amplification (Table 5.2):

Table 5.2 PCR program for validation of the RT-qPCR primers

PCR program

Process		Temperature [°C]	Time	
Hot start		94	10 min	
Amplification	Denaturation	94	30 s	30 cycles
	Annealing	62	30 s	
	Elongation	72	30 s	
Final elongation		72	10 min	
Cooling		8	∞	

5.7.3.1 Analysis of amplified products via agarose gel electrophoresis

The amplified products were either stored at -20°C or directly loaded onto a 3 % agarose gel (150 ml TAE buffer, 4.5 g agarose) containing 20 µl of the gel stain Roti®Safe. The gel was run at 110 V for 30-40 min and bands detected via the gel documentation software Infinity-Capt (Vilber, Germany).

5.7.4 RT-qPCR

To compare cells regarding their mRNA expression of target genes, RT-qPCR was performed [221]. Therefore, a mastermix containing 0.5 µM of both forward and reverse primer of the gene to be analyzed and the 2 x LightCycler® 480 SYBR Green I Master Mix (Roche, Austria) diluted with DEPC-treated H_2O was prepared and transferred into a 96-well plate. For reference, an additional mastermix was prepared with primers for the housekeeping gene Hypoxanthine-guanine phosphoribosyltransferase 1 (*HPRT1*). The cDNA templates were prediluted with DEPC-treated H_2O to a concentration of ~ 250 ng and added to the corresponding wells. RT-qPCR was performed with the LightCycler® 480 (Roche, Austria) according to the following program (Table 5.3):

Table 5.3 RT-qPCR program for analysis of the respective target genes in HAP1 cells and neutrophils

RT-qPCR program

Process		**Temperature [°C]**	**Time**	
Preincubation		50	2 min	
		95	10 min	
Amplification	Denaturation	95	15 s	
	Annealing	62	30 sec	40 cycles
	Elongation	72	30 sec	
Melting curve acquisition		95	10 min	
		60	1 min	
Cooling		40	10 min	

Data was acquired using the LightCycler® 480 Software (Roche, Austria).

5.8 Protein analytics

5.8.1 Preparation of whole-cell lysates

Treated or untreated HAP1 cells were placed on ice and washed once with cold DPBS. Cells were then lysed in RIPA buffer (Sigma Aldrich, Germany) containing phosphatase and protease inhibitors and incubated for at least 5 min on ice. Cell lysis was completed by rotation for 30 min at 4°C, and remaining cell debris was removed by centrifugation for 5 min with 12 500 rpm at 4°C. The supernatant representing the whole-cell lysate was transferred into a new reaction tube and either treated with phosphatase (see next paragraph) or directly used for Western Blot analysis.

5.8.1.1 Phosphatase treatment

To validate phospho-specificity of the self-made TRPM7 pSer1511 antibody (kindly provided by Dr. Chubanov, Walther-Straub-Institute, LMU Munich) used for characterization of the HAP1 TRPM7 KI clone (see 6.2.1), HAP1 whole-cell lysates were treated with the FastAP Thermosensitive alkaline phosphatase (Thermo Fisher Scientific, USA) prior to Western Blot analysis. Thus, the corresponding samples were first diluted with the respective amount of 10 x FastAP buffer, mixed together with 10 U (~10 µl) of FastAP phosphatase and subsequently incubated for 1 h at 37°C. The reaction was stopped by directly placing the mixtures on ice and diluting them with 4 x Laemmli buffer. The samples were either directly applied to the SDS-PAGE or stored at -20 °C until usage.

5.8.2 Nuclear extraction

In order to separate the nucleus from the cytosol, the 'Nuclear Extract Kit' (Active Motif, USA) was utilized. Before beginning the experiment, all reagents were prepared according to manufacturer's instructions. Treated or untreated cells were placed on ice, washed once with DPBS/Phosphatase Inhibitors solution and incubated with Hypotonic Buffer for 15 min on ice. Then, the 'Detergent' (provided with kit) was added and cells were vortexed at high speed for 10 s. Samples were transferred into 1.5 ml reaction tubes and centrifuged at 14 000 rcf for 30 s. The supernatants (cytoplasmic fraction) were transferred into new 1.5 ml reaction tubes and placed on ice. Meanwhile, pellets were resuspended in Complete Lysis Buffer, vortexed at high speed for 10 s and shaken for 30 min at 4°C. After another centrifugation at 14 000 rcf for 10 min at 4°C, the supernatant (nuclear fraction) was transferred into a new reaction tube; finally, all fractions were stored at -80°C until usage.

5.8.3 SDS-polyacrylamide gel electrophoresis (SDS-PAGE)

To analyze cells regarding their proteome (e.g. protein levels, phosphorylation state), SDS-PAGE was applied. Dependent on the size of the protein of interest, separation gels containing either 8 % or 10 % percent of acrylamide/bisacrylamide were used for adequate segregation (see Table 5.4). If not yet done, samples were diluted with 4 x Laemmli buffer and the cells were subsequently heated for 5 min (temperatures indicated in Table 5.4) for complete protein degradation. Samples were then directly applied to the gels which were run at 100-120 V for 2-3 h (dependent on percentage of gel and size of protein of interest) at RT.

Table 5.4 SDS-gel percentages and lysate heating temperatures in respect to the individual proteins to be analyzed in the HAP1 cells

Protein of interest	Amount of acrylamide/bisacrylamid [%]	Heating temperature [°C]
Akt	10	95
ERK1/2	10	95
GSK3	10	95
NFATc1-c4	10	95
TRPM7	8	60

5.8.4 Western Blotting and immunodetection

For further antibody-based detection, proteins were transferred onto a previously in transfer buffer equilibrated nitrocellulose membrane via the Western Blot technique using the tank-blotting system. For sufficient transfer of all protein, blots were run with either 400 mA for 2.5-3 h or 180 mA overnight at 4°C and the success of transfer was visualized using Ponceau S solution which reversibly and unspecifically stains proteins of all sizes. The dye was removed by washing blots with TBST and the remaining free binding sites of the membrane were blocked with 5 % BSA in TBST for 1 h at RT or 3 h at 4°C on a rocking shaker. For protein detection, blots were incubated with the corresponding primary antibody diluted in 5 % BSA TBST (for dilution factors of the applied primary antibodies see 4.9.1) overnight at 4°C. The next day, membranes were washed three times with TBST for 5 min each at RT and incubated with the corresponding HRP-conjugated secondary antibody diluted in TBST (for dilution factors, see 4.9.2) for 1 h at RT. Blots were washed again three times with TBST for 5 min each and, subsequently incubated with ECL-1 and ECL-2 solution (1:1 ratio) for 1 min and immunoreactive bands were detected using the software Chemi-Capt 5000 (Vilber, Germany). Data was subsequently analyzed using ImageJ (Wayne Rasband, NIH).

5.9 COX activity assay

To measure basal COX enzymatic activity in the HAP1 cells, a fluorometric COX activity assay kit (Abcam, UK) was applied. One day prior to the experiment, cells were seeded in cell dishes (10 cm) with a density of 3-5 x 10^6 mio/dish and grown overnight at 37°C and 5 % CO_2. The next day, cells were first washed once with 4 ml cold DPBS. Then, cells were detached in 1.5 ml fresh DPBS with a cell scraper, resuspended and transferred into a 50 ml reaction tube. After rinsing of the dishes once more with 4 ml DPBS and combining these washing fractions with the corresponding cell suspensions, cells were counted using a Neubauer chamber. Cells were then centrifuged at 1500 rpm

for 5 min, the supernatant was discarded and cells were diluted in lysis buffer (0.1 M Tris/HCl, pH 7.8 with 1 mM EDTA and cOmplete™ protease inhibitor cocktail) at a density of 2.5 x 10^7 cells/ml, transferred into a 1.5 ml reaction tube and kept on ice. Cell lysis was completed by sonicating the suspensions for 1 min on ice, and another centrifugation at 10 000 rcf for 15 min served to pellet the cell debris. The supernatant was again transferred into a new 1.5 ml reaction tube and the samples were kept on ice until usage.

Before starting with the actual experiment, all reagents from the kit were prepared as instructed in the assay protocol so that they were ready to use. The assay was performed according to the manufacturer's instructions, and each condition was prepared as duplicate. After final addition of the substrate solution (arachidonic acid/NaOH), fluorescence was measured immediately at a wavelength of 587 nm (excitation at 535 nm) in a kinetic mode every 25 s for 30 min using the Fluostar Omega (BMG Labtech, Germany); data were extracted with the MARS data analysis software (BMG Labtech, Germany).

5.10 General transfection protocol for HEK-293 cells

For transfection (e.g. for generation of the stable HEK-NFAT cell line or the dual-luciferase reporter gene assay, see 5.10.1 respectively 5.11), HEK-293 cells were seeded in 6-well plates one day prior to transfection. When they preferably reached a confluence of ~ 60% on the next day, culturing medium was changed to medium without supplements. While the cells adjusted to the immediate FBS-withdrawal, the transfection mix containing the plasmid of interest and the transfection reagent (Lipofectamin or Turbofect) was prepared. Therefore, both the plasmid DNA (1 µg/well) and transfection reagent (3 µl/1 µg DNA) were independently diluted in medium without supplements (50 µl/well) and incubated for 5 min at RT. Then, the plasmid DNA and the transfection reagent mixes were added together and incubated for another 30 min at RT. The solution was subsequently carefully added to the wells (100 µl/well) drop by drop and the cells incubated for 4 h at 37°C, 5 % CO_2. Afterwards, medium was changed back to medium with supplements for cultivation overnight at 37°C, 5 % CO_2. Cells were used for experiments after 16-24 h after transfection.

5.10.1 Generation of a stable HEK-293 NFAT reporter (HEK-NFAT) cell line

To create the stable HEK-NFAT reporter cell line for validation of the results observed in the transiently transfected HEK-293 cells, HEK-293 cells were transfected with the NFAT reporter gene (Promega, Germany) and a pcDNA4 vector (Thermo Fisher Scientific, USA) introducing Zeocin resistance for subsequent selection of positive clones. To raise the chance respectively the number of

clones later surviving the selection with the antibiotic, four different approaches (named II-V) using different amounts and thus ratios of DNA as well as a positive (I) and a negative control (VI) were taken (see Table 5.5). The positive control was a combination of pcDNA4 giving the Zeocin resistance and the 'empty' vector pcDNA3.1 carrying no information worth mentioning in context of this experiment. Accordingly, the negative control included the NFAT-luciferase reporter and the pcDNA3.1 vector.

Table 5.5 Composition of the different approaches for generation of the HEK-NFAT cell line

Name	Positive control (I)	II	III	IV	V	Negative control (VI)
pcDNA3.1 [ng]	450	/	/	/	50	100
pcDNA4 [ng}	50	50	50	100	50	/
NFAT-luc [ng]	/	450	950	900	400	900
Total DNA amount [ng]	500	500	1000	1000	500	1000
Ratio pcDNA4/NFAT-luc	/	1:10	1:20	1:10	1:5	/
Lipofectamin [µl]	1,5	1,5	3	3	3	1,5

Cells were transfected in 6-wells using Lipofectamin according to the conventional protocol (see 5.10). After the transfection, cells remained in medium without supplements for overnight cultivation. Early on the next day, cells were carefully washed with 2 ml DPBS once and detached with another 2 ml DPBS. A twentieth of each well was transferred into a new T175 flask prepared with 25 ml of medium with supplements. Approximately 6-8 h later, 500 µg/ml Zeocin were added to start the selection. New medium with fresh Zeocin was added every two to three days for 3-4 weeks. While all cells derived from the negative control as well as from the approach III and V died, both the positive control and the approaches II and IV yielded to clones surviving Zeocin treatment. Testing NFAT-reporter activity by addition of the reconstituted luciferase substrate and measuring luminescence at 560 nm (also see 5.11 for more details), cells from both cultures II and IV proved to be stably expressing the NFAT reporter gene and were therefore used for further experiments.

5.11 Dual luciferase reporter assay in HEK-293 cells

For both transfection methods, cells were initially seeded in PDL-coated 12-well plates 2 days prior to the actual experiment with a concentration of 2 x 10^5/well.

a) Dual luciferase reporter assay in transiently transfected HEK-293 cells:

To investigate NFAT activity in transiently transfected cells, a dual-luciferase reporter gene assay was performed. Therefore, the HEK-293 cells were triple transfected; next to the NFAT reporter gene and

the TRPM7-coding plasmid, a third construct - the *Renilla* luciferase - needed be inserted (for more background information, also see 6.1.5). Thus, HEK-293 cells were co-transfected with 500 ng NFAT reporter plasmid, 50 ng *Renilla* luciferase control vector and 400 ng either GFP-tagged TRPM7 WT or TRPM7 KI construct or pcDNA3.1 (according to 5.10 using Lipofectamin). After the overnight incubation in normal growth medium, supplemental FBS was removed for 4 h to starve the cells. After the incubation, medium was withdrawn and cells were lysed with 200 µl reporter assay lysis buffer for 5-10 min at RT. Meanwhile, the luciferase substrate solution and the Stop & Glo® substrate solution were prepared according to the manufacturer's instructions (Promega, Germany). Then, 180 µl of cell lysate were transferred into a solid white 96-well plate which was placed in the Fluostar Omega (BMG Labtech, Germany) for data acquisition. After initially measuring the GFP-signal at 509 nm (excitation at 488 nm; intensity is proportional to expression of TRPM7 constructs), a time-resolved measurement of the firefly luciferase activity at 560 nm was performed: first, the 'background' luminescence was acquired for 2 s, and then 20 µl of the reconstituted luciferase substrate were injected and luminescence was measured with a frequency of 1 Hz for another 8 s. The firefly luciferase signal was later determined by calculating the mean of the acquired 8 values for each sample corrected for the background. The experiment was finalized by addition of 10 µl of the diluted Stop & Glo® substrate to measure *Renilla* luciferase activity at 480 nm. Data were extracted using MARS data analysis software (BMG Labtech, Germany).

b) Dual luciferase reporter assay in the stable HEK-NFAT reporter cell line:

Given the stable expression of the NFAT-reporter in the HEK-NFAT cell line, no additional vector for normalization (*Renilla* luciferase) was required. HEK-NFAT cells were co-transfected with either GFP-tagged TRPM7 WT or TRPM7 KI construct and pcDNA3.1. To analyze if TRPM7-driven effects are expression level dependent, different quantities of TRPM7 WT or KI cDNA expression constructs ranging from 100-1000 ng were transfected. As all samples were to be transfected with the same amount of DNA, pcDNA3.1 was used to reach 1000 ng total in each well. The assay was performed as described in 5.11 a).

5.12 Aequorin-based Ca^{2+} measurements in HEK-293 cells

The analysis of TRPM7's impact on the basal Ca^{2+} levels in HEK-293 cells was done in the Ca^{2+}-sensing HEK-G5α cell line (see 5.1.2.2). Accordingly, cells were seeded in 6-well plates with a density of 1.5 x 10^5/well and co-transfected with 500 ng either TRPM7 WT or TRPM7 KI construct and 500 ng pcDNA3.1 (according to chapter 5.10 using Turbofect). After the overnight incubation in normal, supplemented growth medium, supplements were withdrawn for 4 h to starve the cells. The medium was then replaced by 400 µl/well preheated (37°C) coelenterazine solution (coelenterazine diluted

1:1000 in pure DMEM without phenol red). Cells were incubated for 20 min at RT in the dark, washed down and 90 µl of each well was transferred into a solid white 96-well plate (each sample was measured as triplicate). Signal intensity of each sample was acquired at 509 nm using the Fluostar Omega (BMG Labtech, Germany) and data were extracted using MARS data analysis software (BMG Labtech, Germany).

5.13 Statistical analysis

Data evaluation and statistical analysis was performed using the softwares Igor Pro, Microsoft Excel and GraphPad Prism. Data are displayed as mean ± standard error of the mean (SEM). Statistical significance was determined using either the paired or unpaired student's t-test or the two-way ANOVA and was accepted at a p value of <0.05.

6 Results

6.1 TRPM7 in cell signaling

6.1.1 Characterization of the HAP1 TRPM7 KO clone

Before studying TRPM7's impact on cell signaling events, the knockout of TRPM7 in the HAP1 cell model needed to be confirmed. Therefore, genomic DNA of both HAP1 TRPM7 wild-type (WT) and KO cells was extracted and – in cooperation with Eurofins Genomics (Munich, Germany) – sequenced with primers amplifying the altered region of the human *TRPM7* gene.

The TRPM7 KO is generated by depletion of 17 nucleotides within exon 4 of the TRPM7-coding sequence, which is located on chromosome 15 of the human genome (Figure 6.1A) [222]. Alignment of the sequencing results acquired for the TRPM7 WT and KO clone reveals that the TRPM7 KO indeed lacks 17 nucleotides when compared to WT (Figure 6.1B). Comparison of Figure A and B shows that this missing sequence exactly matches the base pair region 50,648,788 – 50,648,804 in the forward strand of chromosome 15 (compare Figure 6.1A and 6.1B). As published by our coworkers Chubanov et al., this deletion within the TRPM7-coding sequence causes a frame-shift within the *TRPM7* gene [195].

However, since only a small part of the *TRPM7* gene is depleted, it remains unclear if this mutation results in total protein ablation – for example if gene transcription or mRNA translation are hampered and/or the products are degraded immediately – or if parts of the protein are still being expressed in a correct or scrambled form. Western Blot analysis with a C-terminal α-TRPM7 antibody suggested that the HAP1 TRPM7 KO cells do not express TRPM7 [195]. However, any specific antibody detecting TRPM7 usually binds only a small region of the protein, wherefore expression of functional parts of TRPM7 can't be fully excluded by immunoelectrophoresis.

Hence, I further validated TRPM7 protein extinction by testing functionality of the TRPM7 channel; therefore, channel activity of the HAP1 TRPM7 WT and KO clone was acquired via electrophysiological measurements. To maximize currents, both the internal pipette solution and the external bath solution contained 0 mM Mg^{2+}, since TRPM7 is inhibited by internal Mg^{2+} and Mg-ATP (also see introduction, 3.2.1.2). In order to be able to adequately compare single measurements, currents of individual cells were normalized to the respective cell sizes (defined by the capacity, also see methods, 5.4) and expressed as current density (pA/pF, left panel) [223, 224]. Furthermore, representative traces were extracted at 150 s and plotted as current-voltage relationship. This I/V-curve enables the comparison of basic channel parameters such as its equilibrium potential and the voltage range of activation.

In the performed patch clamp experiments using whole-cell configuration, the TRPM7 WT clone displays the typical TRPM7 current development over time – which is a large outwardly rectifying current created by monovalents with only small inward-directed divalent cation flux – and current-voltage (I/V) relationship, while the KO clone shows no increase in TRPM7-like currents (Figure 6.1C). Thus, the genetic modification in the HAP1 TRPM7 KO cell clone disrupts the expression of a functional protein, which allows to study TRPM7's signaling role in this cell model.

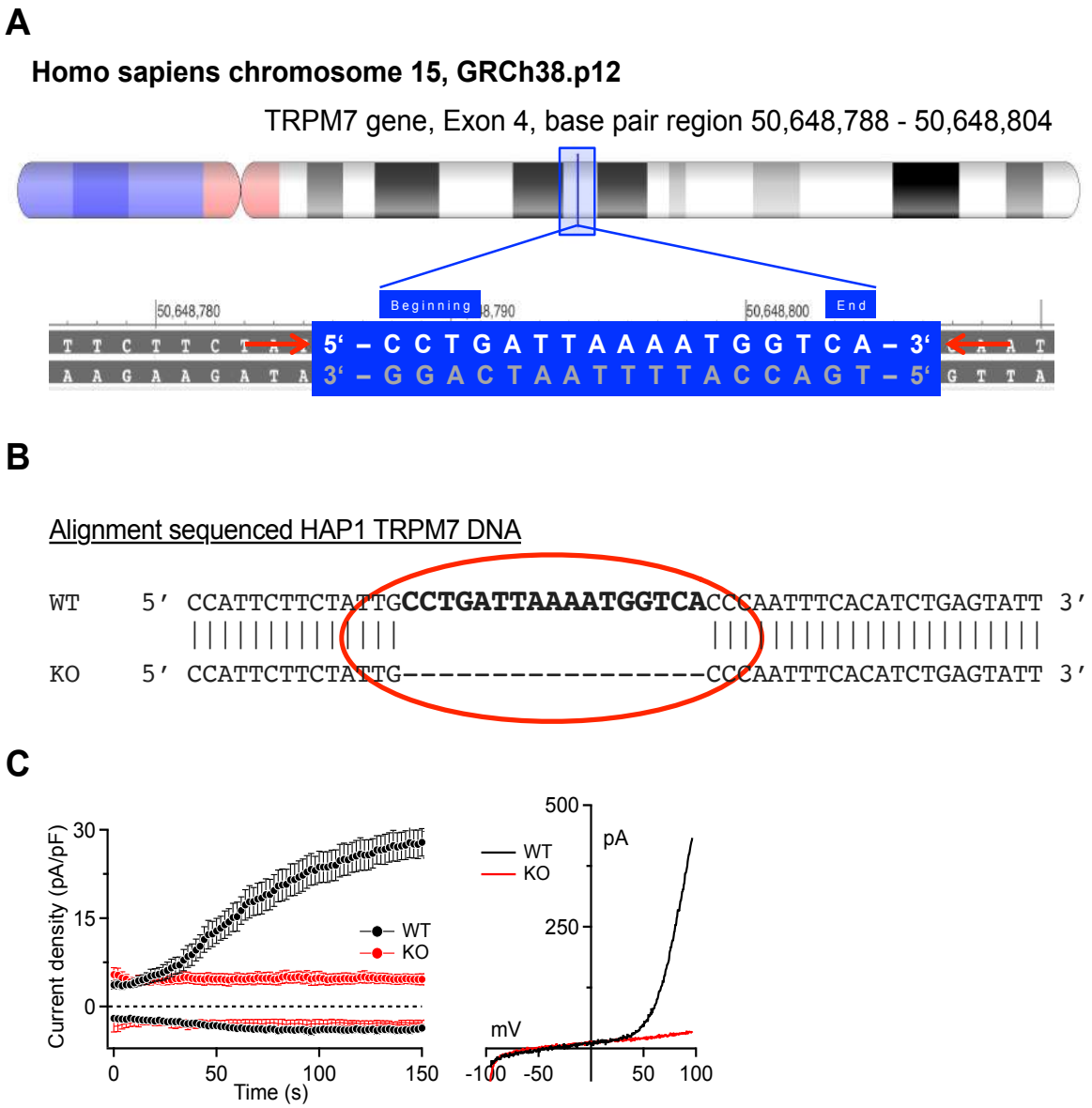

Figure 6.1 Verification of the HAP1 TRPM7 KO clone. (A) The TRPM7 knockout (KO) clone is generated by deletion of 17 nucleotides within exon 4 of the human *TRPM7* gene on chromosome 15; the exact region of the mutation is highlighted (see enlargement in blue) and spans the base pairs (bps) 50,648,788 – 50,648,804 of chromosome 15. **(B)** Alignment of sequenced DNA from wild-type (WT, upper row) and TRPM7 KO (lower row) HAP1 cells shows that the deletion of the 17 nucleotides (see above) in the KO was successful. **(C)** Functional analysis of TRPM7 currents in HAP1 TRPM7 WT (black) and KO (red) cells by patch clamp experiments (n=4-5). Measurements were conducted in the whole-cell configuration in the absence of extra- and intracellular Mg^{2+} to avoid TRPM7 inhibition and thus maximize TRPM7 currents. Current densities at +80 and -80 mV are plotted *vs*. time in seconds (left panel) and representative current-voltage (I/V) relationships of traces extracted at 150 s are presented (right panel). Other than in WT, functional TRPM7 current is absent in the TRPM7 KO cells.

6.1.2 Impact of TRPM7 on ion homeostasis

As outlined in the introduction (see 3.1.2), the ubiquitously expressed TRPM7 channel-kinase plays an important role in systemic and cellular Mg^{2+} and Ca^{2+} homeostasis. Accordingly, depletion of the TRPM7 protein in the HAP1 cells could affect the intracellular concentrations of Mg^{2+} and Ca^{2+}, as well as – due to the conductivity of the channel to other divalent cations – affecting other cellular ion concentrations [51].

To investigate potential alterations, I performed ICP-MS for both clones in cooperation with ALS Scandinavia (Luleå, Sweden). This method allows a highly accurate analysis of the abundance and concentration of different inorganic compounds in liquid or solid material (i.e. metals and traces metals). Like every mass spectrometric technology, the process is subdivided into three working steps: Ionization, ion separation (by mass selection) and detection. In ICP-MS, ICP describes the ionization source. Generation of a high-frequency current creates a microwave field that induces the ionization of the inert gas argon. The resulting argon plasma reaches temperatures up to 10 000°C which are used to resolve chemical bonds within a sample and ionize the single atoms ('ionization'). In the subsequently following sector field (SF) mass analyzer, the ions are accelerated in a static electric and/or magnetic field and separated by trajectory deflection, according to their mass-to-charge (M/Z) ratio [225]. Ion separation is thereby based on the principle that the lighter and more charged an ion is, the more its trajectory will be bent. Finally, the incoming signal is amplified by an electron multiplier integrated in the detector, which – in combination with the SF mass analyzer – guarantees a high resolution ('detection').

Ion content of resting HAP1 cells was determined in parts per million (ppm), and each ion concentration was individually normalized to sulfur (S) (correspondingly to [195]). As this element is present in the AAs cysteine and methionine, its concentration serves as indication for the protein amount which is correlated to the mass of the respective sample [226]. In addition, sulfur-normalized data of the KO were also calculated as percent of WT (set to 100 %), thereby allowing a direct comparison of both genotypes.

Comparing first Mg^{2+} concentration in HAP1 cells of both genotypes, it is obvious that absolute Mg^{2+} levels are significantly lower in TRPM7-deficient HAP1 cells (Figure 6.2A, left panel). The same is true directly comparing Mg^{2+} concentrations of TRPM7 WT to KO cells which reveals a reduction of ~30 % (Figure 6.2A, right panel). In contrast, internal Ca^{2+} concentrations under resting conditions are not significantly affected by TRPM7 deletion (Figure 6.2B).

TRPM7 also conducts essential trace metal ions, such as Zn^{2+}, Mn^{2+} or cobalt (Co^{2+}), with the highest preference for Zn^{2+} [51]. Examining trace metal ion concentrations, it becomes obvious that knockout of TRPM7 causes a slight but highly significant ($p < 0.005$) reduction in absolute cellular

Zn^{2+} concentrations (Figure 6.2C, left panel). Calculating the relative Zn^{2+} amount, it becomes evident that HAP1 TRPM7 KO cells display a decrease of about ~13 % in Zn^{2+} levels when compared to WT (Figure 6.2C, right panel). Furthermore, it was found that TRPM7 depletion also significantly reduces the cellular copper (Cu^{2+}) concentration, as TRPM7 KO cells only contain about two thirds as much as WT (reduction of ~34 %, Figure 6.2D, right panel). Due to their low abundance, most of the other permeates of the TRPM7 channel – such as Ni^{2+}, Co^{2+}, Mn^{2+} – were not detectable via ICP-MS, as intracellular concentrations of these trace-metals is usually very low. Therefore, these data were not included.

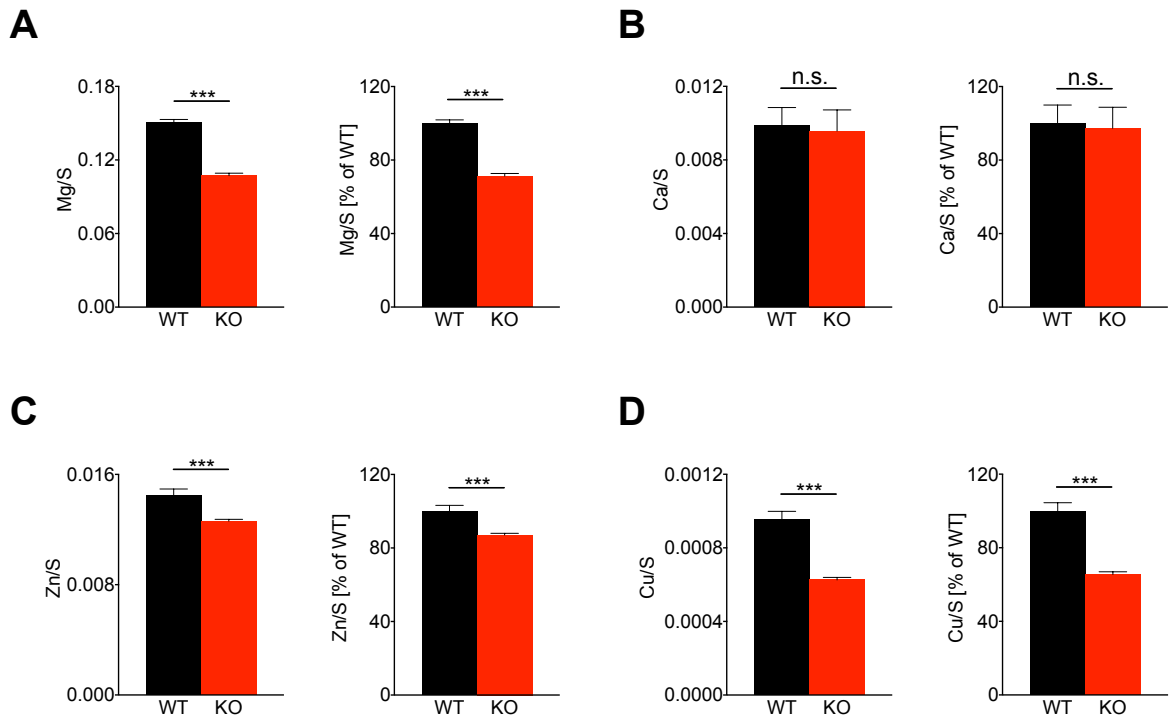

Figure 6.2 Ion levels in HAP1 TRPM7 WT and KO cells. Concentrations of **(A)** Mg^{2+}, **(B)** Ca^{2+}, **(C)** Zn^{2+} and **(D)** Cu^{2+} measured via ICP-MS in resting HAP1 TRPM7 WT (black) and KO (red) cells (n=4). Concentrations are displayed as raw data (counts of respective ion in ppm normalized to counts of sulphur (S) in ppm, left panels) as well as normalized to WT for direct comparison (set to 100 %, right panels). Both evaluations reveal that Mg^{2+}, Zn^{2+} and Cu^{2+} are all highly significantly reduced in HAP1 TRPM7 KO cells compared to WT cells, while internal Ca^{2+}-concentration is not affected by TRPM7 depletion. Data are presented as mean ± s.e.m. Statistics: unpaired student's t-test *** $p<0.005$; n.s.: not significant

I conclude that TRPM7 controls cellular Mg^{2+} levels in HAP1 cells, but is also relevant for Zn^{2+} and Cu^{2+} homeostasis, which both play an important role as enzymatic cofactors [227-229]. In addition, the results indicate that TRPM7 is dispensable for maintenance of basal cellular Ca^{2+} concentrations. However, the existing large gradient (~20 000 fold) between physiological external and internal cytosolic Ca^{2+} concentration ($[Ca^{2+}]_{ext}$= 1-2 mM, $[Ca^{2+}]_{i/cyt}$=~100 nM) predisposes ICP-MS measurements of cytosolic Ca^{2+} relatively sensitive to contamination by residual external Ca^{2+} [230]. Therefore, albeit HAP1 TRPM7 WT and KO cells were intensively washed with Ca^{2+}- (and Mg^{2+}-) free DPBS before

ICP-MS analysis, especially the values for Ca^{2+} could be distorted by Ca^{2+}-ions remaining from the culture medium sticking to the outer cell membrane. To exclude such a falsification of the results acquired with ICP-MS, I next employed the ratiometric Fura-2 AM based Ca^{2+} imaging technique [217] as additional method to determine internal Ca^{2+} concentrations in the HAP1 TRPM7 clones. Other than ICP-MS, Ca^{2+} imaging visualizes levels and alterations of intracellular Ca^{2+} in individual living cells instead of measuring the total ion content present in dried cell pellets.

In order to detect internal Ca^{2+}, the cells are stained with the Ca^{2+}-sensitive dye Fura-2 AM, which allows time-resolved quantification of Ca^{2+} concentrations using fluorescence microscopy. Fura-2 AM is composed of two components: One is the Ca^{2+}-chelator and thus -indicator (Fura-2) and the other is the AM ester group, which ensures membrane crossing and thus facilitates the cellular uptake of the dye; moreover, subsequent cleavage of the AM group by cellular esterases then traps Fura-2 inside the cell [217]. Importantly, binding of free Ca^{2+} to Fura-2 changes its excitation wavelength from originally 380 nm (Ca^{2+}-free/-unbound form) to 340 nm (Ca^{2+}-bound form) while its emission wavelength of 510 nm remains the same [217]. Thus, Ca^{2+} concentration can be directly calculated with the ratio of signal intensities acquired at 380 nm and 340 nm excitation, respectively. One advantage of this method is the use of the ratio of 340/380 nm, which cancels out confounding valuables such as differing indicator concentrations or cellular distribution.

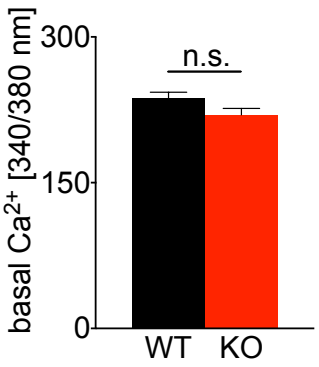

Figure 6.3 Single cell analysis of internal Ca^{2+} concentration in HAP1 TRPM7 WT and KO cells. Ca^{2+} levels in resting HAP1 TRPM7 WT and KO cells were acquired via ratiometric Fura-2 AM based Ca^{2+} imaging (n=10-19). Ca^{2+} concentrations are displayed as ratio of fluorescence at 340 and 380 nm excitation. Although the basal intracellular Ca^{2+} is slightly reduced in the HAP1 TRPM7 KO clone compared to WT, this decrease is not significantly. Data are presented as mean ± s.e.m. Statistics: unpaired student's t-test n.s.: not significant

As illustrated in Figure 6.3, the HAP1 TRPM7 KO cells again show no significant difference in basal intracellular Ca^{2+} concentrations compared to WT cells. Hence, the Ca^{2+} imaging experiments confirm the ICP-MS results obtained for Ca^{2+}, which neither revealed alterations upon TRPM7 depletion. Consequently, TRPM7 is indeed redundant for Ca^{2+} household in resting HAP1 cells.

6.1.3 TRPM7-directed phosphorylation of cell signaling molecules

Within the last decade, several studies suggested that TRPM7 controls basic cellular functions and thereby also contributes to tumor development and progression by facilitating the phosphorylation and thus activation of different cell signaling kinases and transcription factors such as Akt, ERK1/2, STAT3 [154-157, 160, 169-172, 174, 177, 178]. However, the published results are partially controversial, and in some cases (for example ERK1/2 phosphorylation) the exact function of TRPM7 remains unclear. Thus, in order to validate respectively further elucidate the impact of TRPM7 on the above-mentioned signaling cascades, I first analyzed the phosphorylation status of different cell signaling molecules in HAP1 TRPM7 WT and KO cells using Western Blot analysis. Regarding the herein examined targets for TRPM7, the experiments included not only proteins implicated in TRPM7-controlled cancerous processes (Akt, ERK1/2 and STAT3), but also involved the Akt downstream kinase GSK3β and the very recently published target of the TRPM7 kinase, SMAD2 [83, 231]. Dependent on the size of the target protein to be detected, either the glyceraldehyde 3-phosphatase dehydrogenase (GAPDH) or LaminB1 served as loading control of the analyzed whole-cell lysates; the enzyme GAPDH (molecular weight, MW: 38 kDa) was used for Akt, STAT3 and SMAD2 (all >50 kDa), wherefore LaminB1 (MW: 65 kDa) was used for GSK3β and ERK1/2 (both <50 kDa).

Figure 6.4 shows representative Western Blot images and the corresponding statistical analysis upon quantification of the phosphorylated forms of the signaling kinases Akt, GSK3β and ERK1/2 in HAP1 TRPM7 WT and KO cell lysates. As the FBS, which is usually supplemented to the cell culture medium, contains a broad spectrum of growth factors and other proteins that could influence signaling pathways to different extents [207], HAP1 cells were cultured with (+) and without (-) FBS for 3 hours. The signal intensity of each phosphorylation band was determined via the ImageJ software and normalized to its corresponding loading control. For adequate comparison, the WT signal intensity ratio of each protein was set to 100 % and the KO put in relation.

To uncover potential FBS-caused changes in the phosphorylation state of the examined proteins, cells cultured in media containing 10 % FBS or cells incubated in FBS-free media were analyzed separately (Figure 6.4). Compared to WT, TRPM7 KO cells show a strong reduction in phosphorylation of both Akt Ser473 and GSK3β Ser9 (Figure 6.4A and B). Although the total signal intensity decreases upon FBS withdrawal in both genotypes, the reduction in phosphorylation is always stronger in the KO cells in comparison to WT (Figure 6.4A and B, left panels). Evaluating the phosphorylation state via ImageJ, it becomes clear that under both culturing conditions – with and without FBS – the KO shows reduced phosphorylation of Akt and GSK3β relative to WT. Moreover, calculating the statistical significance

shows that the phosphorylation of Akt (with FBS) and GSK3β (without FBS) is significantly reduced in the TRPM7 KO clone in comparison to WT (Figure 6.4A and B, right panels).

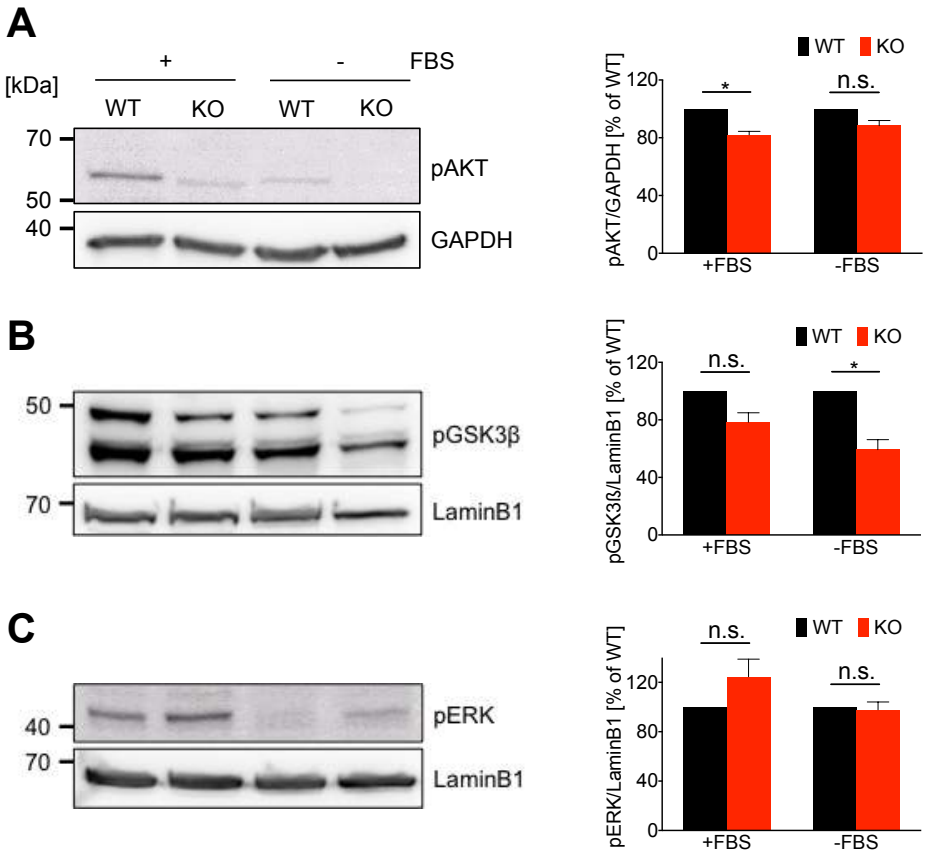

Figure 6.4 Basal phosphorylation levels of cell signaling molecules in HAP1 TRPM7 WT and KO cells. Representative Western Blot images (left panels) and statistical analysis (right panels) of **(A)** AKT pSer473 (pAKT, 60 kDa) **(B)** GSK3β pSer9 (pGSK3β, 47 kDa) and **(C)** ERK1/2 pTyr204 (pERK, 42/44 kDa) in FBS-treated (+) and untreated (-) HAP1 TRPM7 WT and KO cells (n=3-4). Band intensities of each phosphorylation signal was determined via ImageJ and normalized to its respective loading control (GAPDH, 38 kDa; LaminB1, 65 kDa). To cancel out larger variances between the individual experiments, KO values are calculated as percent of WT (set to 100 %). Evaluation of treated and untreated samples illustrates a significant reduction of pAKT (A) in FBS-treated and pGSK3β (B) in untreated HAP TRPM7 KO cells when compared to WT. In contrast, independently of FBS presence, no significant changes are observable for pERK (C). Protein size is expressed in kilo Dalton (kDa). Data are presented as mean ± s.e.m. Statistics: paired student's t-test * $p<0.05$; n.s.: not significant

In contrast to Akt and GSK3β, the Western Blot image suggests that ERK1/2 is more phosphorylated in KO than in WT cells when cultured with 10 % FBS (Figure 6.4C, left panel). Although FBS withdrawal reduces ERK1/2 phosphorylation in both the TRPM7 WT and KO clone, ERK1/2 phosphorylation still seems to be stronger in the KO cells (Figure 6.4C, left panel). These findings are partially confirmed quantifying the amount of phosphorylated ERK1/2 with ImageJ: Treating the cells with FBS indeed increases ERK1/2 phosphorylation upon TRPM7 depletion, although not in a significant extend (Figure 6.4C, right panel, right columns). However, the increase in ERK1/2 phosphorylation is no longer detectable upon serum starvation (Figure 6.4C, right panel, left columns).

Next, I analyzed the phosphorylation state of the two transcription factors STAT3 and SMAD2, as they were previously put in relation to TRPM7 [83, 178, 232]. However, the detected basal phosphorylation levels were really low in both FBS-treated and untreated cells and almost not detectable (Figure 6.5). Thus, the blots were not further evaluated via ImageJ, as signal intensities allowed no accurate analysis.

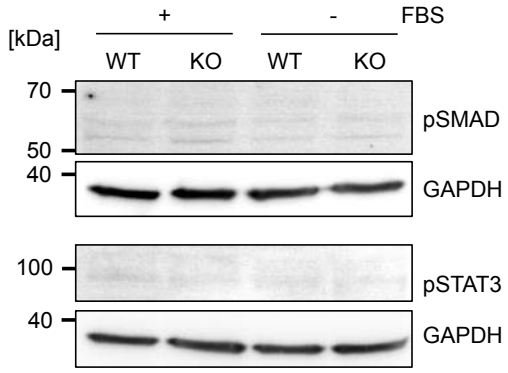

Figure 6.5 Basal phosphorylation levels of the transcription factors SMAD2 and STAT3 in HAP1 TRPM7 WT and KO cells. Representative Western Blot images of SMAD2 pSer465/467 (pSMAD2, 60 kDa, upper panel) and STAT3 pTyr705 (pSTAT3, 86/91 kDa, bottom panel) in FBS-treated (+) and untreated (-) HAP1 TRPM7 WT and KO cells (n=3-4). Due to the very low phosphorylation status of these transcription factors in resting cells, no phospho-specific signals were detectable. Loading control: GAPDH (38 kDa). Protein size is expressed in kDa.

Taken together, I was able to show that TRPM7 significantly affects the phosphorylation of both Akt and GSK3β but not ERK1/2 in resting HAP1 cells. The investigated phosphorylation of Akt at Ser473 is activating the kinase and promotes further phosphorylation of downstream targets such as GSK3β [231]. In contrast to Akt, the investigated GSK3β phosphorylation site Ser9 acts as self-inhibitory mechanism [231, 233]. Being located in both the cytosol and the nucleus, this glycogen synthase kinase controls various cell functions through its impact on numerous transcription factors. Among others, GSK3β phosphorylates the nuclear factor of activated T cells (NFAT) within a nuclear export sequence (NES) and thereby induces its nuclear export [234]. Thus, the increase in GSK3β activity in KO clones could potentially alter NFAT localization within the HAP1 cells, wherefore I investigated nuclear NFAT levels next.

6.1.4 Effect of TRPM7 on subcellular NFAT localization

As explained above, increase in the GSK3β Ser9 phosphorylation reduces its activity and thereby leads to accumulation of NFAT in the nucleus [234, 235]. Hence, the observed reduction of GSK3β Ser9 phosphorylation in the TRPM7-depleted HAP1 cells might cause a decrease in nuclear NFAT levels while increasing its cytosolic concentrations; therefore, the TRPM7 KO could show alterations in subcellular NFAT localization.

Before examining cellular distribution via separate analysis of nuclear and cytoplasmic fraction of NFAT in HAP1 TRPM7 WT and KO cells, I first examined which NFAT family members are expressed in the HAP1 cells. Therefore, I performed Western Blot analysis of whole-cell lysates of WT HAP1 cells. The representative Western Blot images in Figure 6.6 illustrate that all Ca^{2+}-regulated NFATs (NFATc1-4) are present except for NFATc2. NFATc1 and NFATc4 show multiple bands with different intensities, which indicate the presence of different isoforms (NFATc1) or protein phosphorylation states (NFATc4), respectively [236-239]. Nevertheless, also other posttranslational modifications, such as poly ADP-ribosylation, sumoylation and ubiquitination could influence protein size and thus migration of NFAT in the SDS-PAGE [240-244]. While band intensities of NFATc1 and c3 proved to be repeatedly stable in consecutive experiments, both the de- and hyperphosphorylated forms of NFATc4 – supposedly indicated by the bands at 140 and 160 kDa according to the supplier (Santa Cruz, Germany) [236, 237] – showed more variations in the individual experiments (data not shown) aggravating interpretation. Thus, I focused on the first-mentioned NFAT family members (c1 and c3) when analyzing NFAT nuclear accumulation in resting HAP1 TRPM7 WT and KO cells.

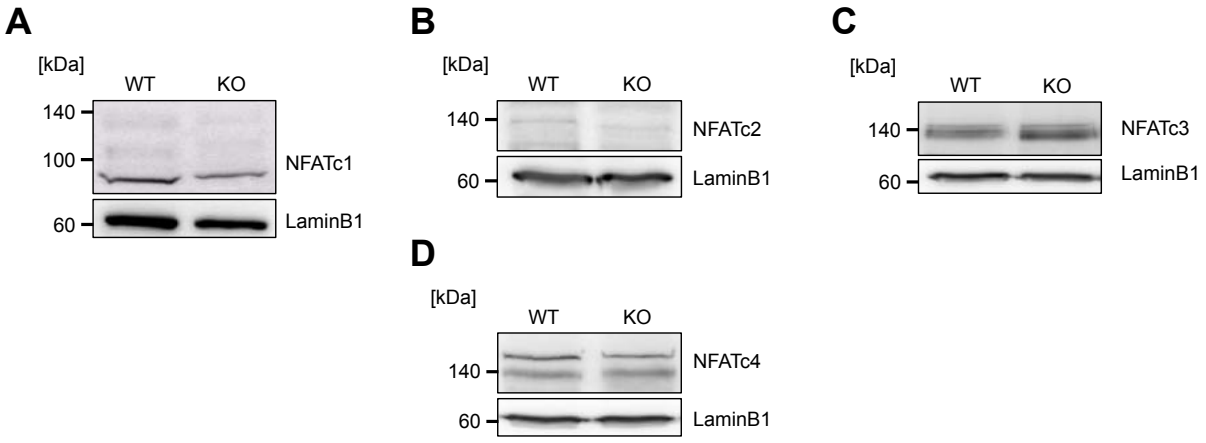

Figure 6.6 NFATc1-c4 expression in HAP1 TRPM7 WT and KO cells. Representative Western Blots of the Ca^{2+}-responsive NFAT family members **(A)** NFATc1 (90/110/140 kDa), **(B)** NFATc2 (135 kDa), **(C)** NFATc3 (130 kDa) and **(D)** NFATc4 (140/160 kDa) expressed in HAP1 TRPM7 WT and KO cells (n=2-4). Numbers in brackets indicate protein sizes of the respective bands expected for the different NFAT family members. Multiple respectively double bands indicate different protein isoforms (NFATc1) or phosphorylation states (NFATc4) as well as other possible posttranslational modifications. Note that all family members are expressed in both HAP1 cell clones except NFATc2. Loading control: LaminB1 (65 kDa). Protein size is expressed in kDa.

For separation of the nucleus from the cytosol, I utilized a commercial nuclear extract kit (Active Motif, USA), which allows obtaining cytosolic cellular components through a 'mild' osmosis-based lysis. The applied 'hypotonic lysis buffer' induces swelling and thus permeabilization of the cell membrane, and addition of the supplemented 'detergent' subsequently results in the release of cytosolic components. The following fast centrifugation step yields in the supernatant representing the cytoplasmic fraction. Further

treatment of the remaining pellet with a more stringent 'cell lysis buffer' dissolves the so far untouched nucleus, and the nuclear fraction is then obtained by separating the lysate from remaining cell debris with another l centrifugation. Figure 6.7A displays representative Western Blots images and quantification analysis of 4-8 individual nuclear cell preparations of NFATc1 (upper panel) and NFATc3 (lower panel). Due to their prevalence in the respective compartments (nucleus, cytosol), LaminB1 and GAPDH served as loading controls for the corresponding fractions. For data evaluation, signal intensities of the NFAT immunoreactive bands were measured by densitometry, expressed relative to the corresponding loading control and KO values were then normalized to WT samples set to 100 %. For both NFAT family members, the Western Blot images (left panel) as well as the statistical analysis (right panel) reveal a significant reduction of nuclear NFAT levels in the HAP1 TRPM7 KO clone when compared to WT. While the concentration of nuclear NFATc1 decreases by about ~12 %, NFATc3 levels decrease by even ~40 % in the KO cells.

To check if the reduced nuclear NFAT levels are accompanied by an increase in the NFAT concentration in the cytosol, I examined the corresponding cytoplasmic fractions. Although the representative Western Blot images suggest that the cytosol contains slightly more NFATc1 and c3 in the KO (Figure 6.7B, left panel), normalization to the loading control proofs that there are no significant differences between the TRPM7 WT and KO HAP1 cells regarding NFAT cytosolic concentrations (Figure 6.7B, right panel).

Since the decrease of nuclear NFAT levels in the KO apparently is not directly associated with an increase in cytosolic NFAT concentrations, I addressed the question if the total concentrations of NFATc1 and c3 are reduced in the HAP1 TRPM7 KO clone in comparison to WT as an additional control. To compare total protein expression of NFATc1 and c3 independently from their localization, I prepared HAP1 TRPM7 WT and KO whole-cell lysates and analyzed them via antibody-directed detection of NFATc1 respectively c3 in Western Blot. Signal intensities of the NFAT bands were normalized to the signals of the corresponding loading controls (LaminB1), and the resulting KO values were subsequently calculated as percent of WT (set to 100 %). Representative Western Blot images and bar graphs of these control experiments (Figure 6.7C) depict that, although KO cells overall express ~6 % more NFATc1 and ~16 % less NFATc3 than WT cells, neither expression of those two family members is significantly altered upon TRPM7 deletion.

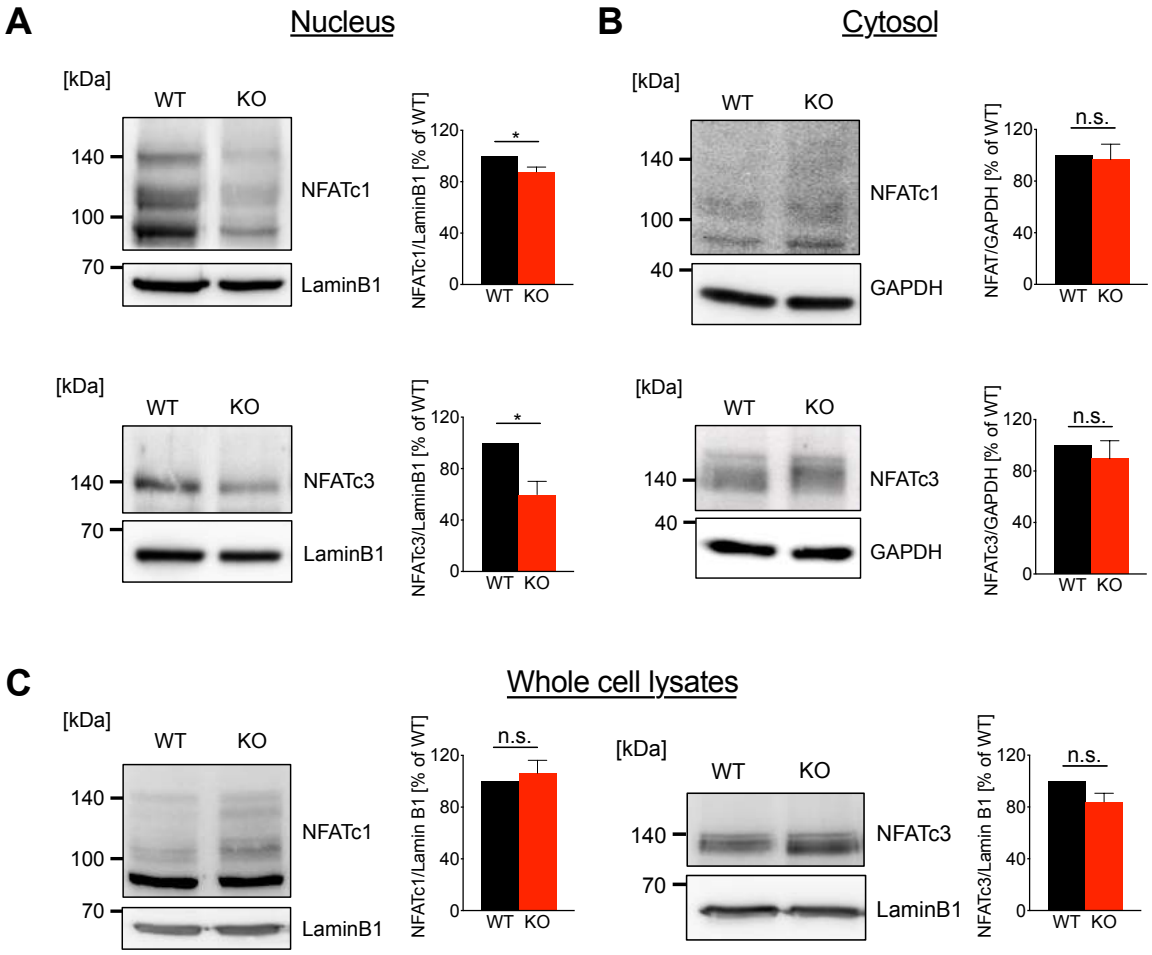

Figure 6.7 Subcellular NFAT localization in resting HAP1 TRPM7 WT and KO cells. Representative Western Blot images and quantification analysis of NFATc1 (90/110/140 kDa, upper panels) and NFATc3 (130 kDa, lower panels) in **(A)** the nucleus and **(B)** the cytosol in resting HAP1 TRPM7 WT and KO cells (n=4-8). For statistical analysis, signal intensities of both family members were normalized to their corresponding nuclear (LaminB1, 65 kDa) or cytosolic (GAPDH, 38 kDa) loading control and HAP1 TRPM7 KO values were calculated as percent of WT (set to 100 %). Note that both NFATc1 and NFATc3 are significantly reduced in the nuclear fraction of the HAP1 TRPM7 KO mutant, while their concentration is not significantly altered in the corresponding cytoplasmic fractions. **(C)** Representative Western Blot images and quantification analysis regarding the total protein concentration of NFATc1 (left panel) and NFATc3 (right panel) in whole-cell RIPA lysates of resting HAP1 TRPM7 WT and KO cells (KO expressed as percent of WT). Although detecting a slight increase (NFATc1) respectively a moderate reduction (NFATc3) regarding the expression levels of NFATcs in HAP TRPM7 KO cells, neither NFATc1 nor NFATc3 total protein expression is significantly changed in the HAP1 TRPM7 KO cells. Protein size is expressed in kDa. Data are presented as mean ± s.e.m. Statistics: paired student's t-test * $p<0.05$; n.s.: not significant

I conclude that TRPM7 antagonizes NFAT nuclear export and thus facilitates NFAT nuclear accumulation through promotion of GSK3β Ser9 phosphorylation. Nevertheless, the TRPM7 KO-induced reduction of nuclear localized NFAT does not necessarily imply a decline in NFAT-dependent gene expression. Hence, I next analyzed if the HAP1 TRPM7 KO cells also show a defect in NFAT transcriptional activity.

6.1.5 Impact of TRPM7 on NFAT-dependent gene expression using the dual-luciferase reporter gene assay

A convenient method for studying gene expression induced by particular transcription factors is the dual-luciferase reporter gene assay. It is based on a reporter gene encoding for a fluorescent protein or enzyme - here: firefly luciferase – that is directly attached to a promoter region recognized by the transcription factor of interest. Thus, the expression of the firefly luciferase depends on induction of gene expression by binding of the corresponding transcription factor to its promoter, and accordingly, transcription factor activity is directly correlated to the enzymatic activity, which can be measured by bioluminescence. The oxidative decarboxylation of the firefly luciferase substrate D-luciferin results in oxyluciferin, which is – by its nature – singlet-excited, meaning that one of the paired electrons is excited to an higher energy level but still retains its original spin. Therefore, when returning to its ground state, it emits light with a wavelength of λ_{max} = 560 nm [245, 246]. Yet, the activity of the firefly luciferase does not exclusively depend on transcription factor activity, but also varies with cell number and, even more important, the transfection rate. To exclude falsification of the results by these parameters, a second luciferase named *Renilla* serves as reference [247-249]. This luciferase converts coelenterazine to coelenteramide which emits light at a wavelength of λ_{max} = 470-480 nm [250, 251]. The *Renilla* luciferase expression relies on the above-mentioned factors varying general gene expression, such as cell number and transfection rate, but occurs independent of specific transcription factors. Thus, its activity can be used for normalization of the firefly luciferase signal [249].

Accordingly, my initial approach was to transfect the HAP1 TRPM7 WT and KO cells with an NFAT reporter gene and a *Renilla* luciferase vector as internal expression control and thereafter to measure NFAT-dependent gene expression and thus determine NFAT transcriptional activity. But before directly applying the dual-luciferase NFAT reporter gene assay, transfection efficiency of the HAP1 cells had to be evaluated first. To simplify these test experiments and be able to rapidly visualize transfection rates, a G5α construct was used which comprises GFP emitting a green fluorescent signal (λ_{max} = 509 nm) upon excitation at 488 nm (also see 6.1.6).

Unfortunately, the fluorescence-based monitoring revealed that transfection of the HAP1 cells with G5α resulted in very low transfection rates. Neither changing the transfection reagent from Lipofectamin to Turbofect or Xfect nor varying the DNA- and/or transfection reagent amount was able to increase the transfection rate which ranged between ~15 and ~30 % (not visually logged). Therefore, in default of obtaining a suitable amount of transfected HAP1 cells, I switched to wild-type HEK-293 cells overexpressing TRPM7 as alternative model system to study transcriptional activity of NFAT.

6.1.5.1 Effect of the TRPM7 on NFAT-dependent gene expression using the dual-luciferase NFAT-reporter gene assay in transiently transfected HEK-293 cells

As described for the initial experiments with HAP1 cells, the dual-luciferase reporter gene assay system was performed in HEK-293 cells using transient overexpression (for detailed description see methods, 5.11). Next to the NFAT reporter gene and the *Renilla* luciferase vector, HEK-293 cells were either transfected with a control vector pcDNA3.1 ('mock') or the vector containing the murine wild-type TRPM7 (TRPM7 WT) protein fused to the fluorescent tag GFP (λ_{max} = 509 nm).

As described in 6.1.3, the mix of various growth factors present in FBS is able to induce numerous signaling pathways and consequently could potentially cover TRPM7-dependent effects on NFAT transcriptional activity [252]. To avoid such an FBS-dependent gene regulation, cells were serum-starved for 4 hours prior to the luciferase measurements. Data evaluation was done by normalization of the firefly to the *Renilla* luciferase activity obtained for mock- respective TRPM7 WT-overexpressing HEK-293 cells, and subsequently, the resulting TRPM7 WT values were calculated as percent of mock (set to 100 %).

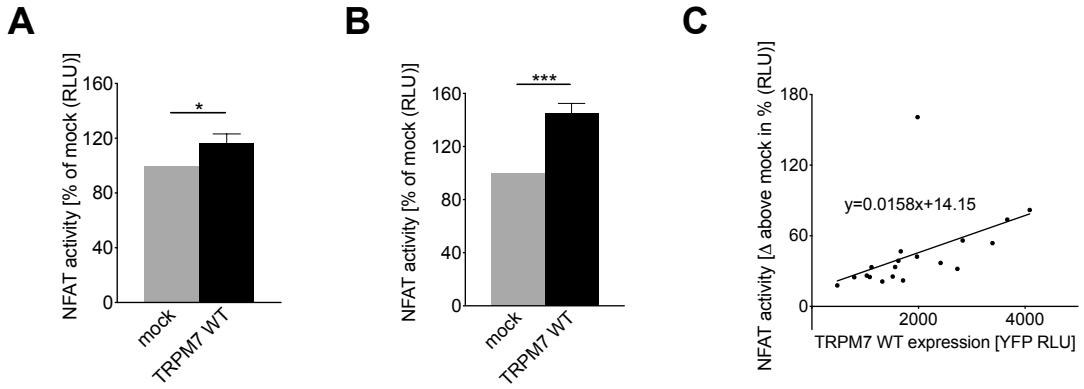

Figure 6.8 NFAT transcriptional activity in TRPM7 WT overexpressing HEK-293 cells. (A) NFAT transcriptional activity in transiently transfected HEK-293 cells co-expressing the NFAT luciferase reporter (500 ng) and the *Renilla* luciferase control vector (50 ng) together with either 400 ng pcDNA3.1 as control ([mock], grey) or 400 ng TRPM7 WT protein ([TRPM7 WT], black, displayed as percent of mock, n=7]). **(B)** NFAT transcriptional activity in a stable HEK-NFAT cell line transiently co-expressing pcDNA3.1 as control ('mock') or TRPM7 WT protein ([TRPM7 WT], displayed as percent of mock, n=19). Amount of transfected TRPM7 WT DNA ranged from 100-1000 ng and was complemented by pcDNA3.1 DNA if necessary to reach a DNA amount of 1000 ng total. **(C)** NFAT transcriptional activity plotted as function of TRPM7 WT expression in the stable HEK-NFAT cell line (n=19). TRMP7 WT data were normalized to the control (pcDNA3.1 alone, [mock], set to 100 %), and subsequently, NFAT activity of the control (which equals 100 %) was subtracted from the resulting TRPM7 WT NFAT activity values. Thus, TRPM7-dependent increase in NFAT activity is expressed as 'Δ above mock in %'. Amount of transfected TRPM7 WT DNA ranged from 100-1000 ng and was complemented by pcDNA3.1 DNA if necessary to reach a DNA amount of 1000 ng total. NFAT activity was measured in and is displayed as relative light units (RLU) of the firefly luciferase substrate oxyluciferin (λ_{max} = 560 nm) and TRPM7 expression is displayed as RLU of GFP (λ_{max} = 509 nm). In both transient and stable HEK-293 NFAT reporter cells, TRPM7 overexpression significantly elevates NFAT transcriptional activity in comparison to mock (A and B). Furthermore, NFAT-dependent gene transcription is augmented with increasing TRPM7 expression levels (**C**). Data are presented as mean ± s.e.m. Statistics: paired student's t-test * $p<0.05$; *** $p<0.005$

Figure 6.8A shows that transient TRPM7 WT overexpression significantly increases NFAT activity around ~17 % compared to mock, indicating that TRPM7 facilitates NFAT-dependent gene expression. However, although the use of *Renilla* luciferase for normalization helps to exclude variables which could distort measurements of NFAT-dependent gene expression (see above), it is useful to substantiate the results with a cell line stably expressing the NFAT luciferase reporter. Thus, the luciferase experiments were repeated in a stable HEK-NFAT reporter cell line that allows standardization of NFAT-coupled luciferase expression.

6.1.5.2 Effect of TRPM7 on NFAT-dependent gene expression in a stable HEK-NFAT reporter cell line

As described above, the stable HEK-NFAT reporter cell line has the advantage of all cells uniformly expressing the NFAT firefly luciferase reporter gene, thus making additional expression of the *Renilla* luciferase for normalization redundant. Hence, a HEK-293 cell line constantly expressing an NFAT firefly luciferase reporter was generated (herein named 'HEK-NFAT', see methods, 5.10.1) and transfected with the control vector mock or the GFP-tagged TRPM7 WT construct. Again, cells expressing mock were used as controls with the NFAT activity set to 100 %, and the activity of TRPM7 WT-expressing cells was calculated as percent of mock. As illustrated in Figure 6.8B, TRPM7 WT overexpression highly significantly ($p<0.005$) enhances NFAT transcriptional activity about ~45 % in comparison to mock. Moreover, the TRPM7-induced increase in NFAT-dependent gene expression is concentration dependent, as higher TRPM7 WT expression levels – measured via the fluorescent tag GFP – correlate with augmented NFAT firefly luciferase activity (Figure 6.8C).

Taken together, TRPM7 WT overexpression indeed promotes NFAT transcriptional activity in HEK-293 cells. Although this result matches the conclusions regarding NFAT localization drawn from the comparison of the HAP1 TRPM7 WT *vs.* KO model (see Figure 6.7), it not necessarily given that the HAP1 cells show the same TRPM7-dependent NFAT-driven gene induction. As a matter of fact, an overexpression system largely differs from a KO system and potentially shows additional alterations induced by enhanced protein expression; hence, the TRPM7 overexpression in the HEK-293 cells might influence other factors – which not necessarily must be affected by TRPM7 KO in the HAP1 cells – promoting NFAT transcriptional activity. One main mechanism triggering NFAT nuclear translocation and activity is the increase in cytosolic Ca^{2+} [253]. Given that TRPM7 is a Ca^{2+}-conducting channel, its overexpression might influence intracellular Ca^{2+} levels in HEK-293 cells; therefore, I next analyzed internal Ca^{2+} concentrations in TRPM7 WT overexpressing HEK-293 cells.

6.1.6 Effect of TRPM7 on Ca^{2+} homeostasis in HEK-G5α cells

In order to monitor basal Ca^{2+} levels in TRPM7 overexpressing HEK-293 cells, another stable cell line was utilized. The HEK-G5α cells (kindly provided by Dr. Breit, Walther-Straub-Institute, LMU

Munich) constitutively express a fusion protein composed of the enzymatic part of the biological Ca^{2+} sensor aequorin (apoaequorin) and GFP, a combination that allows relatively sensitive measurements of the cytosolic Ca^{2+} concentration [196, 202]. In the presence of bound Ca^{2+}, (apo)aequorin is able to oxidize its substrate coelenterazine to coelenteramid which then emits blue light (λ_{max} = 470-480 nm) [251, 254]. Instead of directly measuring the emission, the relatively low light quantum yield (number of emitted photons per Ca^{2+}-bound protein) of this enzymatic reaction is increased by chemiluminescence resonance energy transfer (CRET). Through the close proximity of the two components, the energy is not being emitted by coelenteramid but directly transferred to GFP, which is excited and in turn emits green light (λ_{max} = 509 nm). Accordingly, this system allows sensitive Ca^{2+} measurements without introducing an external fluorescent dye or requiring excitation at a specific wavelength and thereby bypasses problems such as toxicity, photobleaching or autofluorescence [196].

For the measurements, HEK-G5α cells were transfected with either the control vector pcDNA3.1 ('mock') or the TRPM7 WT construct (both introduced above, see 6.1.5). To adequately compare the results, data of the TRPM7 WT were calculated as percent of mock (set to 100 %).

Transient overexpression of TRPM7 WT in HEK-G5α cells significantly elevates Ca^{2+} levels by ~22 % in comparison to mock-transfected cells (Figure 6.9). Hence, the TRPM7 overexpression-induced increase in NFAT transcriptional activity (see 6.1.5) is directly associated with a rise in intracellular Ca^{2+} concentrations upon TRPM7 overexpression, suggesting that in HEK-293 cells, the observed upregulation of NFAT-dependent gene expression is most likely caused by increased Ca^{2+} influx through the TRPM7 channel and thus Ca^{2+}-dependent.

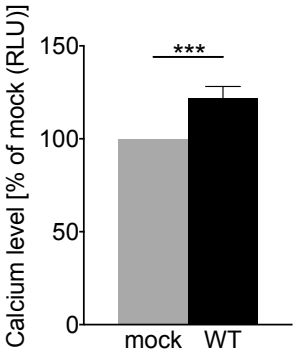

Figure 6.9 Basal Ca^{2+} levels in TRPM7 WT overexpressing HEK-G5α cells. Ca^{2+} concentration in mock-transfected (grey) and TRPM7 WT-overexpressing (black) HEK-G5α cells (n=8). Ca^{2+} concentration is illustrated as relative light units (RLU) of GFP (λ_{max} = 509) and WT data are normalized to mock (set to 100 %). When compared to mock, TRPM7 overexpression highly significantly elevates internal Ca^{2+} concentration in HEK-G5α cells. Data are presented as mean ± s.e.m. Statistics: paired student's t-test *** p<0.005

In contrast, knockout of native TRPM7 in HAP1 cells significantly reduces the level of nuclear localized NFAT (as shown in 6.1.4) but does not alter the basal intracellular Ca^{2+} concentration (shown in 6.1.2). Consequently, in HAP1 cells, TRPM7 promotes NFAT nuclear localization independently of Ca^{2+}, indicating the existence of a different mechanism by which the channel-kinase interferes with NFAT.

Irrespective of the differential outcome regarding Ca^{2+} in the TRPM7-depleted HAP1 cells and the TRPM7-overexpressing HEK-293 cells, the results demonstrate that TRPM7 substantially affects NFAT localization and transcriptional activity in human cells. Since NFAT controls the expression of various genes, I decided to employ another technique, namely RT-qPCR, to closer examine NFAT-dependent gene expression in HAP1 TRPM7 WT and KO cells.

6.1.7 Impact of TRPM7 on NFAT-dependent target gene expression using RT-qPCR

NFAT affects a variety of genes and induces their expression either alone or in cooperation with other transcription factors and cofactors. Thus, TRPM7 might be involved in the up- and/or downregulation of these genes through its impact on NFAT localization in HAP1 cells (see 6.1.4). To closer examine target genes induced by NFAT in the HAP1 TRPM7 WT and KO cells, I applied the widely used RT-qPCR which allows to determine specific gene expression by mRNA quantification [255-257].

Therefore, I investigated the expression of four genes previously shown to rely on NFAT activity: *Cyclooxygenase-2 (COX-2)*, *Interleukin-2 (IL-2)*, *Inositol 1,4,5-triphosphate receptor type 1* (*IP_3R1)* and *Myc* [258-264]. Before starting the actual quantification of the respective mRNA transcripts, classical reverse transcription PCR (RT-PCR) followed by agarose gel electrophoresis was used to determine if the HAP1 cells actually express the described NFAT target genes.

Figure 6.10 reveals that both HAP1 cell clones express *COX-2*, *IP_3R1* and *Myc* but lack *IL-2*. Accordingly, the first three were chosen for further RT-qPCR analysis.

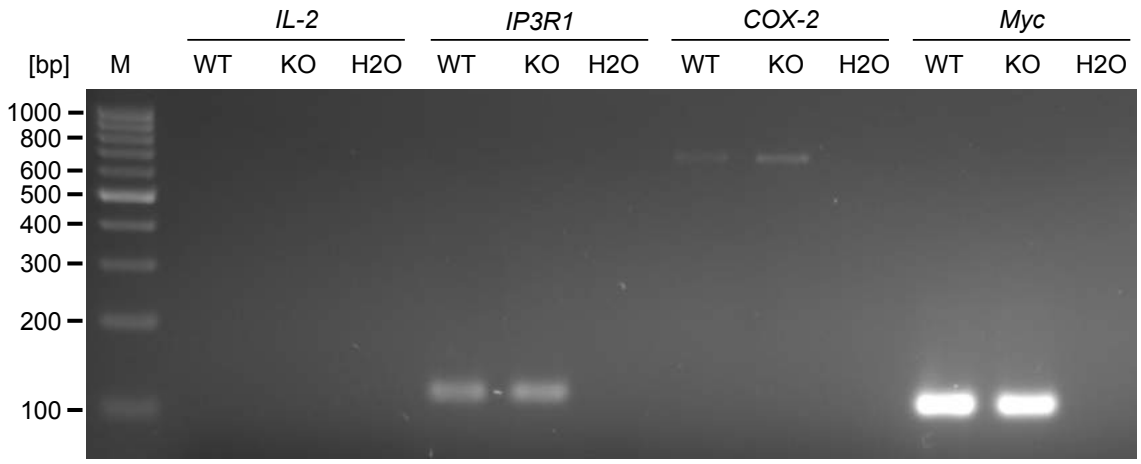

Figure 6.10 Expression of NFAT-inducible genes in HAP1 TRPM7 WT and KO cells. Analysis of the mRNA expression of the NFAT-dependent genes *IL-2*, *IP$_3$R1*, *COX-2* and *Myc* in HAP1 TRPM7 WT and KO cells. Water (H_2O) served as negative control; the DNA ladder (Marker [*M*]) indicates the size of the amplified PCR products measured in base pairs (*bp*). Note that the *IP$_3$R1*, *COX-2* and *Myc* are expressed in both HAP1 cell clones wherefore *IL-2* is not.

Figure 6.11 documents the results obtained from 6-20 independent preparations of the two genotypic cell lines. Data of every gene of interest were normalized to the housekeeping gene *HPRT1* and expressed as relative gene expression ($2^{(-\Delta CP)}$).

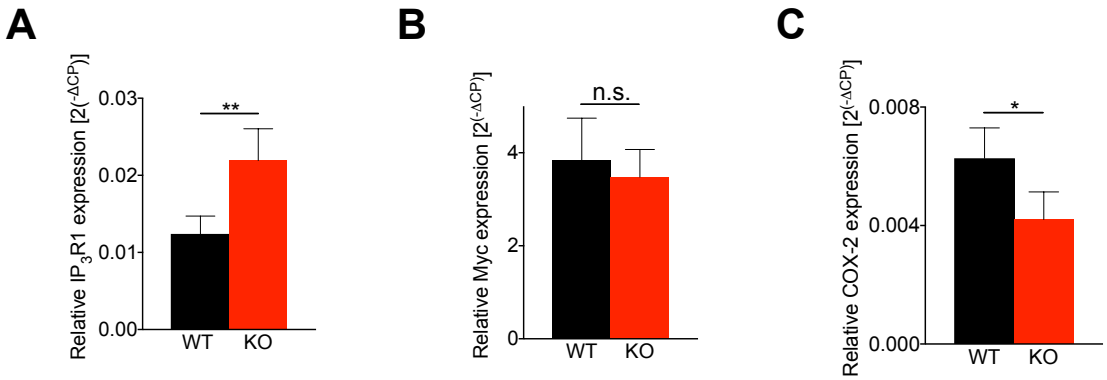

Figure 6.11 Quantity of *IP$_3$R1*, *Myc* and *COX-2* mRNA in HAP1 TRPM7 WT and KO cells. Relative mRNA expression (measured via RT-qPCR) of **(A)** *IP$_3$R1* (n=6), **(B)** *Myc* (n=6) and **(C)** *COX-2* (n=18-20) in resting HAP1 TRPM7 WT and KO cells. For analysis, the particular signals were normalized to the reference gene *HPRT1* and expressed as relative gene expression ($2^{(-\Delta CP)}$). Note a significant increase in *IP$_3$R1* expression (A) as well as a significant reduction in *COX-2* expression (C) in HAP1 TRPM7 KO cells compared to WT. *Myc* mRNA levels however are not effected by TRPM7-depletion (B). Data are presented as mean ± s.e.m. Statistics: ratio paired t-test *p<0.05, **p<0.01; n.s.: not significant

Regarding *IP$_3$R1*, depletion of TRPM7 leads to a significant increase in transcription when compared to WT (~0.012 compared to ~0.022, Figure 6.11A). In contrast, *Myc* gene expression is not affected by TRPM7, as there is no apparent difference in the amount of *Myc* mRNA comparing WT and KO samples (Figure 6.11B). Opposed to these findings, *COX-2* mRNA levels are significantly reduced if TRPM7 is absent (Figure 6.11C): Relative to WT, HAP1 TRPM7 KO cells express only about two thirds as much *COX-2* (~0.0063 compared to ~0.0042).

In summary, both mRNA levels of *IP$_3$R1* and *COX-2* differ in the KO clone. Surprisingly, TRPM7 differentially affects *IP$_3$R1* and *COX-2* gene regulation: While *IP$_3$R1* gene expression is significantly augmented upon TRPM7 depletion, *COX-2* gene expression is – in contrast – dramatically downregulated.

6.1.8 Effect of TRPM7 on COX-2 activity

COX-2, also known as prostaglandin-endoperoxide synthase 2 (PTGS2), is – together with the other cyclooxygenase isoform COX-1 – the rate-limiting enzyme for prostaglandin (PG) synthesis and thus plays an essential role in pain, inflammation and other diseases, such as several types of cancer and neuropathological disorders [265-274]. Given its clinical relevance, I next addressed the question if the substantial reduction of *COX-2* mRNA in the HAP1 TRPM7 KO cells results in diminished COX-2 enzymatic activity, which not necessarily must be the case [274-277]. To investigate COX-2 activity, I utilized a fluorometric COX Activity Assay (Abcam, UK), which quantifies COX activity by the conversion of its substrate arachidonic acid into PG G_2 (PGG_2); the amount of subsequently metabolized PGG_2 and thus COX activity is reflected by an increase in fluorescence (measured at an emission wavelength of λ_{max} = 587 nm, excitation at 535 nm; for more details, see specification by the supplier). Thus, following preparation of the assay, the enzymatic reaction was initialized by arachidonic acid administration (resembling time point 0, t=0), and subsequently, the increase in fluorescence (measured in relative fluorescence units, RFU) was monitored every 25 s for 30 min.

Figure 6.12A displays the respective increase in fluorescence in the DMSO-treated (see below) HAP1 TRPM7 WT and KO samples plotted *versus* time (raw data sets, displayed as [RFU]). First of all, it becomes apparent that the assay exhibits a very high background signal (RFUs at t=0, $RFUt_0$). Nevertheless, looking at the kinetic of the substrate conversion resembling COX activity, TRPM7 WT cells clearly show a small, but continuous increase in fluorescence over time, while no substantial elevation in fluorescence was detectable for the TRPM7 KO cells (Fig. 6.12A). To exclude larger variations between the individual experiments regarding the background signal, raw data were further evaluated by calculating the increase in fluorescence over time (expressed as ΔRFU) by subtracting the background signal ($RFUt_0$) from each time point of the corresponding measurement. Instead of making these calculations for the two graphs shown in 6.12A resembling the mean of all TRPM7 WT and KO samples, this was done for each experiment (n) individually. Subsequently, the means and the standard error of the means (SEMs) of both TRPM7 WT and KO were calculated, and the results are displayed in Figure 6.12B. Similar to Figure 6.12A, the kinetics show that, while WT demonstrates a considerable increase in fluorescence over time, no elevation in fluorescence and thus COX activity is observed for the TRPM7 KO mutant. Furthermore, this calculation demonstrates that the large variations visible before in Fig. 6.12A (resembled by the large SEMs) were, as expected, rather due to variances in the initial background signal between the individual

experiments and are not actually genotype-dependent fluctuations in the effect of TRPM7 on COX activity. Comparing and statistically analyzing each time point individually by a two-way ANOVA illustrates that the TRPM7 KO mutant displays a significant ($p<0.05$) reduction of COX activity from time point 17 min 55 s respectively highly significant reduction ($p<0.01$) from time point 20 min until the end of the measurement in comparison to WT.

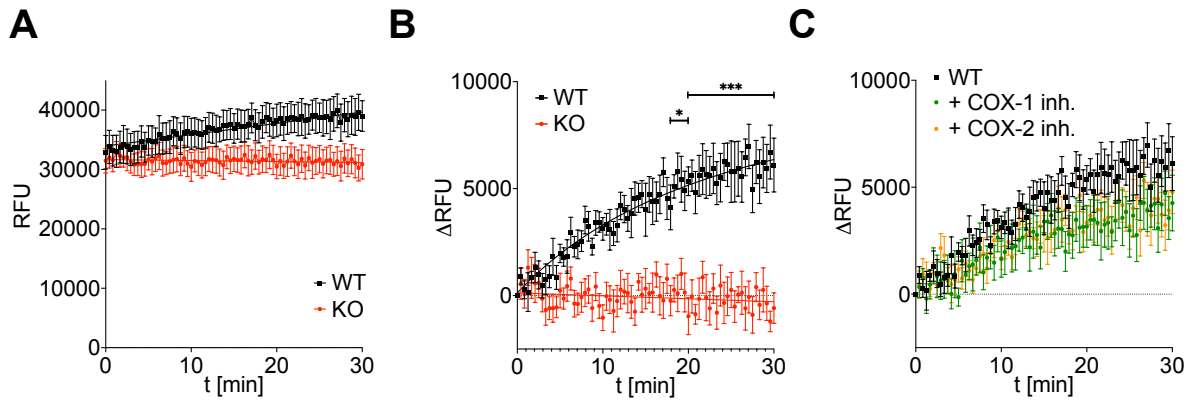

Figure 6.12 COX-2 activity in HAP1 TRPM7 WT and KO cells. Basal cyclooxygenase (COX) enzymatic activity in HAP1 cell lysates was measured via conversion of the substrate arachidonic acid to a fluorescent substance ($\lambda_{excitation}$ = 535 nm, $\lambda_{emission}$ = 587 nm; n=4); the resulting increase in fluorescence was measured every 25 s for 30 min. **(A)** Increase in fluorescence (resembling COX activity) over time in the DMSO-treated HAP1 TRPM7 WT and KO cells. Data are displayed as relative fluorescence units (RFU, raw data) plotted *versus* time. Note that, despite the very high fluorescent background signal recorded for both genotypes, the TRPM7 WT cells clearly display an increase in fluorescence and thus COX activity over time, while the signal in the TRPM7 KO cells does not substantially change. **(B)** Total increase in fluorescence resembling COX activity over time in the HAP1 TRPM7 WT and KO cells. To exclude larger variances between the individual experiments (n), fluorescent background signal were subtracted from every time point of the measurement for each trace individually before averaging and calculating the statistics. The resulting kinetics are displayed as ΔRFU and plotted *versus* time. As in (A), the KO shows diminished COX activity in comparison to WT, as the kinetic displays no increase in fluorescence. Statistics reveal that, when comparing the respective monitored fluorescence of the TRPM7 WT and KO samples for each time point separately, COX activity is significantly attenuated in the HAP1 TRPM7 KO cells from time point 17 min 55 sec (indicated by the bar, *) respectively highly significantly attenuated from time point 20 min (indicated by the bar, ***) until the end of the measurement. **(C)** Effect of the inhibition of COX-1 respectively COX-2 on the fluorescent increase resembling COX activity monitored for the HAP1 TRPM7 WT cells. To analyze if the observed increase is indeed COX related and to further specify which of the two COX isoforms, COX-1 and/or COX-2, is responsible for substrate conversion in the HAP1 cells, two different inhibitors specific for COX-1 (SC-560) and COX-2 (Celecoxib) were applied; inhibitor-treated samples were compared to samples treated with DMSO as solvent-control. Analogues to (B), data was evaluated by subtracting the fluorescent background signals from every time point of the measurement for each experiment individually before averaging and calculating the statistics; the resulting kinetics are displayed as ΔRFU and plotted *versus* time. The illustration shows that both the COX-1 and the COX-2 inhibitor affect COX activity by attenuating the increase in fluorescence in comparison to DMSO. Thus, both COX-1 and COX-2 seem to contribute to substrate conversion in HAP1 TRPM7 WT cells, and conclusively, depletion of TRPM7 affects both COX isoforms. Data are presented as mean ± s.e.m. Statistics: two-way ANOVA *p<0.05; ***p<0.005

As both illustrations, Figure 6.12A and B, demonstrate that the TRMP7 KO shows no increase in fluorescence over time, I conclude that depletion of TRPM7 almost fully extinguishes COX activity in the HAP1 cells. To further investigate how the two COX family members COX-1 and COX-2 contribute to

the observed increase in fluorescence resembling substrate conversion in the HAP1 TRPM7 WT cells and thereby also conclude which of these two isozymes is affected by the depletion of TRPM7, I applied the two inhibitors SC-560 and Celecoxib (supplied with the assay) specifically blocking COX-1 (SC-560) and COX-2 (Celecoxib) [278, 279]. As both substances were dissolved in DMSO, the solvent (used in the same dilution as applied for the inhibitors, 2 %) was added to the control samples containing no inhibitor. Again, fluorescence was measured every 25 s for 30 min after initialization of the reaction by arachidonic acid administration. Analogous to Figure 6.12B, raw data were evaluated by subtracting the background signal ($RLUt_0$) of each trace for every sample (WT DMSO, WT + COX-1 inh., WT + COX-2 inh.) individually before calculating the means and the statistics; the resulting kinetics are displayed in Figure 6.12C. Despite the partly high errors of the DMSO-, COX-1 inhibitor- and COX-2 inhibitor-treated samples, Figure 6.12C shows that, in comparison to DMSO, both inhibitors diminish the total increase in fluorescence and thus COX activity observed for the HAP1 TRPM7 WT cells to almost the same extent. statistically analyzing the data via a two way ANOVA this time comparing the means of all time points of the DMSO-, the COX-1 inhibitor- and the COX-2 inhibitor-treated WT samples demonstrates that both the COX-1 and the COX-2 inhibitor highly significantly ($p<0.01$) attenuate the fluorescent increase (significance not shown). Thus, I conclude that the observed increase in fluorescence in the DMSO-treated WT samples is attributable to both isozymes. Linking this result to the finding that the HAP1 TRPM7 KO mutant almost shows no substrate conversion (see Figure 6.12A and B), I hypothesize that the depletion of TRPM7 significantly diminishes the enzymatic activity of both COX-1 and COX-2. Associating these results with the previous findings for COX-2, I conclude that TRPM7 is not only essential for controlling *COX-2* gene expression but also significantly affects COX-2 enzymatic activity."

6.1.9 Effect of TRPM7 on the induction of *COX-2* gene expression

One difference between the cyclooxygenases 1 and 2 is that COX-1 is constitutively present in most organs, while COX-2 synthesis, showing low to no expression in most tissues, is induced by various factors including hormones, growth factors, bacterial endotoxins and cytokines [280-282]. However, defining COX-2 as the 'inducible' isoform, which is still a widespread habit, is not absolutely correct, since the enzyme is at least constitutively expressed in some organs (kidney, brain, gastro-intestinal tract) [283-285]. Nevertheless, activation of *COX-2* gene expression resembles a critical mechanism in many inflammatory processes, wherefore I chose to investigate if TRPM7 is involved in inducible *COX-2* mRNA production. As HAP1 cells do not display the surface receptors such as toll-like receptor 4 (TLR4) [286] established for proper activation of *COX-2* mRNA synthesis (demonstrated by a non-official genomic analysis of Horizon Discovery, Cambridge, UK; not shown), I chose forskolin as stimulus [214]. This natural compound stimulates adenylyl cyclase which in turn converts ATP to the second messenger cAMP, a known activator of *COX-2* gene expression [287-289]. As additional controls, cells were either

exposed to 0.1 % DMSO – which served as drug diluent and was therefore applied in the same dilution as forskolin – or left untreated to uncover potential DMSO-dependent, TRPM7-unspecific effects on *COX-2* gene expression.

HAP1 TRPM7 WT and KO cells were either stimulated with 50 µM forskolin, incubated with 0.1 % DMSO or left untreated for one hour. Inducible *COX-2* expression was subsequently analyzed via mRNA quantification using RT-qPCR as before (also see 6.1.7). Also here, *COX-2* data of untreated, DMSO-exposed and forskolin-treated samples were normalized to the housekeeping gene *HPRT1* (shown as $2^{(-\Delta CP)}$).

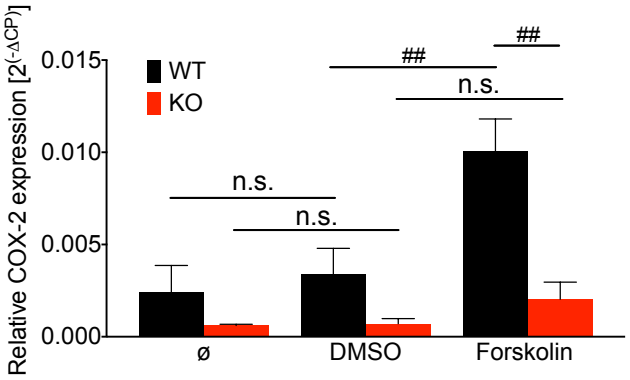

Figure 6.13 Inducible *COX-2* mRNA expression in HAP1 TRPM7 WT and KO cells. Relative expression of *COX-2* mRNA (measured via RT-qPCR) in HAP1 TRPM7 WT and KO cells stimulated with 50 µM forskolin or treated with DMSO as control for 1 h (n=4). For analysis, the particular signals were normalized to the reference gene *HPRT1*. Treatment with forskolin substantially increases *COX-2* mRNA expression in HAP1 TRPM7 WT cells, while *COX-2* gene induction is significantly less pronounced in the HAP1 TRPM7 KO cells. Data are presented as mean ± s.e.m. Statistics: two-way ANOVA $^{\#\#}$ $p<0.01$, n.s.: not significant

In comparison to DMSO, stimulation with 50 µM forskolin significantly increases *COX-2* mRNA levels in the HAP1 TRPM7 WT cells around threefold (DMSO: ~0.0033, forskolin: ~0.010, Figure 6.13). In contrast, forskolin treatment causes only a slight, but not significant increase of the initial low *COX-2* mRNA concentration in HAP1 TRPM7 KO cells when compared to DMSO (DMSO: ~0.0006, forskolin: ~0.002, Figure 6.13). Hence, forskolin indeed significantly stimulates *COX-2* mRNA production and thus induces *COX-2* gene expression in HAP1 TRPM7 WT, but not KO cells. Moreover, direct comparison of the forskolin-treated HAP1 TRPM7 WT and KO clone reveals that TRPM7 facilitates this inducible *COX-2* mRNA synthesis, as the forskolin-triggered augmentation of *COX-2* mRNA levels is about five times higher in WT than in KO (WT: ~0.010 compared to KO: 0.002, Figure 6.13). Importantly, although comparison of the untreated and DMSO-exposed control samples demonstrates that one hour incubation with 0.1 % DMSO minimally increases *COX-2* mRNA levels in both HAP1 TRPM7 WT and KO clone (Figure 6.13), this change is not significant. Consequently, one can conclude that DMSO has no substantial impact on *COX-2* gene expression.

Taken together, TRPM7 seems to plays a role in constitutive as well as inducible *COX-2* gene expression.

6.2 Role of the TRPM7 kinase domain in the cell signaling pathways

To understand if and to what extent the TRPM7 kinase is involved in Akt, GSK3β, NFAT and COX-2 directed signaling cascades, I utilized the novel kinase-dead HAP1 mutant cell model. As introduced above, the HAP1 TRPM7 KI clone carries a point mutation at the active site of the kinase (K1648R) depleting kinase activity. Hence, this cell line provides a suitable tool to precisely discriminate TRPM7 protein *vs.* kinase activity-specific functions.

6.2.1 Characterization of the kinase-dead HAP1 TRPM7 KI clone

Initially, the mutant HAP1 TRPM7 KI cells had to be analyzed analogously to the HAP1 KO clone (see 6.1.1). The correct insertion of the kinase inactivating point mutation was first examined by alignment of HAP1 TRPM7 WT and KI cDNA sequences. As mentioned in the methods (see 5.1.1.1), kinase activity is depleted by replacing lysine (K) to arginine (R) at position 1648 located within the enzymatic pocket of the kinase domain (K1648R). Therefore, the respective lysine-coding base triplett (AAA) was exchanged to an arginine-coding one (CGG). Sequencing of the HAP1 TRPM7 WT and KI cDNA illustrates that the genetic mutation was successful (Figure 6.14A); furthermore, computational translation (via Expasy Translate Tool) of the mutated genetic sequence into the corresponding protein sequence demonstrates that the nucleotide substitution results in the anticipated exchange of lysine to arginine (Figure 6.14B). For proving that the mutation at the catalytic site of the kinase is indeed causing its inactivation, Western Blot technique was applied. As only a few targets of the TRPM7 kinase are known yet (also see introduction, 3.2.2.2), I chose a polyclonal antibody kindly provided by Dr. Chubanov (Walther-Straub-Institute, LMU Munich) which binds to the phosphorylated TRPM7-autophosphorylation site Ser1511 [75]. In HAP1 TRPM7 WT cells displaying intact autophosphorylation, this antibody should detect the Ser1511-phosphorylated form of TRPM7 and thus show a band at approx. 220 kDa (molecular weight of full-length TRPM7). If kinase enzymatic function is indeed depleted in the TRPM7 KI clone, TRPM7 autophosphorylation is disrupted and the anti-TRPM7 pSer1511 antibody should not bind, which is reflected by lack of the corresponding signal. To additionally validate phospho-specifity of this antibody and thus verify the TRPM7 Ser1511 phosphorylation signal, half of the HAP1 TRPM7 WT and KI cell lysates were additionally treated with an alkaline phosphatase (in specific: FastAP Thermosensitive Alkaline Phosphatase, Thermo Fisher Scientific, USA) and subsequently compared to the untreated WT and KI samples. This enzyme ensures the rapid dephosphorylation of proteins and thus can be used to distinguish between phospho-specific and phospho-unspecific bands resulting from potential antibody cross-reactivity [290].

The Western Blot shown in Figure 6.15A illustrates that the phospho-specific anti-TRPM7 pSer1511 antibody labels a protein band at 220 kDa (molecular mass of full-length TRPM7) in the HAP1 TRPM7 WT cells (Figure 6.15A, first left lane). However, the respective signal is missing in the TRPM7 KI clone (Figure 6.15A, second left lane) as well as in the phosphatase-treated WT and KI samples (Figure 6.15A, right lanes). This indicates that the detected band in the WT indeed represents Ser1511-phosphorylated full-length TRPM7, and the result is substantiated by the absence of the corresponding signal in the phosphatase-treated sample. Thus, my results confirm that the TRPM7 KI cells indeed lack kinase activity.

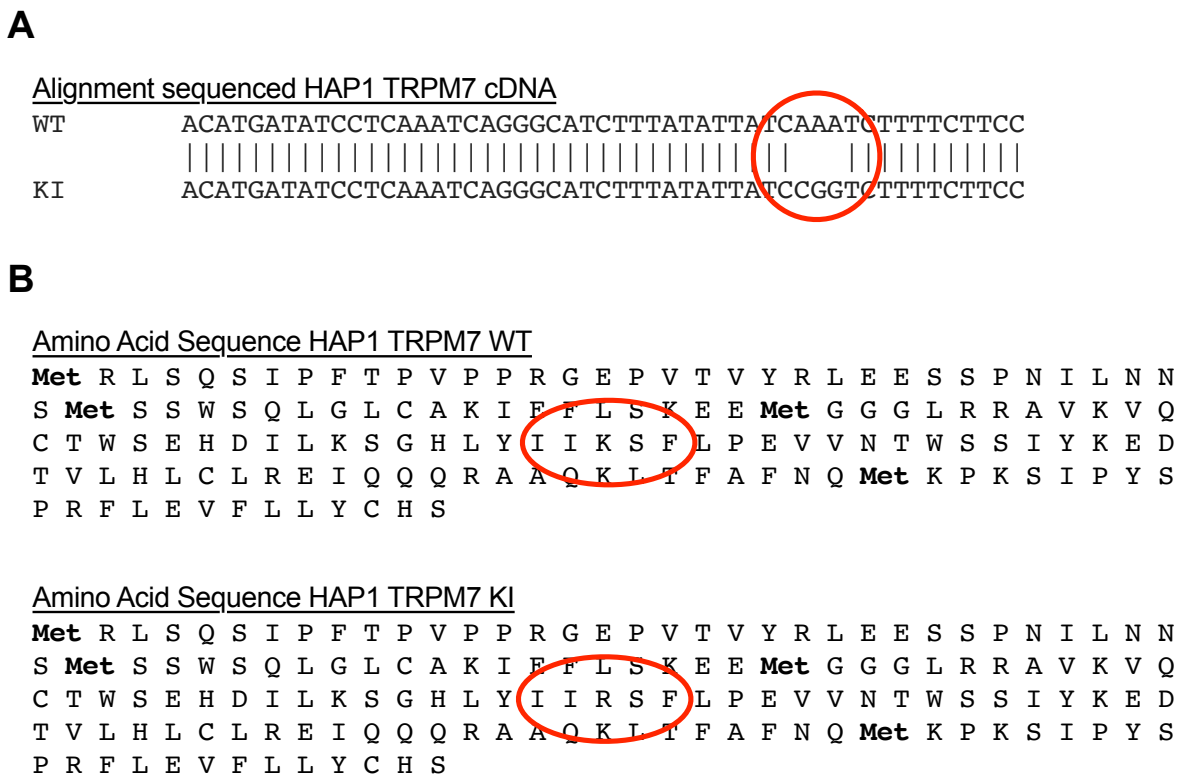

Figure 6.14 Verification of the HAP1 TRPM7 KI clone. (A) Alignment of sequenced wild-type (WT) and TRPM7 knock-in (KI) cDNA. For direct comparison of HAP1 TRPM7 WT and KI genetic sequences, mRNA of both cell clones was extracted, translated into cDNA and the respective altered region subsequently sequenced by Eurofins Genomics (with primers flanking the site of mutation). Extracted section shows the kinase inactivating base triplett exchange of the three nucleotides coding for lysine (AAA) to arginine (CGG) **(B)** Amino Acid (AA) sequences of the TRPM7 WT and KI clone resulting from the mRNA transcript (corresponding cDNA sequence partially shown in (A)). Note the substitution of lysine (K) to arginine (R) in the HAP1 TRPM7 KI clone.

Next, it was essential to clarify if kinase inactivation affects channel conductivity. This is of special importance since it was previously published that modifications regarding the kinase domain can alter channel conductivity (also see introduction, 3.2.4) [34, 36, 98]. Although K1646R-caused kinase disruption in mice, which is identical to the here inserted human mutation K1648R, did not change properties of the TRPM7 channel [83, 117, 118], this finding needed to be reaffirmed for the human TRPM7 KI cell line.

Therefore, TRPM7 currents of HAP1 TRPM7 WT and KI cells were measured via the whole-cell patch clamp technique (for more detailed description, see 6.1.1 or methods, 5.4). Overall comparison of the HAP1 TRPM7 KI clone with WT reveals that neither kinetics nor the amplitude of the TRPM7 current is significantly altered (Figure 6.15B). Intriguingly, data suggest that the HAP1 TRPM7 KI displays a higher basal current density than WT (see beginning of the measurement; WT: 3.17 pA/pF compared to KI: 7.28 pA/pF) and a slower and less steep current development over time; however, these differences are not significant (Figure 6.15B, left panel). Furthermore, traces at 150 s show the same current-voltage relationship for HAP1 TRPM7 WT and KI cells (Figure 6.15B, right panel). Overall, the presented data suggest that kinase depletion does not significantly change basic channel parameters of TRPM7 in the human HAP1 cell line, which is in accordance with the results acquired for the K1646R mutation in mice [117, 118]. Thus, the K1648R mutation inactivates the TRPM7 kinase domain without altering channel conductance, wherefore the HAP1 TRPM7 KI cells present a suitable tool to closer examine TRPM7 kinase activity function independently of the TRPM7 channel.

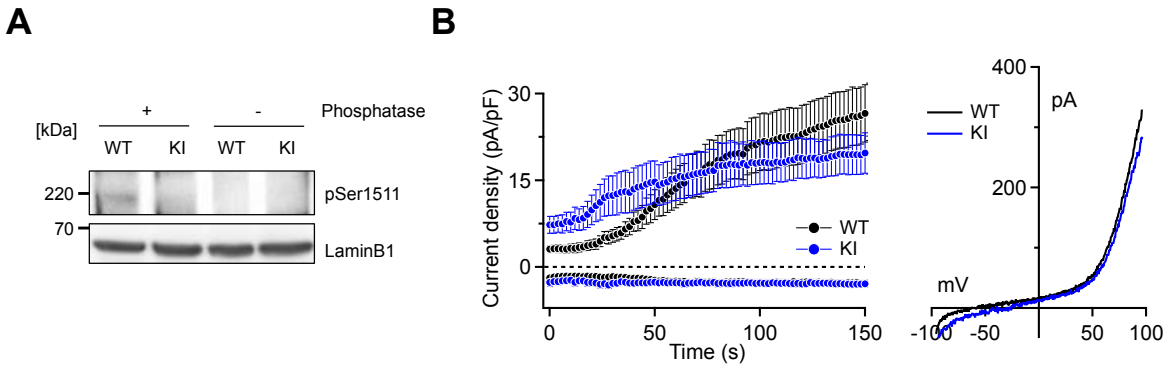

Figure 6.15 Characterization of the HAP1 TRPM7 KI clone. (A) Western Blot image of untreated (left) and phosphatase-treated (serving as control, right) HAP1 TRPM7 WT and KI lysates stained for the autophosphorylation site Ser1511. Note that the corresponding signal visible for the TRPM7 WT is missing in the TRPM7 KI clone (left lanes) as well as in the phosphatase-treated samples (right lanes). Loading control: LaminB1 (65 kDa). **(B)** Functional analysis of TRPM7 currents in HAP1 TRPM7 WT (black) and KI (blue) cells by patch clamp experiments (n=5-8). Measurements were conducted in the whole-cell configuration in the absence of extra- and intracellular Mg^{2+} to maximize TRPM7 currents. Current densities at +80 and -80 mV are plotted *vs.* time in seconds (left panel) and representative current-voltage relationships of traces extracted at 150 s are presented (right panel). Although TRPM7 current kinetics are slightly altered in HAP1 TRPM7 KI cells compared to WT, current development over time and equilibrium potential are not significantly altered.

6.2.2 Impact of the TRPM7 kinase activity on ion homeostasis

Despite the registered intact function of the channel in the HAP1 TRPM7 KI clone (see Figure 6.15B, channel conductance), inactivation of the kinase could potentially alter cellular ion homeostasis indirectly by other mechanisms [119, 138, 291, 292]. To address this question, cell lysates of the kinase-dead mutant were analyzed via ICP-MS identical to the KO mutant (see 6.1.2). With regard to TRPM7's described conductance, special focus was put on Mg^{2+} and Ca^{2+}, but also Zn^{2+} and Cu^{2+} [51]. Again, data were

evaluated by normalizing the values of each ion to sulfur (S) (Figure 6.16, left panels) and by calculating the KI data in percent of WT (set to 100 %, Figure 6.16, right panels).

Other than the HAP1 TRPM7 KO cells (see 6.1.2), the HAP1 TRPM7 KI cells do not reveal any changes regarding these four divalent cations: As illustrated in Figure 6.16, kinase activity neither affects Mg^{2+} (Figure 16A) nor Ca^{2+} homeostasis (Figure 6.16B) in a significant manner. Likewise, also levels of the trace elements Zn^{2+} and Cu^{2+} are the same for both the HAP1 TRPM7 KI and WT clone (Figure 6.16C and D). Thus, one can conclude that kinase depletion does not interfere with intracellular ion homeostasis in resting HAP1 cells.

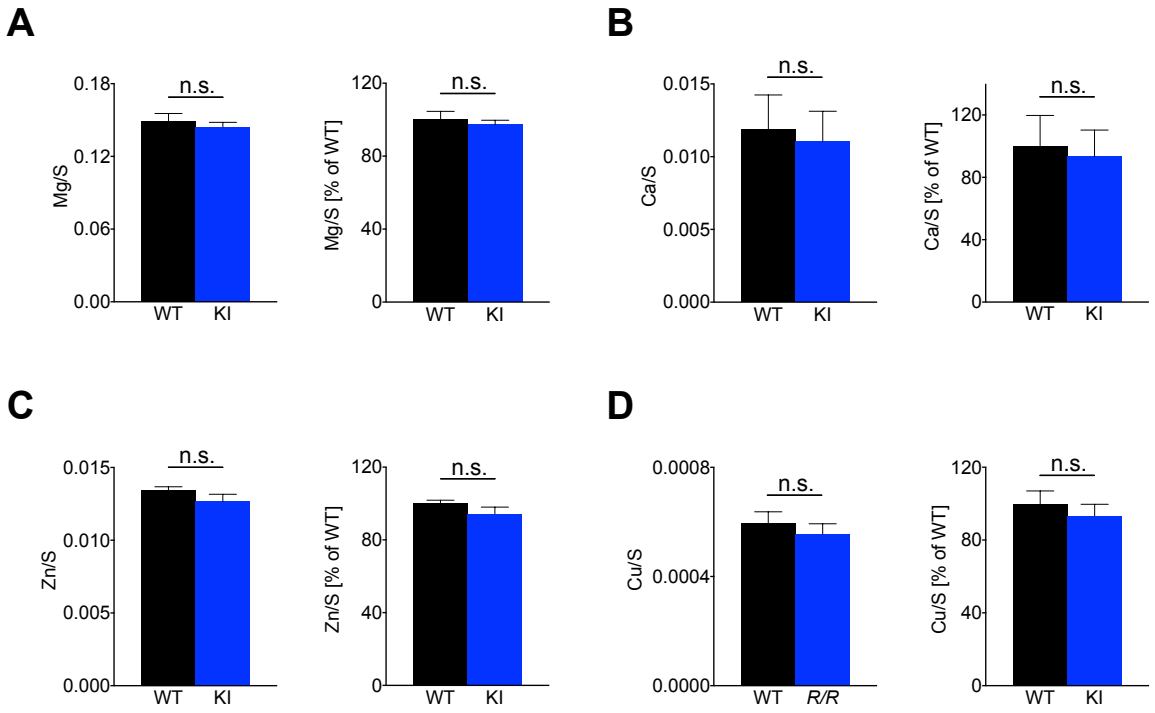

Figure 6.16 Ion levels in HAP1 TRPM7 WT and KI cells. Concentrations of **(A)** Mg^{2+}, **(B)** Ca^{2+}, **(C)** Zn^{2+} and **(D)** Cu^{2+} measured via ICP-MS in resting HAP1 TRPM7 WT (black) and TRPM7 KI (blue) cells (n=4). Concentrations are displayed as raw data (counts of respective ion in ppm, normalized to counts of sulphur (S) in ppm, left panels) as well as normalized to WT for direct comparison (set to 100 % right panels). Both evaluations reveal no alterations regarding concentration of investigated ions in the HAP1 TRPM7 KI clone compared to WT. Data are presented as mean ± s.e.m. Statistics: unpaired student's t-test ns: not significant

However, due to the above-mentioned sensitivity of intracellular Ca^{2+} measurements to contamination by residual external Ca^{2+} (see 6.1.2), Ca^{2+} concentrations in the HAP1 TRPM7 KI clone were additionally acquired via the ratiometric Fura-2 AM based Ca^{2+} imaging technique analogously to the previous experiments with the KO-mutant form (see 6.1.2). Comparing the 340/380 nm ratios of TRPM7 WT and KI shows that kinase-inactivation does not change basal intracellular Ca^{2+} concentration (Figure 6.17). Hence, outcome of the Ca^{2+} imaging measurements is

consistent with the ICP-MS results regarding Ca^{2+} and thus substantiates the hypothesis that TRPM7 kinase activity is not altering basal Ca^{2+} levels in HAP1 cells.

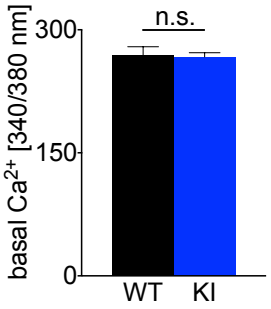

Figure 6.17 Single cell analysis of internal calcium concentration in HAP1 TRPM7 WT and KI cells. Ca^{2+} levels in resting HAP1 TRPM7 WT and KI cells acquired via ratiometric Fura-2 AM based Ca^{2+} imaging (n=10-22). Ca^{2+} concentrations are displayed as ratio of fluorescence at 340 and 380 nm. Intracellular Ca^{2+} concentration is about the same in HAP1 TRPM7 WT and KI cells. Data are presented as mean ± s.e.m. Statistics: unpaired student's t-test n.s.: not significant

6.2.3 Regulation of *COX-2* gene expression by TRPM7 kinase activity in HAP1 cells

As COX-2 is essential for controlling the immune response but also promotes tumor progression (see 6.1.8 and 6.1.9, respectively), it is important to understand whether the observed differences in the *COX-2* gene expression in the TRPM7-deficient HAP1 cells are due to the lack of TRPM7 kinase activity. Therefore, I examined if *COX-2* mRNA levels are affected by impairment of the TRPM7 kinase function. Since COX-2 in some organs is constitutively expressed whereas in other systems it is induced by specific signals (e.g. LPS [293]), RT-qPCR experiments were performed to compare *COX-2* mRNA concentrations of resting HAP1 TRPM7 WT and KI cells as well as upon increasing cAMP production caused by forskolin stimulation (analogously to the previous experiments, see 6.1.7 and 6.1.9) [280-285, 287].

6.2.3.1 Impact of TRPM7 kinase activity on constitutive *COX-2* gene expression

To properly analyze *COX-2* gene expression via its mRNA concentration, RT-qPCR WT and KI *COX-2* mRNA data were normalized to the housekeeping gene *HPRT1* and expressed as relative *COX-2* expression ($2^{(-\Delta CP)}$). The evaluation reveals a substantial reduction of *COX-2* mRNA concentration in the HAP1 TRPM7 KI clone when compared to WT (Figure 6.18). In comparison to the WT, the *COX-2* mRNA level is significantly decreased in the TRPM7 KI clone when data are referenced to HPRT1 (WT: ~0.00137; KI: ~0.00083, Figure 6.18).

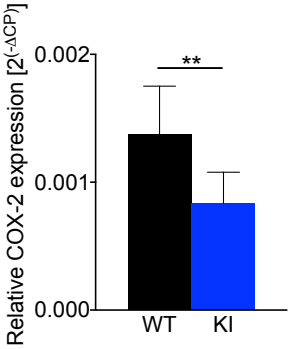

Figure 6.18 Constitutive *COX-2* mRNA expression in HAP1 TRPM7 WT and KI cells. *COX-2* mRNA expression (measured via RT-qPCR) in resting HAP1 TRPM7 WT and KI cells (n=8-10). For analysis, the particular signals were first normalized to the reference gene *HPRT1* and then presented as relative *COX-2* expression ($2^{(-\Delta CP)}$). Note a significant reduction in *COX-2* expression in HAP1 TRPM7 KI cells compared to WT. Data are presented as mean ± s.e.m. Statistics: ratio paired t-test **p<0.01

6.2.3.2 Impact of TRPM7 kinase activity on inducible *COX-2* gene expression

Similar to the previously described experiments, *COX-2* mRNA synthesis in the HAP1 cells was stimulated by addition of 50 µM of the adenylyl cyclase activator forskolin to fresh culture medium followed by an one hour incubation. In addition, cells were either incubated with 0.1 % DMSO (drug diluent, applied in the same concentration as forskolin) for one hour or left untreated; both of theses samples served as controls (also see 6.1.9). Data evaluation was accomplished by normalization of raw data to the housekeeping gene *HPRT1* (shown as $2^{(-\Delta CP)}$).

First of all, in comparison to the respective DMSO samples, forskolin treatment significantly enhances *COX-2* mRNA production in HAP1 WT cells (from ~0.001 to ~0.005), whereas it has a smaller, but still significant effect on HAP1 TRPM7 KI cells (from ~0.0009 to ~0.003, Figure 6.19). Thus, forskolin indeed induces *COX-2* gene expression in both HAP1 TRPM7 WT and KI cells. However, direct comparison of the forskolin-treated WT and KI samples illustrates that the induced *COX-2* mRNA synthesis in HAP1 TRPM7 KI clone is only about 60 % as much as in WT (WT: ~0.005, KI: ~0.003, Figure 6.19). Furthermore, the control samples reveal that DMSO has no effect on *COX-2* gene expression in both investigated TRPM7 genotypes since there are no significant differences between the *COX-2* mRNA concentrations of the respective untreated and DMSO-exposed samples (Figure 19).

When comparing the HAP1 TRPM7 KI results to the results acquired for the TRPM7 KO clone, it becomes evident that the repressive effect of the TRPM7 kinase inactivation on inducible *COX-2* gene expression is less pronounced as the one caused by depletion of the full-length protein; while HAP1 TRPM7 KI cells display about 60 % as much *COX-2* mRNA as WT upon forskolin stimulation (Figure 6.19), HAP1 TRPM7 KO *COX-2* mRNA levels are only about 20 % compared to WT (see Figure 6.13).

The results lead to the conclusion that the activity of the TRPM7 kinase has a significant impact on both constitutive as well as inducible *COX-2* gene expression. As described above, *COX-2* gene expression is directly controlled by the transcription factor NFAT (also see 6.1.7). Interestingly, results showed that NFAT nuclear localization as well as transcriptional activity is altered upon depletion respectively overexpression of full-length TRPM7 (see 6.1.4 and 6.1.5). Thus, the intact TRPM7 kinase might potentiate *COX-2* gene expression by facilitating NFAT nuclear localization and NFAT-dependent transcription. To assess if TRPM7 kinase activity indeed modulates these NFAT parameters, I utilized antibody-directed detection of NFAT in Western Blot for investigating NFAT nuclear localization (in HAP1 TRPM7 KI cells) as well as the dual-luciferase reporter gene assay for studying NFAT transcriptional activity (in HEK-293 cells overexpressing a TRPM7 KI construct).

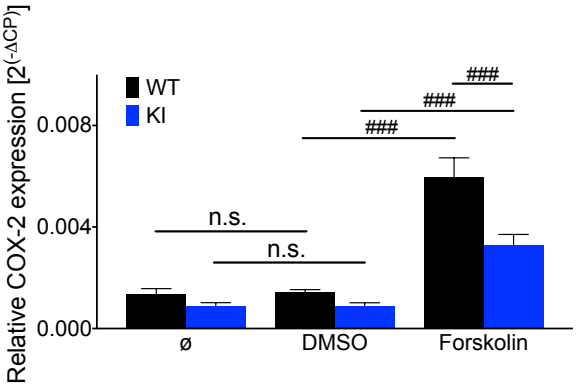

Figure 6.19 Inducible *COX-2* mRNA expression in HAP1 TRPM7 WT and KI cells. Relative *COX-2* mRNA expression (measured via RT-qPCR) in HAP1 TRPM7 WT and KI cells stimulated with 50 µM forskolin or treated with DMSO as control for 1 h (n=4-5). For analysis, the particular Cp values were normalized to the reference gene *HPRT1*. Treatment with forskolin significantly increases *COX-2* mRNA expression in both HAP1 TRPM7 WT and KI cells, yet the increase is less distinct in the KI wherefore the mutant significantly differs from WT. Data are presented as mean ± s.e.m. Statistics: two-way ANOVA ### $p<0.005$; n.s.: not significant

6.2.4 Effect of TRPM7 kinase activity on subcellular NFAT localization

Equivalent to the experiments with the HAP1 TRPM7 KO cells (see 6.1.4), I next examined the basal nuclear localization of NFATc1 in the HAP1 TRPM7 KI clone via immunoelectrophoresis. Again, the signal intensities were measured via ImageJ, the results normalized to the corresponding loading controls (LaminB1 and GAPDH) and the TRPM7 KI data were subsequently calculated in percent of WT (set to 100 %) (also see 6.1.4).

The representative Western Blot results shown in Figure 6.20A depict that, in contrast to the KO clone, lack of TRPM7 kinase activity does not influence the nuclear localization of NFATc1 in resting cells. Both the nuclear and the cytosolic level do not significantly differ in the HAP1 TRPM7 KI cells when compared to WT fractions (Figure 6.20A respectively B). The additional control regarding the total expression of NFATc1 via whole-cell lysates shows that total NFATc1 levels are about the same in TRPM7 WT and KI cells (Figure 6.20C).

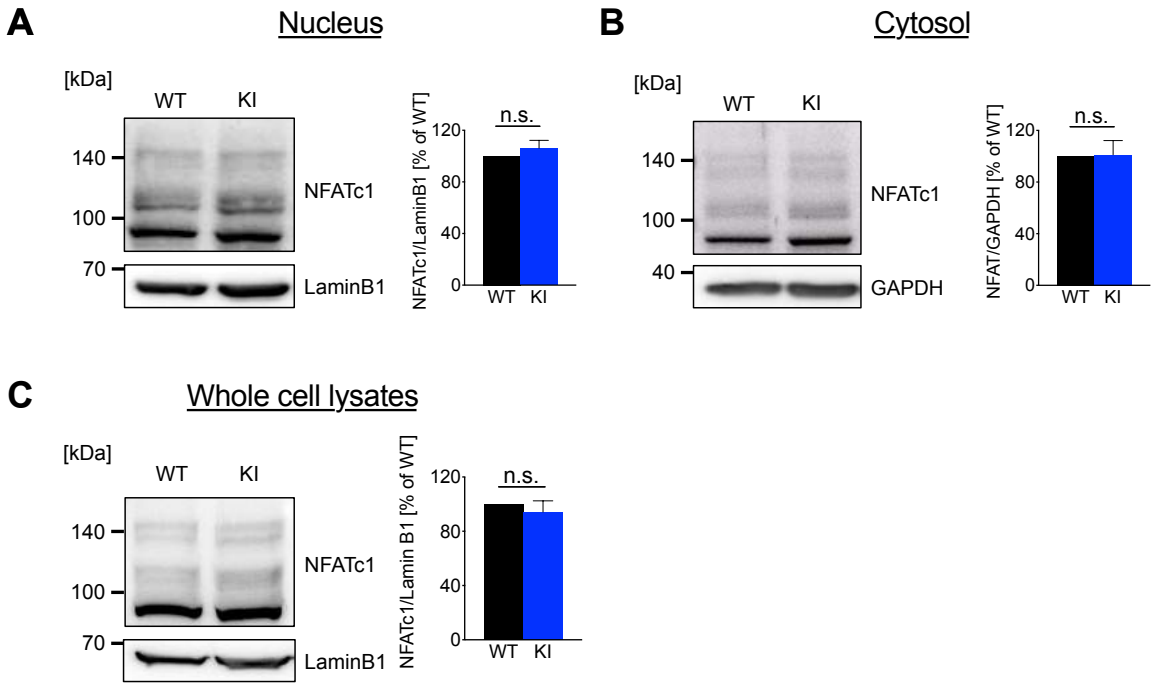

Figure 6.20 Subcellular NFATc1 translocation in resting HAP1 TRPM7 WT and KI cells. Representative Western Blot images and statistical analysis of NFATc1 in **(A)** the nucleus and **(B)** the cytosol in resting HAP1 TRPM7 WT and KI cells (n=5-10). For statistical analysis, signal intensities of both family members were normalized to their corresponding nuclear (LaminB1) or cytosolic (GAPDH) loading control; subsequently, HAP1 TRPM7 KI values were calculated as percent of WT (set to 100 %). Neither nuclear nor cytosolic concentration of NFATc1 of the HAP1 TRPM7 KI significantly differs from WT. **(C)** Representative Western Blot image and quantification analysis regarding the total concentration of NFATc1 in whole-cell RIPA lysates of resting HAP1 TRPM7 WT and KI cells (KI expressed as percent of WT). Consistent with the data presented in (A) and (B), total NFATc1 level is about the same in HAP1 TRPM7 WT and KI cells. Data are presented as mean ± s.e.m. Statistics: paired student's t-test n.s.: not significant

So far, the results suggest that the TRPM7 kinase activity is not linked to basal subcellular NFATc1 distribution. However, whether transcription of NFATc1 is affected by kinase inactivation is not clear. Therefore, I proceeded with the above described dual-luciferase reporter gene assay (see 6.1.5) to investigate NFAT-dependent gene expression in TRPM7 KI overexpressing HEK-293 cells.

6.2.5 Regulatory effect of TRPM7 kinase on NFAT-dependent gene expression

Again, when starting to investigate NFAT transcriptional activity via the above introduced dual-luciferase reporter gene assay (see 6.1.5), I faced the problem of the HAP1 cells being difficult to transfect. Hence, analogues to the experiments with the TRPM7 KO clone (see 6.1.5), I conducted the dual-luciferase reporter gene assay in HEK-293 cells overexpressing the murine TRPM7 KI construct carrying the kinase inactivating point mutation K1646R which is analogous to the K1648R mutation present in the HAP1 TRPM7 KI cell line.

6.2.5.1 Effect of the TRPM7 kinase-dead mutant on NFAT-dependent gene expression using the dual-luciferase NFAT-reporter gene assay in transiently transfected HEK-293 cells

Initially, the effect of the TRPM7 kinase activity on NFAT-dependent gene expression was tested using transient overexpression; accordingly, HEK-293 cells were co-transfected with the NFAT firefly luciferase reporter gene and the expression control luciferase *Renilla* (for more details see 6.1.5), and in addition, either the control vector pcDNA3.1 ('mock') or the GFP-tagged TRPM7 kinase-inactivated construct carrying the point mutation K1646R (herein named TRPM7 KI) was inserted. Data were normalized by relating the firefly luciferase signal to the *Renilla* luciferase signal and TRPM7 KI values were subsequently calculated as percent of mock (set to 100 %). Figure 6.21A illustrates that the expression of kinase-mutated TRPM7 does not significantly alter NFAT transcriptional activity in HEK-293 cells when compared to the control. Direct comparison of this result to the data acquired for the overexpression of TRPM7 WT protein in the dual-luciferase reporter gene assay (see 6.1.5.1) reveals that kinase inactivation significantly impacts the TRPM7 overexpression-promoted NFAT transcriptional activity which was previously reported herein (Figure 6.21D). While TRPM7 WT overexpression augments NFAT-dependent gene expression about ~17 % in HEK-293 cells, TRPM7 KI overexpression has no effect (Figure 6.21D) in comparison to to mock. Accordingly, it seems that TRPM7-directed upregulation of NFAT-driven gene expression requires a functional TRPM7 kinase.

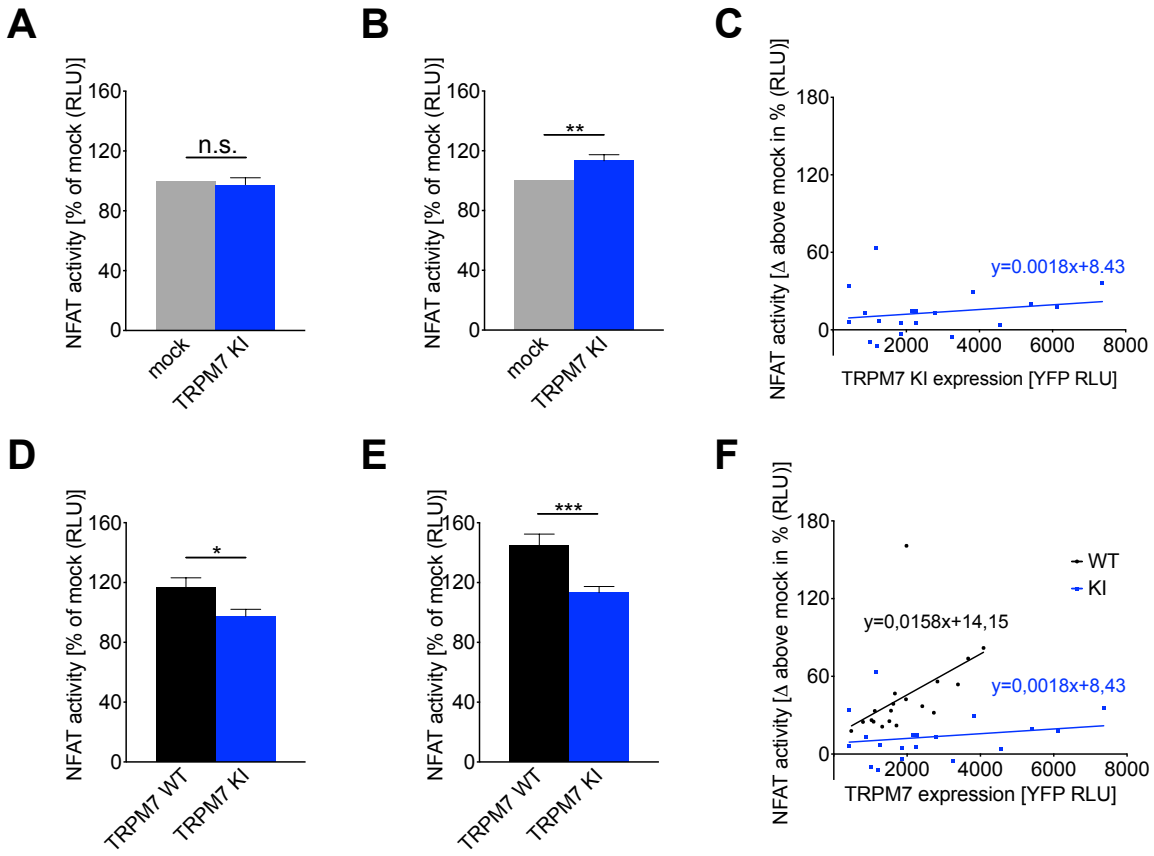

Figure 6.21 NFAT transcriptional activity in TRPM7 WT or KI overexpressing HEK-293 cells. (A) NFAT transcriptional activity in transiently transfected HEK-293 cells co-expressing the NFAT firefly luciferase reporter (500 ng) and the *Renilla* luciferase control vector (50 ng) together with 400 ng pcDNA3.1 as control ('mock', grey) or TRPM7 KI protein ([TRPM7 KI], blue, displayed as percent of mock, n=5). **(B)** NFAT transcriptional activity in the stable HEK-NFAT cell line transiently co-expressing pcDNA3.1 as control ('mock') or TRPM7 KI protein ([TRPM7 KI], displayed as percent of mock, n=19). Amount of transfected TRPM7 KI DNA ranged from 100-1000 ng and was complemented by pcDNA3.1 DNA if necessary to reach a DNA amount of 1000 ng total. **(C)** NFAT transcriptional activity plotted as function of TRPM7 KI expression in the stable HEK-NFAT cell line (n=19). TRMP7 KI data were normalized to the control ('mock', set to 100 %) and subsequently, NFAT activity of the control (which equals 100%) was subtracted from the resulting TRPM7 KI NFAT activity values. Thus, TRPM7-dependent increase in NFAT activity is expressed as 'Δ above mock in %'. Amount of transfected TRPM7 KI DNA ranged from 100-1000 ng and was complemented by pcDNA3.1 DNA if necessary to reach a DNA amount of 1000 ng total. NFAT activity is displayed as RLU of the firefly luciferase substrate oxyluciferin (λ_{max} = 560 nm), and KI data are normalized to mock (set to 100 %)**.** TRPM7 expression is displayed as RLU of GFP (λ_{max} = 509 nm). While ineffective in the transient HEK-293 NFAT reporter cells, mutant TRPM7 overexpression in stable HEK-NFAT cells slightly but significantly elevates NFAT activity in comparison to mock (A and B). Furthermore, NFAT-dependent gene transcription is minimal augmented with increasing TRPM7 expression levels (C). **(D-E)** Direct comparison of NFAT transcriptional activity induced by TRPM7 WT and KI overexpression in (**D**) transiently transfected HEK cells and (**E**) the stable HEK-NFAT cell line (merged from Fig. 6.8 and 6.21A and B, displayed as percent of mock). **(F)** Comparison of the concentration-dependent increase in NFAT activity induced by TRPM7 WT or KI overexpression in stable HEK-NFAT cells (merged from Fig. 6.8 and 6.21C). Statistical analysis shows that TRPM7 kinase-inactivation significantly decreases TRPM7-induced NFAT-dependent gene expression in both transient and stable HEK-293 NFAT reporter cells (D and E). Comparison of the slope describing the TRPM7 concentration dependence of NFAT activity is approximately ten times higher for the TRPM7 WT (0.0158) than for the TRPM7 KI (0.0018) construct (F), substantiating a role for the kinase domain in NFAT-dependent gene expression in HEK-293 cells. Data are presented as mean ± s.e.m. Statistics: paired and unpaired student's t-test * p<0.05; ** p<0.01; *** p<0.005; n.s.: not significant

6.2.5.2 Effect of the TRPM7 kinase-dead mutant on NFAT-dependent gene expression in a stable HEK-293 reporter cell line

As mentioned above, performing the dual-luciferase reporter gene assay in transiently transfected cells necessitates a control measuring the general gene expression rate (here: *Renilla* luciferase), which is predominantly dependent on cell number and transfection rate (see 6.1.5). To be able to exclude this additional control, make measurements more consistent and thus verify the obtained results, the NFAT firefly luciferase reporter gene assay was repeated in the herein generated stable HEK-NFAT reporter cell line overexpressing either the control vector pcDNA3.1 ('mock') or kinase-inactivated TRPM7 (see 6.1.5.2). For analysis, TRPM7 KI data were calculated as percent of mock (set to 100 %).

Surprisingly, introduction of enzymatically inactive TRPM7 in the stable HEK-NFAT reporter cell line only slightly but significantly increases NFAT transcriptional activity by about 13 % (Figure 6.21B). Furthermore, this effect is concentration-dependent, as elevated TRPM7 KI expression – measured via the GFP signal – directly correlates with a raise in NFAT-induced gene expression (Figure 6.21C). However, direct comparison of the results acquired for TRPM7 WT (see 6.1.5.2) *vs.* TRPM7 KI overexpression in the HEK-NFAT reporter cell line reveals that the promotion of NFAT-dependent gene expression by TRPM7 is significantly reduced upon kinase depletion (Figure 6.21E); thus, overexpression of the TRPM7 WT protein increases NFAT transcriptional activity by about 45 % (in comparison to mock, not shown here), whereas TRPM7 KI protein overexpression elevates NFAT-dependent gene expression only by about 13 % (in comparison to mock, not shown here) in HEK-NFAT reporter cells (Figure 6.21E). In addition, correlation of the TRPM7 expression level and NFAT-dependent gene expression which is reflected by the slopes in Figure 6.21F proves to be much higher for TRPM7 WT-transfected than in TRPM7 KI-transfected HEK-NFAT reporter cells (WT: 0.0158, KI: 0.0018).

While the experiments using transient transfection of HEK-293 cells suggest that the kinase function is required for the TRMP7-dependent enhancement of NFAT transcriptional activity, the results acquired with the stable HEK-NFAT cell line indicate that the kinase participates in, but not exclusively controls this TRPM7-directed NFAT transcriptional activation. As mentioned before, NFAT is directly activated by increasing cytosolic Ca^{2+} concentrations (see 6.1.5) [253]. Consequently, the observed increase in NFAT-dependent gene expression induced by the TRPM7 KI mutant (see 6.2.5.2) might be due to an enhanced Ca^{2+} influx through the functional TRPM7 channel. Potential differences in cytosolic Ca^{2+} concentrations could also explain the differential outcomes regarding NFAT nuclear localization (see 6.2.4) in HAP1 TRPM7 KI cells and NFAT transcriptional activity (see 6.2.5) in TRPM7 KI overexpressing HEK-NFAT reporter cells. Hence, I next determined the Ca^{2+} concentrations in TRPM7 KI overexpressing HEK-G5α.

6.2.6 Impact of TRPM7 kinase activity on Ca^{2+} homeostasis in HEK-G5α cells

Congruent to the previously described experiments (see 6.1.6), basal Ca^{2+} levels in HEK-293 cells were obtained with the HEK-G5α cell line stably expressing the Ca^{2+}-binding protein apoaequorin fused to GFP introduced above (see 6.1.6). By CRET from Ca^{2+}-bound apoprotein to GFP, these cells allow relative sensitive measurements of internal Ca^{2+} concentrations (for more details, see 6.1.6).

Figure 6.22A depicts that transient overexpression of the kinase-dead TRPM7 mutant (TRPM7 KI) has no significant impact on the internal Ca^{2+} concentration in comparison to the control vector pcDNA3.1 ('mock') (Figure 6.22A). Direct comparison of this result obtained for the kinase-dead TRPM7 mutant to the results acquired for TRPM7 WT (see 6.1.6) demonstrates that TRPM7 kinase activity is required for TRPM7-induced increase in intracellular Ca^{2+} (Figure 6.22B); while the Ca^{2+} concentration is not (substantially) altered in TRPM7 KI overexpressing HEK-G5α (in comparison to mock, not shown), overexpression of TRPM7 WT significantly raises Ca^{2+} levels by almost 22 % (in comparison to mock, not shown) (Figure 6.22B).

Assuming that in HEK-293 cells the TRPM7-induced effect on NFAT-dependent gene expression is conducted through Ca^{2+} as hypothesized (see 6.1.5), this result is in agreement with the inactivated kinase showing no increase in NFAT transcriptional activity in transient overexpression experiments (see 6.2.5.1). However, it contradicts the slight but significant augmentation of NFAT activity observed for TRPM7 KI overexpression in the stable HEK-NFAT-reporter cell line (see 6.2.5.2).

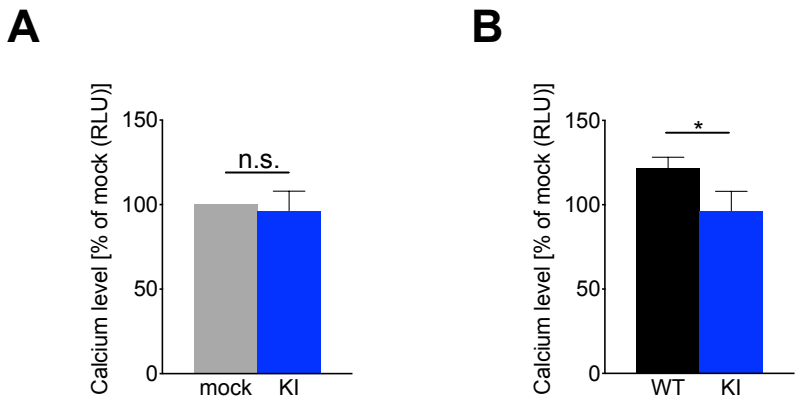

Figure 6.22 Basal Ca^{2+} levels in TRPM7 WT or KI overexpressing HEK-G5α cells. (**A**) Ca^{2+} concentration in mock-transfected (grey) or TRPM7 KI-overexpressing (blue) HEK-G5α cells (n=8). Ca^{2+} concentration is illustrated as RLU of GFP (λ_{max} = 509) and KI data were normalized to mock (set to 100 %). Overexpression of the kinase-depleted TRPM7 protein does not change internal Ca^{2+} concentration in HEK-G5α cells. (**B**) Direct comparison of Ca^{2+} levels in TRPM7 WT or KI overexpressing HEK-G5α cells (merged from Figure 6.9 and 6.22, displayed as percent of mock). While TRPM7 WT overexpression significantly increases intracellular Ca^{2+} concentration in the HEK-G5α cell line in comparison to mock (not shown), TRPM7 KI overexpression has no effect regarding the intracellular Ca^{2+} level. Data are presented as mean ± s.e.m. Statistics: paired and unpaired student's t-test * $p<0.05$; n.s.: not significant

Taken together, the results suggest that TRPM7's kinase activity is required for Ca^{2+} homeostasis in HEK-293 cells and thereby potentially controls NFAT-dependent gene expression.

The finding that kinase activity is required for the TRPM7-directed rise in intracellular Ca^{2+} in HEK-293 cells contradicts the experimental outcome of basal Ca^{2+} analysis in HAP1 TRPM7 KI cells (see 6.2.2), where kinase depletion does not change intracellular Ca^{2+} concentrations (see 6.2.2). Thus, in contrast to HEK-293 cells, TRPM7 kinase activity shows to be dispensable for maintenance of basal internal Ca^{2+} levels in HAP1 cells.

So far, the experiments lead to the conclusion that, although being redundant for basal Ca^{2+} homeostasis and NFATc1 nuclear localization, TRPM7 kinase activity is involved in *COX-2* gene expression in HAP1 cells. Thus, the kinase-induced activation of *COX-2* gene expression seems to occur independently from the transcription factor NFAT. Considering that the previous experiments in the HAP1 TRPM7 KO clone suggest that TRPM7 affects NFAT subcellular localization through promoting phosphorylation of the NFAT export kinase GSK3β (see 6.1.3), one would assume that the TRPM7 kinase inactivation has no impact on GSK3β phosphorylation either. Thus, to investigate this hypothesis and determine through which upstream signaling molecule(s) the TRPM7 kinase activity potentially regulates *COX-2* gene expression, I next analyzed the phosphorylation status of Akt, GSK3β and ERK1/2 in the HAP1 TRPM7 KI mutant.

6.2.7 Effect of the TRPM7 kinase activity on the phosphorylation of cell signaling proteins

As Western Blot analysis via specific phospho-antibodies proofed to be suitable for visualization of Akt, GSK3β and ERK1/2 phosphorylation before (see 6.1.3), this technique was also applied for analysis of the TRPM7 kinase-dead HAP1 clone. Analogues to 6.1.3, cells were cultured with and without FBS for three hours, lysed and analyzed via Western Blotting and ImageJ. For data evaluation, phosphorylation signal intensities of the respective protein were normalized to the signal intensity of the loading control (either GAPDH or LaminB1) and subsequently the results acquired for the TRPM7 KI clone were calculated as percent of WT (set to 100 %). Figure 6.23 illustrates that the kinase has differential effects on all three targets. At first sight, the Akt pSer473 Western Blot shows no alterations between the TRPM7 WT and KI samples, which is mostly due to comparatively low signal intensities (Figure 6.23A, left panel). Evaluation of the bands via ImageJ yet reveals that Akt Ser473 phosphorylation in the HAP1 TRPM7 KI cells is, independently from FBS withdrawal, slightly reduced by ~11-13 % compared to WT (Figure 6.23A, middle panel), but this reduction is only significant for the normally cultured but not for the serum-starved cells (Figure 6.23A, middle panel). In contrast, kinase inactivation significantly enhances GSK3β Ser9 phosphorylation by ~18 % (Figure 6.23B). Comparison of the normally cultured and serum-starved

cells however reveals that this effect is FBS-dependent, as there are no differences detectable between the mutated and wild-type HAP1 TRPM7 clone upon FBS withdrawal (Figure 6.23B, left and middle panel). Thus, in consideration of numerous potential off-target effects of FBS [207], I conclude that the TRPM7 kinase is not involved in GSK3β phosphorylation at Ser9. The last signal transducer I examined was ERK1/2.

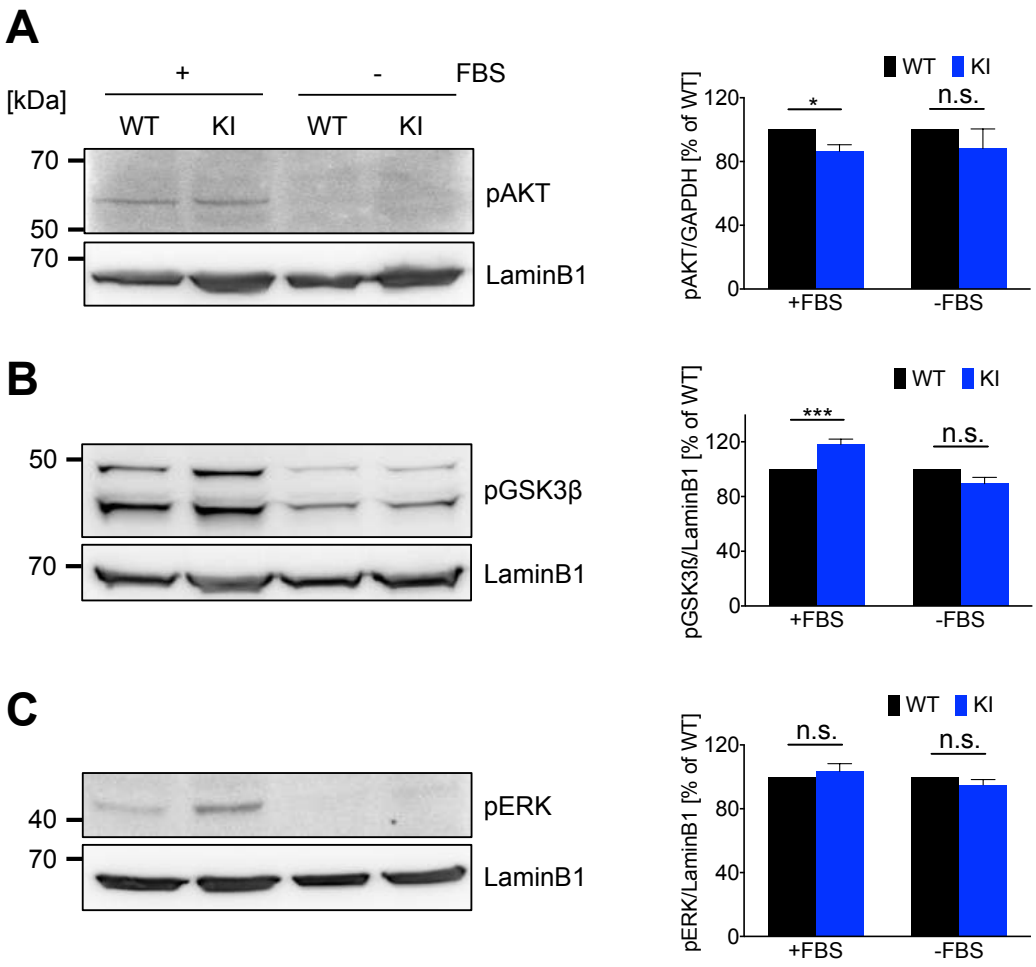

Figure 6.23 Basal phosphorylation levels of cell signaling molecules in HAP1 TRPM7 WT and KI cells. Representative Western Blot images (left panels) and statistical analysis (right panels) of **(A)** AKT pSer473 (pAKT, 60 kDa), **(B)** GSK3β pSer9 (pGSK3β, 47 kDa) and **(C)** ERK1/2 pTyr204 (pERK, 42/44 kDa) in FBS-treated (+) and untreated (-) HAP1 TRPM7 WT and KI cells (n=3-4). Band intensities of each phosphorylation signal was determined via ImageJ and normalized to the loading control LaminB1 (65 kDa). To cancel out larger variances between the individual experiments, KI values are calculated as percent of WT (set to 100 %). Although not directly noticeable in the Western Blot images, statistical evaluation illustrates a significant reduction of pAKT (A) and a highly significant increase of pGSK3β (B) in FBS-treated HAP TRPM7 KI cells when compared to WT, whereas serum starved-samples reveal no differences regarding pAKT and pGSK3β between WT and KI samples (right panels). Also phosphorylation of ERK1/2 (C) is – independently of FBS treatment of the cells – the same in HAP1 TRPM7 WT and KI cells (right panels). Protein size is expressed in kDa. Data are presented as mean ± s.e.m. Statistics: paired student's t-test * $p<0.05$; *** $p<0.005$; n.s.: not significant

Although visual analysis of the Western Blot images might suggest differences, statistical analysis via ImageJ displays that neither for the normally cultured nor serum-starved TRPM7 KI clone, ERK1/2

Tyr204 phosphorylation is altered in comparison to TRPM7 WT (Figure 6.23C, left and middle panel). Taken together, this indicates that the TRPM7 kinase is dispensable for ERK1/2 Tyr204 phosphorylation. In summary, the kinase domain seems to play a significant role in phosphorylation of Akt at Ser473 phosphorylation but neither contributes to GSK3β Ser9 nor to ERK1/2 Tyr204 phosphorylation. With regard to the GSK3β being one of the main kinases priming NFAT for nuclear export [234], this outcome of the phosphorylation analysis of cell signaling kinases is in agreement with about equal NFAT amounts within the nucleus found in HAP1 TRPM7 WT and KI cells (see 6.2.4). If GSK3β is inhibited by phosphorylation at Ser9 [233] in the TRPM7 kinase-mutated HAP1 cells just as much as in the wild-type HAP1 cells, NFAT transport is unchanged. Interestingly, the activation-causing phosphorylation of the prevalent GSK3β upstream kinase Akt at Ser473 slightly decreases upon TRPM7 phosphotransferase inactivation. One would assume that this affects GSK3β as well, but several studies showed that there exist other kinases (such as PKA or PKC) that could compensate for the missing Akt phosphorylation-dependent activation of GSK3β [233, 294-296]. Hence, the findings for Akt and GSK3β are not necessarily contradictory.

6.3 Effect of pharmacological inhibition of the TRPM7 channel and/or kinase on *COX-2* gene expression in neutrophils

Besides trying to elucidate the mechanism behind TRPM7's regulative role in *COX-2* gene expression and enzymatic activity, I wanted to test if TRPM7 represents a pharmacological target for attenuating inducible *COX-2* gene expression. For this approach, I applied the two TRPM7 inhibitors NS8593 and TG100-115 (also see introduction, 3.2.3) to freshly isolated, primary neutrophils to target both the full-length protein as well as its kinase activity only. As TG100-115 also blocks different PI3K isoforms, I additionally used a combination of the two inhibitors IPI-549 and GSK2292767 targeting PI3K-γ and PI3K-δ, respectively, to distinguish TRPM7 kinase and PI3K-specific effects on *COX-2* mRNA production [212, 297, 298]. Furthermore, the solvent DMSO (0.1 %, matching the highest employed drug concentration) served as control. Following a 30 min preincubation with the inhibitors listed above, *COX-2* mRNA production in the neutrophils was induced with the common stimulus LPS. Already low concentrations of this bacterial endotoxin significantly upregulate *COX-2* gene expression and protein expression in neutrophils [213]. Samples were collected after 120 min of stimulation and *COX-2* gene expression was subsequently analyzed via mRNA quantification using RT-qPCR. For comparison, the resulting COX-2 data for each sample was normalized to the respective values for the housekeeping gene *HPRT1* (shown as $2^{(-\Delta CP)}$). Figure 6.24 illustrates that neither DMSO nor any of the drugs (mentioned above) significantly change constitutive *COX-2* mRNA

expression in resting neutrophils. As expected, administration of 10 ng/ml LPS for two hours significantly increases *COX-2* mRNA production in the control (from ~109 to ~370) and the DMSO (from ~94 to ~435) sample around fourfold. Preliminary incubation with 30 µM NS8593 for 30 min attenuates the LPS-caused effect by about half compared to DMSO (from ~88 to 225). Interestingly, kinase-specific inhibition with 20 µM TG100-115 represses LPS-stimulation even more and reduces induced *COX-2* mRNA synthesis to one fifth in comparison to DMSO (from ~65 to ~120). This surprising effect could be explained by the side effect of TG100-115, which – next to the TRPM7

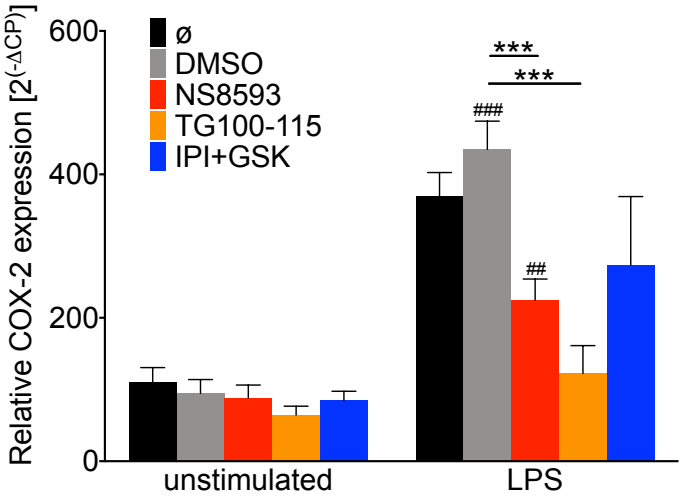

Figure 6.24 LPS-triggered induction of *COX-2* gene expression in primary human neutrophils treated with different TRPM7 inhibitors. Relative *COX-2* gene expression (measured via RT-qPCR) in freshly isolated neutrophils treated with TRPM7 inhibitors. The cells were incubated with one of the following inhibitors: NS8593 (30 µM), TG100-115 (20 µM) or a combination of IPI-549 and GSK2292767 (160 and 100 nM, respectively), DMSO or nothing (ø, control) for 30 min and subsequently stimulated with 10 ng/ml LPS for 120 min (n=4-9). Unstimulated samples (left set of bar graphs) show that plain drug administration without subsequent LPS application has no effect on neutrophilic *COX-2* mRNA levels. LPS-treatment for 120 min on the other hand highly significantly increases *COX-2* mRNA expression in the control, DMSO- and NS8593-treated samples, yet the induction is only about half as high in presence of NS8593 when compared to DMSO. Furthermore, preliminary incubation with the TRPM7-kinase inhibitor TG100-115 almost fully prevents LPS-induced *COX-2* mRNA upregulation in a highly significant manner in comparison to DMSO. However, specific inhibition of the PI3K isoforms PI3K-γ and PI3K-δ demonstrates that part of the TG100-115-caused inhibition of *COX-2* mRNA production is due to the side effects of TG100-115 on those two kinases. In comparison to DMSO, administration of the respective inhibitors IPI-549 (abbreviated IPI) and GSK2292767 (abbreviated GSK) lowers inducible *COX-2* mRNA production about half. Thus, the effect of TG100-115 on LPS-induced *COX-2* mRNA production is not exclusively attributable to its inhibition of the TRPM7 kinase. Data are presented as mean ± s.e.m. Statistics: two-way ANOVA $^{\#\#}$ $p<0.01$, $^{\#\#\#}$ $p<0.005$; unpaired student's t-test *** $p<0.005$

kinase – simultaneously inhibits different PI3K isoforms with a much higher potency. Indeed, blocking both PI3K-γ and PI3K-δ together also counteracts LPS-driven *COX-2* mRNA production, but to a lesser extent than TG100-115, showing about 60 % of the DMSO signal (from ~85 to ~270).

I conclude that the TRPM7 protein plays a significant role in inducible *COX-2* mRNA gene expression in primary neutrophils, with both channel and kinase domain contributing to this regulation. Hence, TRPM7 might represent an interesting target when it comes to pharmacological inhibition of COX-2-mediated inflammatory processes.

7 Discussion

The ubiquitously expressed protein TRPM7 is defined by the unique fusion of an ion channel conducting divalent cations and an alpha-kinase domain phosphorylating serine and threonine residues. Besides being essential for survival, growth and reproduction, the channel-kinase functions in many pathological processes such as tumor development and metastasis, ischemic stroke as well as neurodegenerative and cardiovascular diseases [299]. Developing research shows that, aside from TRPM7's impact on Ca^{2+} and Mg^{2+} homeostasis, the channel-kinase is implicated in numerous cell signaling events (see introduction, 3.2.6). Thus, various studies indicate a fundamental role for the TRPM7 in common signaling pathways such as PI3K/Akt, MAPK/ERK, JAK/STAT or TGF-β/SMAD; yet, the so far presented results are partially contradictory and often do not differentiate between channel and kinase function [45, 83, 151, 155, 160, 169-172, 174, 177, 178, 184].

Given this background, it was my attempt to clarify if and how TRPM7 operates in the signaling cascades mentioned above and thereby discriminate between channel- and/or kinase-directed mechanisms. Moreover, in terms of a TRPM7-dependent control of different signaling pathways, special focus was put on the new discovery of other downstream targets affected by the TRPM7 chanzyme.

Accordingly, the herein presented results depict that the channel-kinase TRPM7 has a significant impact on various cell signaling molecules in immune-derived cell culture (HAP1) cells. Its range of action includes specific channel- and/or kinase-mediated a) phosphorylation of the signal transmitting kinases AKT and GSK3β, b) the nuclear localization of the transcription factor NFAT and, most importantly, c) the regulation of *COX-2* gene expression and enzymatic activity. Separate analysis of the different HAP1 TRPM7 cell models thereby shows that the channel and the kinase unit differentially contribute to these cell signaling events. Remarkably, the promoting effect of TRPM7 on *COX-2* gene expression is also observed for primary immune cells, since pharmacological inhibition of the TRPM7 channel respectively its kinase domain diminishes LPS-induced *COX-2* gene upregulation in neutrophils. In consideration of the pathophysiological background of COX-2, this suggests TRPM7 to be a valuable pharmacological target for future therapy of COX-2-driven diseases. In the following, I will review my results with special regard to domain-specific effects of TRPM7 on different cell signaling events and discuss TRPM7's potential as a pharmacological target for the suppression of COX-2-mediated maladies.

7.1 HAP1 TRPM7 cell models demonstrate to be a suitable tool to study the channel-kinase's function in innate immune cells

Preliminary to the actual experiments focusing on TRPM7's impact on cell signaling, both the HAP1 TRPM7 full-length protein knockout (KO) and the kinase-dead (KI) clone were genetically validated and characterized with respect to their functionality. DNA- respectively cDNA-sequencing of the two HAP1 TRPM7 cell models was able to confirm integrity of the anticipated genetic modifications (see Figures 6.1 and 6.14). In addition, TRPM7 current development was investigated in both HAP1 TRPM7 cell models via the whole-cell patch clamp technique. While lack of the characteristic TRPM7-elicited current in the HAP1 TRPM7 KO clone confirms functional protein extinction [195], annihilation of TRPM7's enzymatic function does not affect channel activity, as current amplitude and kinetics are not significantly altered in HAP1 TRPM7 KI cells compared to WT. This finding reflects the results acquired from TRPM7 kinase inactivation in mice, where the corresponding murine kinase mutation K1646R did not impact channel activity of TRPM7 [118]. Furthermore, phospho-specific Western Blot analysis targeting the TRPM7 autophosphorylation site Ser1511 in HAP1 TRPM7 KI displays that the genetic mutation indeed results in the intended kinase inactivation. Thus, the HAP1 TRPM7 KO model allows studying the role of the full-length protein while the KI model raises the possibility of investigating TRPM7 kinase-specific function(s) only.

7.2 TRPM7 channel moiety is essential for maintenance of Mg^{2+}, Zn^{2+}, but also Cu^{2+} levels in resting cells

At first hand TRPM7 being an ion channel, it was crucial to examine basal ion concentrations in the HAP1 TRPM7 KO and KI clones. Most importantly and in accordance with the literature declaring TRPM7 to be essential for Mg^{2+} homeostasis [34-36], knockout of TRPM7 leads to a significant reduction of the intracellular Mg^{2+} concentration (see Figure 6.2A) in the HAP1 cells. Moreover, culturing the HAP1 cells shows that this drop in internal Mg^{2+} caused by TRPM7 deficiency substantially affects cell cycle progression, as normally cultured HAP1 TRPM7 KO cells go into growth arrest which can be rescued by additional Mg^{2+} supplementation [195]. Together with the studies of Schmitz et al., this emphasizes TRPM7's role for maintenance of cellular Mg^{2+} levels and indicates how TRPM7 controls important cell functions such as proliferation [43]. However, TRPM7's impact on Mg^{2+} levels apparently occurs independently of its phosphotransferase activity, as the HAP1 TRPM7 KI clone does not display any changes regarding their intracellular Mg^{2+} concentration in comparison to WT (see Figure 6.16A). This is in accordance with already published

papers, where the TRPM7 kinase activity showed to be redundant for maintenance of intracellular Mg^{2+} levels [36, 83, 116-118].

Other than observed for Mg^{2+}, Ca^{2+} homeostasis seems to be unaffected by TRPM7 depletion respectively its kinase inactivation, as ICP-MS reveals no significant alterations of Ca^{2+} levels in neither HAP TRPM7 KO nor KI cells (see Figure 6.2B respectively 6.16B). Nevertheless, intracellular Ca^{2+} concentrations are comparably low and ICP-MS resolution is limited, wherefore intracellular Ca^{2+} levels were additionally determined via the Ca^{2+} imaging technique. Yet, measurements with the Ca^{2+}-specific fluorescent dye Fura-2 AM reflect the results acquired with ICP-MS (see Figures 6.3 and 6.17, respectively), which indicates that absence of the TRPM7 channel-kinase or its kinase inactivation do not significantly impact Ca^{2+} household in the HAP1 cells. This is surprising, as TRPM7 is a Ca^{2+} permeable channel and has been shown to function in Ca^{2+}-mediated signaling and activation mechanisms in a channel as well as kinase-dependent manner [49, 119, 138, 291, 292, 300, 301]. However, both ICP-MS and Ca^{2+} imaging experiments were conducted in resting cells, whereas most of the studies claiming TRPM7 and in particular its kinase domain to be relevant for internal Ca^{2+} are based on activated or stimulated cells which require increased Ca^{2+} influx. Hence, although TRPM7 contributes to Ca^{2+}-mediated signaling in activated cells, it might be redundant for maintenance of basal Ca^{2+} levels. In agreement with this notion, several reports show that TRPM7 does not substantially affect resting Ca^{2+} levels, eventually substantiating my findings obtained for the HAP1 cells showing TRPM7 to be dispensable the regulation of basal Ca^{2+} levels [83, 119, 302].

Next to the two main cations Ca^{2+} and Mg^{2+}, I focused on two other divalent ions Zn^{2+} and Cu^{2+} whose concentrations also lay within the evaluable range of the ICP-MS measurements. Being an essential cofactor, Zn^{2+} plays an important role in enzymatic reactions, cell signaling and transcription factor remodeling [227]. Compared to other mono- and divalent cations, Zn^{2+} shows the highest driving force through TRPM7 channel, and several papers have already published TRPM7's contribution to Zn^{2+} transport [51-54, 302]. Thus, the channel-kinase potentiates Zn^{2+}-induced neurotoxicity by promoting Zn^{2+} accumulation in neurons followed by neuronal cell death for example [53, 54]. Furthermore, TRPM7 releases Zn^{2+} from intracellular storage vesicles upon reactive oxygen species (ROS) production and thereby controls cytosolic Zn^{2+} levels and oxidation state(s) [52]. In addition, Clapham et al. hypothesized that the channel and kinase domain work synergistically, as TRPM7 expression increases the intracellular Zn^{2+} concentration whereas the cleaved kinase domain binds to zinc-finger proteins in a Zn^{2+}-dependent manner and thereby activates gene transcription [84]. Substantiating TRPM7's role in Zn^{2+} homeostasis, a very recent paper showed that TRPM7 depletion in HAP1 cells results in a significant decrease of internal Zn^{2+} levels [302]. Furthermore, the same study found that conditional knockout of intestinal, but not renal

TRPM7 results in significantly reduced serum and bone Zn^{2+} levels in mice, indicating that TRPM7 is essential for epithelial transport of Zn^{2+} in the intestine [302]. However, this TRPM7-dependent regulation of organismal Zn^{2+} levels appears to occur separate of its kinase activity, as mutant mice globally expressing a kinase-dead (K1646R) form of TRPM7 reveal no alterations in serum or bone Zn^{2+} concentrations [302].

Compliant with these findings, my investigations show that the internal Zn^{2+} levels are significantly reduced in the HAP1 cells if TRPM7 is absent (see Figure 6.2C). In addition, exploration of the HAP1 TRPM7 KI clone illustrates that TRPM7 most likely controls Zn^{2+} levels through its channel domain, as kinase inactivation has no effect on the internal Zn^{2+} concentration (see Figure 6.16C). Together with the literature, this substantiates the importance of TRPM7 for Zn^{2+} homeostasis, and, corresponding to the already published implications of TRPM7 in Zn^{2+}-mediated events, one could speculate that TRPM7 also affects other processes, e.g. the development and function of the immune, nervous, digestive and skeletal system, by facilitating Zn^{2+} influx [303-305]. Furthermore, although the results suggest the kinase to be redundant for maintenance of Zn^{2+} in resting cells, it does not exclude that TRPM7 kinase-mediated mechanisms rely on Zn^{2+} influx mediated through an active TRPM7 channel domain as Clapham et al. hypothesized [84].

Regarding the trace metal Cu^{2+}, nothing is known yet about the effect of TRPM7 on Cu^{2+} homeostasis; actually, there is not even a proof that Cu^{2+} enters the cell through TRPM7. Nevertheless, the massive reduction of about ~34 % in HAP1 TRPM7 KO (see Figure 6.2D) cells strongly suggests a role of TRPM7 in the maintenance of intracellular Cu^{2+} levels.However, examination of the HAP1 TRPM7 KI cells simultaneously reveals that the TRPM7-dependent control of Cu^{2+} occurs independently of its kinase domain (see Figure 6.16D). Like Zn^{2+}, Cu^{2+} functions as cofactor in enzymatic reactions, mainly enabling redox reactions as present in the respiratory chain or ROS homeostasis [228, 229, 306]. Consequently, by tightly regulating ROS production and elimination, Cu^{2+} is essential for survival, but at the same time Cu^{2+} overload is toxic to eukaryotes [307, 308]. Inherited or evolved dysregulation of the trace element leads to severe syndromes such as Wilson or Menkes disease, neurodegenerative diseases or cancer [309]. Although there is no paper stating a direct connection of TRPM7 and Cu^{2+} yet, some studies hint toward a correlation of TRPM7- and Cu^{2+}-mediated actions. Thus, the channel-kinase has been shown to tightly regulate ROS levels and induces neuronal cell death in dependence of Ca^{2+}, $Mg^{2+}$and Zn^{2+}, indicating that ions entering the cell through the TRPM7 channel contribute to neurodegeneration processes [53, 135, 310]. Accordingly, also Cu^{2+} could be implicated in the TRPM7-dependent balance of ROS and therewith associated diseases.

Given the fact that TRPM7 affects the internal concentrations of Zn^{2+} and Cu^{2+} that both function as essential cofactors, it would be interesting to further evaluate the impact of TRPM7 on metabolic processes relying on Zn^{2+} and/or Cu^{2+} in future studies.

Overall, elemental analysis of both HAP1 TRPM7 KO and KI clone underlines the current understanding of TRPM7 to resemble an essential, non-redundant entry mechanism for Mg^{2+} and Zn^{2+}, whereas it is dispensable for cellular Ca^{2+} uptake under resting conditions. Moreover, the channel-kinase seems to have a significant impact on Cu^{2+} homeostasis, as knockout of TRPM7 results in diminished Cu^{2+} levels. Conclusively, the experiments with the HAP1 TRPM7 KI cells indicate that the observed alterations for Mg^{2+}, Zn^{2+} and Cu^{2+} are due to absence of a functional channel domain, as kinase inactivation has no effect on the influx respectively maintenance of these ions.

7.3 Novel domain-specific role for TRPM7 in COX-2 gene expression and activity

The immunologically relevant enzyme COX-2 is of great importance in mammalians [284, 311, 312]. Despite originally believed to be exclusively expressed upon gene induction, constitutive COX-2 expression has been shown in various organs. Dependent on age, COX-2 is permanently present in tissues including the central nervous system, kidney, intestinal tract and placenta as well as heart, lungs and skin [283, 313-316]. Although COX-2 is not considered to be essential for survival, knockout experiments revealed that only 60 % of mice lacking COX-2 survive postnatal stage [311]. Moreover, viable COX-2-deficient animals often develop severe diseases such as cardiac fibrosis and ischemia, peritonitis or nephropathy (due to organ dysplasia), which emphasizes the importance of the constant expression of COX-2 in these organs [311, 317-319]. Nevertheless, induction of *COX-2* gene expression is just as important, as it is involved in many inflammatory processes and carcinogenesis; correspondingly, gene expression remains aberrantly high in mature cancerous tissues [320-324]. The contribution of COX-2 to these maladies originates from its enzymatic action: Cyclooxygenases initialize PG synthesis through conversion of arachidonic acid to PG H_2 (PGH_2), which is further metabolized into a variety of other lipid compounds [265-267]. Besides regulating elementary physiological functions, these biologically active substances play an important role in immune cell homeostasis and thereby contribute to inflammation as well as inflammation-caused cancer genesis [325-327]. By receptor-specific binding, PGH_2 derivates such as PGE_2 and PGJ_2, for example, function in the proliferation, differentiation and cytokine production of T cells and B cells but also control innate immune reactions by affecting dendritic cells, macrophages and neutrophils. Hence, COX-2 expression serves not only as prognostic marker for different cancer subtypes but also

represents an interesting target for pharmacological treatment of inflammation and tumor progression [326, 328-336].

Interestingly, some papers previously suggested TRPM7 to be implicated in COX-2 expression [91, 337]. Thus, it was shown that TRPM7 promotes COX-2 protein expression in bradykinin-stimulated VSMCs [337]. However, in context of aldosteron-induced signaling, the same group controversially published that TRPM7 attenuates COX-2 protein expression in a kinase-dependent manner in TRPM7-overexpressing HEK-293 cells [91]. Yet, especially the second study lacks profound proof as it was a) was conducted in an overexpression system, thus the observed changes might be caused by compensatory mechanisms and not TRPM7-mediated actions and b) is deficient of adequate controls. Furthermore, both reports draw their conclusion that TRPM7 functions in COX-2 expression by application of the substance 2-APB for validation of TRPM7 specifity. Although this drug is known to block the TRPM7 channel in μM concentrations [71] (also see introduction, 3.2.3), it is very unspecific as it simultaneously affects a broad spectrum of other channels and transport proteins involved in Ca^{2+} homeostasis such as IP_3Rs, SOCCs, SERCA, numerous TRP channels and potassium channels etc. [99, 100, 102-110]. Thus, just because one detects differences upon 2-APB administration, it would be presumptuous to ascribe specific functions to TRPM7, as the inhibitor at the same time targets the above-mentioned molecules and thus very likely causes severe side effects. Accordingly, the observed alterations could be explained via the effect of 2-APB on other channels and transporters regulating intracellular Ca^{2+} concentrations and thus downstream COX-2 expression.

In the present study, I demonstrate that TRPM7 indeed promotes COX-2 gene expression and enzymatic activity in immune cells. Analysis of resting HAP1 cells via RT-qPCR demonstrates that knockout of TRPM7 leads to a significant reduction in constitutive *COX-2* gene expression (see Figure 6.11C). Moreover, stimulation of the HAP1 cells shows that the channel-kinase likewise facilitates inducible *COX-2* gene expression. Administration of forskolin, which increases cAMP levels and thus triggers *COX-2* mRNA production, substantially augments *COX-2* gene expression levels in HAP1 TRPM7 WT cells, whereas no significant change is observed for the HAP1 TRPM7 KO cells (see Figure 6.13). Overall, this forskolin-induced *COX-2* gene upregulation shows to be five times higher if TRPM7 is present. Thus, the channel-kinase is not only essential for constitutive, but also contributes to inducible *COX-2* gene expression.

Incorporating the HAP1 TRPM7 KI model in these studies, it becomes apparent that the kinase activity of TRPM7 carries a central role in the TRPM7-dependent regulation of both constitutive and inducible *COX-2* gene expression. Comparable to the data acquired for the HAP1 TRPM7 KO clone, the HAP1 TRPM7 KI cells express about one third less *COX-2* in comparison to WT under resting conditions (see Figure 6.18). Furthermore, TRPM7 kinase inactivation attenuates forskolin-stimulated

COX-2 gene induction by almost half in HAP1 cells (see Figure 6.19). Correlation of the experimental outcome of the HAP1 TRPM7 WT, KO and KI clone hints towards a TRPM7 kinase-specific regulation of constitutive *COX-2* gene expression, while both channel and kinase mutually control inducible *COX-2* mRNA upregulation.

Intriguingly, further RT-qPCR experiments reveal that this phenotype observed for the HAP1 cells can be mimicked by pharmacological suppression of TRPM7. Primary neutrophils incubated with TRPM7 channel- and/or kinase-specific inhibitors and subsequently stimulated with LPS show significant changes regarding *COX-2* gene induction. Complete block of the TRPM7 channel with NS8593 – which most likely also reduces enzymatic activity of the TRPM7 kinase [119] (also see introduction, 3.2.4) – results in a significant reduction of LPS-induced *COX-2* gene expression by about half when compared to the DSMO control (see Figure 6.24). Interestingly, this repression is even more pronounced if only the TRPM7 kinase is inhibited by administration of TG100-115 (see Figure 6.24). These results are slightly differing from the results obtained with the HAP1 TRPM7 models, where knockout of the full-length protein was more potent to block *COX-2* gene expression than kinase inactivation (compare Figure 6.13 and 6.19). However, application of TG100-115 to neutrophils does not exclusively block the TRPM7 kinase, but primarily inhibits the PI3K isoforms PI3K-γ and PI3K-δ; thus, the results have to be directly compared to the impact of specific PI3K-γ and PI3K-δ inhibitors on inducible *COX-2* gene expression. Corresponding application of the two PI3K inhibitors IPI-549 and GSK2292767 together clearly attenuates the LPS-triggered increase of COX-2 mRNA more than 25 %, but is way less effective than TG100-115. I conclude that part of the TG100-115-caused inhibition of *COX-2* mRNA upregulation by LPS is indeed due to simultaneous PI3K inhibition, as PI3K is known to activate *COX-2* mRNA and protein production through different pathways [338-341]. Nonetheless, this experiment at the same time demonstrates that the observed reduction of *COX-2* gene expression in the TG100-115 treated samples is mainly attributable to pharmacological inhibition of the TRPM7 kinase. Hence, the comprehensive experimental outcome in the neutrophils supports the notion of both the TRPM7 channel and kinase being involved in inducible *COX-2* gene expression.

Given the physiological relevance of COX-2 in different diseases, TRPM7 might represent a valuable pharmacological target for treatment of numerous pathologies such as various types of cancer, Alzheimer's respectively Parkinson's disease, multiple sclerosis and other neurological disorders [269-271, 273]. However, this necessitates that the depletion respectively inactivation of TRPM7 and/or its kinase activity also reduces COX-2 enzymatic activity. Examining the HAP1 cell models regarding the catalytic activity of cyclooxygenases demonstrates that TRPM7 indeed has a significant impact on COX-2-, but also COX-1-mediated substrate conversion. Knockout of TRPM7 in the HAP1 cells

results in a significantly diminished basal COX activity when compared to WT (see Figure 6.12A and B). Further differentiation between the activity of COX-1 and COX-2 shows that the monitored substrate conversion in the HAP1 TRPM7 WT cells is attributable to both isoforms (Figure 6.12C). Linking these results, I conclude that full-length TRPM7 is required for sufficient COX-2 and COX-1-dependent PG synthesis; yet, it remains unclear if this is due to the demonstrated facilitation of *COX-2* gene expression or in some way through directly aiding the conversion process itself.

To unravel if and to what extent the TRPM7 kinase is involved in COX-2 activity, the same fluorometric COX activity assay was conducted in the HAP TRPM7 KI clone. However, this approach did not lead to evaluable results as signal intensities showed to be very low and no cyclooxygenase-specific signal was measureable (results not shown). Thus, kinase impact on basal COX-2 activity still needs to be clarified. One possible experimental setup to do so would be to increase COX-2 protein expression in the HAP1 cells by elevating cAMP levels via administration of forskolin and use these stimulated cell lysates for analysis. Moreover, the neutrophils represent another handy tool to further investigate TRPM7 channel- and/or kinase-specific effects on COX-2 activity. On the one hand, cells could be inhibited with NS8593, TG100-115 and the PI3K inhibitors prior to LPS stimulation (as done when examining inducible *COX-2* gene expression, see Figure 6.24), lysed and subsequently applied to the COX-2 activity assay. Another option is to change the chronological order of the experiment, thus first stimulate the neutrophils with LPS and apply the drugs directly in the COX activity assay. These two experimental setups would kill two birds with one stone, as they a) would clarify the role of TRPM7 respectively its kinase in COX-2 enzymatic activity and b) elucidate if TRPM7's impact on COX-2 activity is just due to upregulating its expression or if TRPM7 directly affects COX-2 enzymatic reactions.

7.4 Cell signaling analysis shows: TRPM7 controls COX-2 through the signaling kinase Akt

Recent work has suggested a role for TRPM7 in cell signaling. The channel-kinase has been shown to operate in prominent pathways such as PI3K/Akt, MAPK/ERK, JAK/STAT and TGF-β/SMAD signaling. However, the individual studies led to partially ambiguous results regarding the exact function of TRPM7, and furthermore, only a few of them differentiated between the impact of the channel and kinase domain throughout the corresponding experiments. Now, given the herewith shown effect of TRPM7 on *COX-2* gene expression and activity and its concomitant potential as an eventual target for attenuation of inflammation, it is of great importance to understand the mechanism behind the TRPM7-dependent regulation of COX-2. Hence, in the following paragraph, I will a) review the observations made for the TRPM7-dependent control of different pathways and b) put these results in context of a possible upstream regulation of COX-2.

Detailed analysis of different signaling pathways in the HAP1 TRPM7 cell models revealed several molecules to be affected by the channel-kinase. An initial comprehensive screen of various cell signaling kinases demonstrated that TRPM7 facilitates site-specific phosphorylation of Akt and GSK3β but not ERK1/2. Total knockout of TRPM7 in the HAP1 cells results in a significant reduction of Akt Ser473 and GSK3β Ser9 phosphorylation, while ERK1/2 Tyr204 phosphorylation remains unaffected (see Figure 6.4). Furthermore, analysis of the HAP1 TRPM7 KI model illustrates that the TRPM7-dependent promotion of Akt Ser473 phosphorylation is at least partially conducted through its kinase domain, as kinase inactivation leads to a small but significant reduction of the corresponding signal (see Figure 6.23). However, the same experiments reveal that the TRPM7 kinase unit is not involved in GSK3β Ser9 phosphorylation, nor does it affect ERK1/2 phosphorylation.

From a mechanistical point of view, the post-translational modification of these molecules has opposing effects; while both Akt (Ser473) and ERK1/2 (Tyr204) are activated upon phosphorylation, phosphorylation of GSK3β (Ser9) results in its inhibition [231, 233, 342]. Taking this information into account, the herein presented results are predominantly congruent with what is known from the literature: TRPM7 has been published to positively regulate PI3K/Akt signaling by triggering Akt phosphorylation which in turn activates other downstream targets such as mTOR [151]. Accordingly, analysis of the phosphorylation status in the HAP1 TRPM7 cell models confirms the importance of TRPM7 for Akt activation. However, I herewith for the first time show that TRPM7 kinase activity is substantively involved in this TRPM7-induced activation of Akt. Moreover, my investigations demonstrate that full-length TRPM7 also inhibits GSK3β by enhancing its phosphorylation at Ser9; yet, this regulation happens independently from its kinase domain.
Importantly, GSK3β itself is a downstream kinase of Akt [343]; thus, the detected diminution in GSK3β Ser9 phosphorylation in absence of TRPM7 (see Figure 6.4) might be directly caused by attenuation of Akt Ser473 phosphorylation. Nevertheless, the decrease in GSK3β Ser9 phosphorylation is not necessarily directly attributable to the reduction of Akt phosphorylation, as its phosphorylation at Ser9 is also regulated by other kinases (e.g. PKA and PKC) and furthermore indirectly controlled by the element lithium (Li^{2+}) [296, 344-346]. Hence, TRPM7 potentially regulates GSK3β activity not through Akt, but instead promotes GSK3β phosphorylation at Ser9 via the activation of PKA and PKC and/or by facilitating Li^{2+} influx.

In terms of MAPK/ERK signaling, TRPM7's role in ERK1/2 activation is controversially discussed: Some groups demonstrated an increase and others a decrease of pERK1/2 signals upon TRPM7 depletion [155, 160, 169-172]. My studies indicate that TRPM7 is not involved in ERK1/2 activation in the HAP1 cells, as ERK1/2 Tyr204 phosphorylation is not affected by knockout or kinase inactivation of TRPM7 (see Figure 6.4 and 6.23). In summary, I conclude that TRPM7's impact on

ERK1/2 is cell type- and stimulus-dependent, and that in resting HAP1 cells, the channel-kinase is dispensable for basal ERK1/2 phosphorylation.

Downstream of the signaling kinases Akt and GSK3β, TRPM7 shows to function in NFAT nuclear localization and transcriptional activity. As mentioned, GSK3β has been shown to determine NFAT-dependent gene transcription; counteracting the Ca^{2+}- activated molecule calcineurin, which is responsible for NFAT dephosphorylation and subsequent nuclear import [347, 348], GSK3β phosphorylates NFAT within its NES and thereby induces its nuclear export [234, 349]. In addition, GSK3β attenuates NFAT transcriptional activity by preventing DNA binding [350, 351]. Thus, the herein observed TRPM7-caused inhibition of GSK3β (see Figure 6.4B) is likely to affect these NFAT parameters. Studying the localization of different NFAT family members in resting HAP1 cells reveals that TRPM7 effectively impacts the cellular distribution of NFATc1 and NFATc3: Knockout of the channel-kinase results in reduced levels of NFATc1 and NFATc3 in the nucleus (see Figure 6.7A). Surprisingly, these reductions are not accompanied by a simultaneous increase of cytosolic NFATc1 and c3 concentrations, as one would expect. This led to the assumption that TRPM7 might affect the total protein expression of these NFAT members; however, analysis of whole-cell lysates indicates that neither NFATc1 nor NFATc3 expression is significantly reduced upon TRPM7 depletion (see Figure 6.7C). Hence, the observed decrease of nuclear NFAT in the HAP1 TRPM7 KO cells is indeed attributable to TRPM7's promoting effect on NFAT nuclear localization and not caused by a TRPM7-dependent alteration of total protein expression of NFAT.

Further investigating the impact of the TRPM7 kinase domain on NFAT nuclear localization in the HAP1 cells shows that the TRPM7-dependent control of nuclear NFATc1 levels occurs separate of its phosphotransferase activity. Thus, depletion of TRPM7 kinase activity does not alter NFATc1 nuclear localization in the HAP1 cells (see Figure 6.20A). Following the hypothesis that TRPM7 affects NFAT through the export kinase GSK3β, this finding is in accordance with the fact that kinase inactivation neither alters GSK3β Ser9 phosphorylation.

Taken together, I presume that the TRPM7 channel-kinase, without its phosphotransferase activity being mandatory, contributes to nuclear NFAT localization through direct or indirect GSK3β phosphorylation in the HAP1 cells. Moreover, a luciferase gene reporter assay in HEK-293 cells shows that TRPM7 also affects NFAT-driven gene expression. In both a transiently transfected as well as in a stable HEK-NFAT reporter cell line, overexpression of TRPM7 WT results in significantly enhanced NFAT transcriptional activity compared to mock (increase of up to ~45 %, see Figure 6.8). Surprisingly, this observed increase in NFAT-driven gene transcription is significantly lower when overexpressing a kinase depleted TRPM7 (TRPM7 KI) vector (increase of ~13 %, see Figure 6.21), indicating that the kinase activity is at least partially required for NFAT induction.

Assuming that NFAT transcriptional activity is directly related to its nuclear localization, these findings stand in contrast to the results obtained for the HAP1 TRPM7 KI cells, which showed no decrease in nuclear NFAT levels compared to WT (see Figure 6.20A). Nevertheless, TRPM7 is a Ca^{2+} permeable channel and NFAT induction strongly depends on Ca^{2+}-dependent calcineurin activation [352]; thus, the increase in NFAT transcriptional activity observed for the transfected HEK-293 cells might be caused by an increased Ca^{2+} influx due to TRPM7 overexpression. Indeed, aequorin-based analysis of Ca^{2+} levels in HEK-G5α cells reveals that overexpression of the TRPM7 WT construct significantly elevates cytosolic Ca^{2+} concentration in HEK-293 cells. Overexpression of the kinase-depleted protein however has no impact on the intracellular Ca^{2+} concentration, which suggests the kinase domain to be relevant for the observed overexpression-induced Ca^{2+} influx. Interestingly, this is in accordance with several recent studies that claim TRPM7's kinase unit to be important for Ca^{2+} homeostasis. Accordingly, TRPM7's phosphotransferase activity was shown to be required for store-operated Ca^{2+} entry (SOCE) activation in TRPM7 overexpressing DT40 B-lymphocytes, murine platelets and activated primary T cells, potentially through targeting stromal interaction molecule (STIM) proteins [119, 138, 291]. In addition, TRPM7's enzymatic domain controls Ca^{2+} store release through thrombin-induced G-protein-coupled receptor signaling [292]. Taken together, the Ca^{2+} experiments in the HEK-G5α cells show that TRPM7 overexpression elevates internal Ca^{2+} levels in a kinase-dependent manner. Correlating these results to the NFAT reporter assay, the observed increase in NFAT transcriptional activity in TRPM7 overexpressing HEK-NFAT reporter cells indeed might be caused by TRPM7's impact on the intracellular Ca^{2+} concentration.

In summary, the NFAT-reporter assay strongly suggests TRPM7 to be implicated in NFAT-dependent gene expression in HEK-293 cells and highlights the kinase domain as an important player in these processes. Thus, the experiments illustrate that TRPM7 elevates NFAT-dependent gene expression in a kinase-dependent manner. However, overexpression of the kinase-dead TRPM7 protein in the stable HEK-NFAT cell line still causes a slight but significant increase in NFAT-dependent gene expression, suggesting that in parts, TRPM7 augments NFAT-dependent gene expression independently of its kinase activity. Hence, although the kinase shows to play a major role in the TRPM7-dependent induction of NFAT, it is not exclusively responsible for its activation. Further examination of the intracellular Ca^{2+} levels in TRPM7-overexpressing HEK-G5α cells reveals that the kinase-dependent increase of NFAT-dependent gene expression is most likely attributable to a kinase-dependent elevation of the internal Ca^{2+} levels, while the small but existent kinase-independent induction of NFAT occurs separately from altering Ca^{2+} concentrations. Considering that TRPM7 kinase depletion had no effect on the internal resting Ca^{2+} concentration in HAP1 cells, the results acquired for HEK-293 cells can't be directly transferred to HAP1 cells, as TRPM7

overexpression apparently causes Ca^{2+} concentrations and possibly also other parameters to change that distort the results.

Overall, my investigations show that TRPM7 promotes phosphorylation of the cell signaling kinases Akt and GSK3β and furthermore facilitates nuclear accumulation of the transcription factor NFAT. While the TRPM7-dependent Akt Ser473 phosphorylation is partially conducted through an active kinase domain, neither GSK3β nor NFAT are affected by TRPM7's phosphotransferase activity. Relating these results to the differential effect of the TRPM7 channel and/or kinase on COX-2, I hypothesize that TRPM7 presumably controls *COX-2* gene expression and enzymatic activity through two different pathways:

In the first place, the TRPM7-dependent enhancement of *COX-2* gene expression is mediated through the Akt-GSK3β -NFAT signaling axis (see Figure 7.1A). Full-length TRPM7 augments phosphorylation of both Akt at Ser473 and GSK3β at Ser9, thus causing Akt activation respectively GSK3β inhibition. The TRPM7-dependent block of GSK3β evokes nuclear accumulation of NFAT, which, according to the literature, in turn activates constitutive as well as inducible *COX-2* gene expression [260, 261]. Moreover, increased gene expression is most likely accompanied by escalated protein expression, which would explain why TRPM7 also promotes COX-2 enzymatic activity; however, the experiments are not eligible to tell if the observed increase in substrate conversion is due to augmented protein expression or potentially caused by a direct interaction of COX-2 and TRPM7.

Reviewing the results with focus on the TRPM7 kinase domain demonstrates that the channel-kinase seems to additionally control *COX-2* gene expression through an alternative route. As shown by the RT-qPCR experiments, TRPM7 kinase activity is required for constitutive *COX-2* gene expression and furthermore also participates in inducible *COX-2* gene expression (see Figure 6.18 and 6.19, respectively). Yet, analysis of the HAP1 TRPM7 KI cells simultaneously reveals that the kinase unit is redundant for GSK3β phosphorylation and NFAT nuclear localization, indicating that the TRPM7 kinase activity regulates *COX-2* gene expression apart from these two molecules. Instead, aligning the results acquired for the molecule Akt in the HAP1 cells with the current literature illustrates that the TRPM7 kinase domain potentially promotes *COX-2* gene expression through the cell signaling kinase Akt. Thus, HAP1 TRPM7 KI cells display a significant decrease in the activation-causing Akt Ser473 phosphorylation. However, several papers have shown that Akt significantly affects *COX-2* gene expression: as being part of the PI3K/Akt signaling pathway, Akt regulates *COX-2* gene expression through the transcription factors nuclear factor kappa-light-chain-enhancer of activated B cells (NFκB) and CREB, and attenuation in Akt phosphorylation results in decreased NFκB nuclear translocation and thus diminished COX-2 induction [353-359]. Interestingly, recent studies

demonstrate that TRPM7 functions in both activation and translocation of these Akt downstream targets NFκB and CREB. Schappe et al. for example showed that in bone marrow-derived macrophages (BMDMs), TRPM7 is necessitated for LPS-stimulated NFκB p65 phosphorylation initiating its nuclear translocation [360]. Moreover, an *in vitro* kinase assay identified CREB to be a potent substrate of the TRPM7 kinase [115]. In accordance, Ogata et al. demonstrated that the TRPM7 kinase unit promotes phosphorylation and thereby activation of CREB during teeth maturation in mice [361]. Overall, these findings substantiate the hypothesis that the observed TRPM7 kinase-dependent augmentation of *COX-2* gene expression is caused by the activation of Akt which initiates a signaling cascade along the transcription factors NFκB and/or CREB (see Figure 7.1B). Nevertheless, it can't be excluded that the TRPM7 kinase potentially affects *COX-2* gene expression by directly targeting nuclear structures that regulate transcriptional activity. According to Clapham et al., the TRPM7 C-terminus enclosing its kinase domain is truncated, translocates to the nucleus and eventually contributes to the expression of specific genes by histone H3 modification [84] (also see introduction, 3.2.6). Likewise, this mechanism could also apply for the HAP1 cells, implying that the enhanced *COX-2* gene expression results from the direct interaction of the truncated TRPM7 kinase domain with corresponding histones in the nucleus (see Figure 7.1B).

Hence, my studies not only uncover TRPM7 to be an important player in *COX-2* gene induction but furthermore indicate that the channel-kinase controls *COX-2* gene expression through more than one pathway. Together with the current literature, the experiments strongly suggest that TRPM7 promotes *COX-2* gene expression through the central molecule Akt, which further activates different downstream targets. On the one hand, the TRPM7-dependent activation of Akt induces inhibition of NFAT export kinase GSK3β, and the resultant nuclear accumulation of NFAT contributes to *COX-2* gene expression. On the other hand, I hypothesize that the TRPM7-induced phosphorylation of Akt stimulates activation and nuclear translocation of the transcription factors NFκB and CREB which again promote *COX-2* gene expression. Most importantly, only the latter postulated Akt – NFκB/CREB – COX-2 cascade relies on TRPM7 kinase activity, whereas signaling along the Akt – GSK3β – NFAT – COX-2 axis occurs independently of the TRPM7 kinase domain. As I propose that TRPM7 presents a promising pharmacological target for the inhibition of COX-2-mediated inflammation and cancer, it is of great importance to further elucidate the mechanisms through which TRPM7 controls COX-2, as this knowledge will help to predict respectively reduce the risk of potential drug side effects.

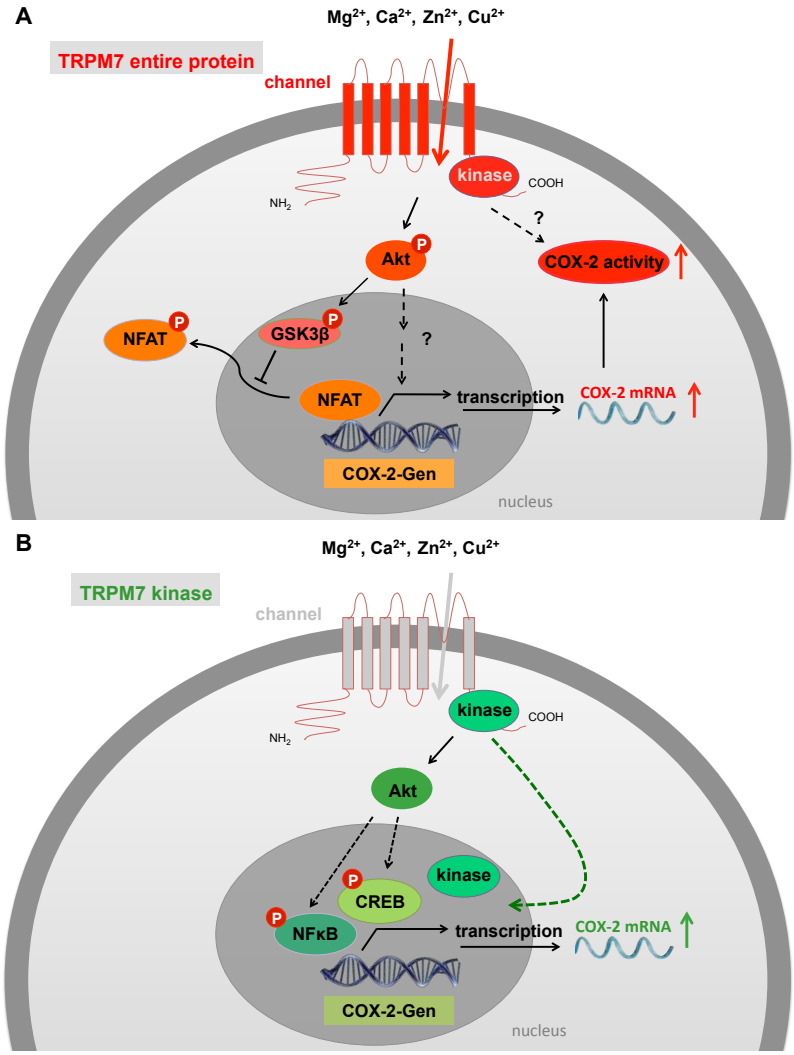

Figure 7.1 Working model for the TRPM7-dependent regulation of *COX-2* gene expression and enzymatic activity in respect to the impact of TRPM7's kinase activity.
(A) Full-length TRPM7 promotes *COX-2* gene expression and activity via the cell signaling molecules Akt, GSK3β and NFAT. TRPM7 facilitates phosphorylation of the signaling kinase Akt (Ser473) and its downstream target GSK3β (Ser9), thus causing activation of Akt respectively inhibition of GSK3β. The phosphorylation-induced block of GSK3β leads to nuclear accumulation of the transcription factor NFAT, which in turn activates the transcription of *COX-2*. The resulting increase in COX-2 mRNA production is accompanied by enhanced COX-2 enzymatic activity. However, it remains unclear if the observed elevation of COX-2 activity is due to the upregulated *COX-2* gene and thus protein expression or if TRPM7 facilitates COX-2-mediated enzymatic reactions through direct interaction with the enzyme. Moreover, it can't be excluded that Akt stimulates *COX-2* gene expression by affecting other signaling molecules promoting *COX-2* gene expression.
(**B**) **The TRPM7 kinase-dependent regulation of *COX-2* gene expression occurs through Akt which is known to control the activity of the transcription factors CREB and NFκB.**Although the TRPM7 kinase domain significantly contributes to TRPM7-induced *COX-2* mRNA production by enhancing the phosphorylation of Akt (Ser473), this does not occur through the signaling molecules GSK3β or NFAT, as kinase inactivation has no impact on GSK3β phosphorylation or NFAT nuclear translocation. However, aligning these results with the current literature, one might speculate that TRPM7 kinase activity potentially controls *COX-2* gene expression by activation of Akt which in turn stimulates the transcription factors NFκB and CREB, thereby initiating *COX-2* gene transcription.
Alternatively, the TRPM7 kinase might stimulate *COX-2* mRNA production by directly interacting with nuclear components. As described by Clapham and coworkers, the C-terminus of TRPM7 enclosing the kinase domain can be truncated and translocate to the nucleus where the kinase then is able to induce transcription of selected genes by histone modification.

Herein demonstrated regulations are indicated by solid lines; currently unknown regulatory mechanisms are indicated by dotted lines; inhibitory actions are indicated by a blunt arrow; activating actions are indicated by a pointed arrow; the green dotted line hints to the translocation of the kinase unit into the nucleus; red arrows point to an increase in COX-2 mRNA transcription and elevated enzmyatic activity, respectively.

7.5 Perspective: TRPM7 kinase as a potential pharmacological target for attenuating COX-2-driven diseases

Corresponding to its clinical relevance, search for COX-2 inhibitors started as early as in the seventies, when the non-steroidal anti-inflammatory drug (NSAID) aspirin showed to effectively block PG synthesis [362]. With evolving research, more and more beneficial actions of NSAIDs came to light, wherefore they found broad use in therapy. Unfortunately, increasing administration also unmasked that classical NSAIDs comprise severe adverse effects, including risk elevation for gastrointestinal injuries, cardiovascular diseases and, dependent on predispositions, renal dysfunction [363, 364]. Primarily believed to be caused by simultaneous inhibition of the second present cyclooxygenase isoform COX-1, side effects were to be reduced by improving NSAIDs to selectively inhibit COX-2 [365]. But despite all efforts, most of these new pharmaceuticals also show some of the side effects observed with the classical, non-selective NSAID (nsNSAID) administration [365-368]. In many cases, these new substances called 'coxibs' negatively affect cardiorenal function, reproductive actions and thrombotic events [365-368]. Hence, to successfully treat respectively prevent inflammation and cancer, existing drugs have to be further developed but also other targeting strategies should be considered [369].

Although there was a vague indication that TRPM7 functions in COX-2 gene expression in terms of bradykinin- and aldosterone-directed signaling [91, 337], I herewith for the first time present that depletion or inhibition of TRPM7 respectively its kinase activity lead to a significant reduction in constitutive and inducible *COX-2* gene expression. Furthermore, preliminary experiments demonstrate that the channel-kinase – directly or indirectly – also impacts COX-2 catalytic function.

Hence, the discovery of both the TRPM7 channel and kinase positively regulating COX-2 expression and activity offers great potential for future therapy. However, TRPM7 essentially contributes to many physiological processes, which raises the possibility of the pharmacological block of the channel-kinase causing severe side effects [120]. Judging by the outcome of various TRPM7 knockout respectively kinase inactivation studies, I hypothesize that exclusively targeting the TRPM7 kinase domain represents the more decent option, as its actions are more limited and thus the risk of potential adverse reactions might be reduced [35, 45, 117, 118, 291, 370]. Yet, the only better investigated TRPM7 kinase-specific inhibitor on the market so far is TG100-115, and although it has been tested for therapeutical use in a phase II clinical study in terms of it being a PI3K blocker, it is not yet known if it is safe to apply in humans [371, 372]. Thus, besides screening for other drugs specifically inhibiting the TRPM7 kinase domain, further studies will have to show if therapeutic

TG100-115 application is feasible in mammals and if it is of use for attenuation of TRPM7 kinase-triggered COX-2 expression and activity.

8 References

1. Clapham, D.E., *TRP channels as cellular sensors.* Nature, 2003. **426**(6966): p. 517-24.
2. Nadolni, W. and S. Zierler, *The Channel-Kinase TRPM7 as Novel Regulator of Immune System Homeostasis.* Cells, 2018. **7**(8).
3. Montell, C. and G.M. Rubin, *Molecular characterization of the Drosophila trp locus: a putative integral membrane protein required for phototransduction.* Neuron, 1989. **2**(4): p. 1313-23.
4. Hardie, R.C. and B. Minke, *The trp gene is essential for a light-activated Ca2+ channel in Drosophila photoreceptors.* Neuron, 1992. **8**(4): p. 643-51.
5. Wes, P.D., et al., *TRPC1, a human homolog of a Drosophila store-operated channel.* Proc Natl Acad Sci U S A, 1995. **92**(21): p. 9652-6.
6. Zhu, X., et al., *Molecular cloning of a widely expressed human homologue for the Drosophila trp gene.* FEBS Lett, 1995. **373**(3): p. 193-8.
7. Nilius, B., *TRP channels in disease.* Biochim Biophys Acta, 2007. **1772**(8): p. 805-12.
8. Montell, C., *The TRP superfamily of cation channels.* Sci STKE, 2005. **2005**(272): p. re3.
9. Venkatachalam, K. and C. Montell, *TRP channels.* Annu Rev Biochem, 2007. **76**: p. 387-417.
10. Ramsey, I.S., M. Delling, and D.E. Clapham, *An introduction to TRP channels.* Annu Rev Physiol, 2006. **68**: p. 619-47.
11. Saimi, Y. and C. Kung, *Calmodulin as an ion channel subunit.* Annu Rev Physiol, 2002. **64**: p. 289-311.
12. Tang, J., et al., *Identification of common binding sites for calmodulin and inositol 1,4,5-trisphosphate receptors on the carboxyl termini of trp channels.* J Biol Chem, 2001. **276**(24): p. 21303-10.
13. Montell, C., L. Birnbaumer, and V. Flockerzi, *The TRP channels, a remarkably functional family.* Cell, 2002. **108**(5): p. 595-8.
14. Zheng, J., *Molecular mechanism of TRP channels.* Compr Physiol, 2013. **3**(1): p. 221-42.
15. Storch, U., et al., *Transient receptor potential channel 1 (TRPC1) reduces calcium permeability in heteromeric channel complexes.* J Biol Chem, 2012. **287**(5): p. 3530-40.
16. Dong, X.P., X. Wang, and H. Xu, *TRP channels of intracellular membranes.* J Neurochem, 2010. **113**(2): p. 313-28.
17. Chubanov, V., L. Mittermeier, and T. Gudermann, *Role of kinase-coupled TRP channels in mineral homeostasis.* Pharmacol Ther, 2018. **184**: p. 159-176.
18. Nilius, B., et al., *Transient receptor potential cation channels in disease.* Physiol Rev, 2007. **87**(1): p. 165-217.
19. Yue, Z., et al., *Role of TRP channels in the cardiovascular system.* Am J Physiol Heart Circ Physiol, 2015. **308**(3): p. H157-82.
20. Gees, M., B. Colsoul, and B. Nilius, *The role of transient receptor potential cation channels in Ca2+ signaling.* Cold Spring Harb Perspect Biol, 2010. **2**(10): p. a003962.
21. Owsianik, G., et al., *Permeation and selectivity of TRP channels.* Annu Rev Physiol, 2006. **68**: p. 685-717.
22. Yeh, B.I., et al., *Conformational changes of pore helix coupled to gating of TRPV5 by protons.* EMBO J, 2005. **24**(18): p. 3224-34.
23. Drews A, L.S., Mohr F, Rizun O, Lambert S, Oberwinkler J, *The fractional calcium current through fast ligand-gated TRPM channels*, in *Acta Physiologica, Joint Meeting of the Scandinavian and German Physiological Societies*. 2010: Copenhagen, Denmark.

24. Earley, S., B.J. Waldron, and J.E. Brayden, *Critical role for transient receptor potential channel TRPM4 in myogenic constriction of cerebral arteries.* Circ Res, 2004. **95**(9): p. 922-9.
25. Brayden, J.E., et al., *Transient receptor potential (TRP) channels, vascular tone and autoregulation of cerebral blood flow.* Clin Exp Pharmacol Physiol, 2008. **35**(9): p. 1116-20.
26. Hagenacker, T., et al., *Sensitization of voltage activated calcium channel currents for capsaicin in nociceptive neurons by tumor-necrosis-factor-alpha.* Brain Res Bull, 2010. **81**(1): p. 157-63.
27. Wu, Z.Z., S.R. Chen, and H.L. Pan, *Signaling mechanisms of down-regulation of voltage-activated Ca2+ channels by transient receptor potential vanilloid type 1 stimulation with olvanil in primary sensory neurons.* Neuroscience, 2006. **141**(1): p. 407-19.
28. Vennekens, R., et al., *Increased IgE-dependent mast cell activation and anaphylactic responses in mice lacking the calcium-activated nonselective cation channel TRPM4.* Nat Immunol, 2007. **8**(3): p. 312-20.
29. Kwan, H.Y., et al., *TRPC1 associates with BK(Ca) channel to form a signal complex in vascular smooth muscle cells.* Circ Res, 2009. **104**(5): p. 670-8.
30. Kim, E.Y., C.P. Alvarez-Baron, and S.E. Dryer, *Canonical transient receptor potential channel (TRPC)3 and TRPC6 associate with large-conductance Ca2+-activated K+ (BKCa) channels: role in BKCa trafficking to the surface of cultured podocytes.* Mol Pharmacol, 2009. **75**(3): p. 466-77.
31. Rohacs, T., *Regulation of transient receptor potential channels by the phospholipase C pathway.* Adv Biol Regul, 2013. **53**(3): p. 341-55.
32. Mandadi, S., P.J. Armati, and B.D. Roufogalis, *Protein kinase C modulation of thermo-sensitive transient receptor potential channels: Implications for pain signaling.* J Nat Sci Biol Med, 2011. **2**(1): p. 13-25.
33. Bouron, A., K. Kiselyov, and J. Oberwinkler, *Permeation, regulation and control of expression of TRP channels by trace metal ions.* Pflugers Arch, 2015. **467**(6): p. 1143-64.
34. Nadler, M.J., et al., *LTRPC7 is a Mg.ATP-regulated divalent cation channel required for cell viability.* Nature, 2001. **411**(6837): p. 590-5.
35. Ryazanova, L.V., et al., *TRPM7 is essential for Mg(2+) homeostasis in mammals.* Nat Commun, 2010. **1**: p. 109.
36. Schmitz, C., et al., *Regulation of vertebrate cellular Mg2+ homeostasis by TRPM7.* Cell, 2003. **114**(2): p. 191-200.
37. Walder, R.Y., et al., *Mice defective in Trpm6 show embryonic mortality and neural tube defects.* Hum Mol Genet, 2009. **18**(22): p. 4367-75.
38. Schlingmann, K.P., et al., *Hypomagnesemia with secondary hypocalcemia is caused by mutations in TRPM6, a new member of the TRPM gene family.* Nat Genet, 2002. **31**(2): p. 166-70.
39. Walder, R.Y., et al., *Mutation of TRPM6 causes familial hypomagnesemia with secondary hypocalcemia.* Nat Genet, 2002. **31**(2): p. 171-4.
40. Voets, T., et al., *TRPM6 forms the Mg2+ influx channel involved in intestinal and renal Mg2+ absorption.* J Biol Chem, 2004. **279**(1): p. 19-25.
41. Fonfria, E., et al., *Tissue distribution profiles of the human TRPM cation channel family.* J Recept Signal Transduct Res, 2006. **26**(3): p. 159-78.
42. Chubanov, V., et al., *Disruption of TRPM6/TRPM7 complex formation by a mutation in the TRPM6 gene causes hypomagnesemia with secondary hypocalcemia.* Proc Natl Acad Sci U S A, 2004. **101**(9): p. 2894-9.

43. Schmitz, C., et al., *The channel kinases TRPM6 and TRPM7 are functionally nonredundant.* J Biol Chem, 2005. **280**(45): p. 37763-71.
44. Ferioli, S., et al., *TRPM6 and TRPM7 differentially contribute to the relief of heteromeric TRPM6/7 channels from inhibition by cytosolic Mg2+ and Mg.ATP.* Sci Rep, 2017. **7**(1): p. 8806.
45. Jin, J., et al., *Deletion of Trpm7 disrupts embryonic development and thymopoiesis without altering Mg2+ homeostasis.* Science, 2008. **322**(5902): p. 756-60.
46. Duncan, L.M., et al., *Down-regulation of the novel gene melastatin correlates with potential for melanoma metastasis.* Cancer Res, 1998. **58**(7): p. 1515-20.
47. Chen, X., *Localization and Functional Analysis of the Calcium Permeable Melastatin-like Channel TRPM3*, in *Institut für Pharmakologie und Toxikologie, Medizin*. 2009, Philipps-Universität Marburg.
48. Pedersen, S.F., G. Owsianik, and B. Nilius, *TRP channels: an overview.* Cell Calcium, 2005. **38**(3-4): p. 233-52.
49. Penner, R. and A. Fleig, *The Mg2+ and Mg(2+)-nucleotide-regulated channel-kinase TRPM7.* Handb Exp Pharmacol, 2007(179): p. 313-28.
50. Winding, P. and M.W. Berchtold, *The chicken B cell line DT40: a novel tool for gene disruption experiments.* J Immunol Methods, 2001. **249**(1-2): p. 1-16.
51. Monteilh-Zoller, M.K., et al., *TRPM7 provides an ion channel mechanism for cellular entry of trace metal ions.* J Gen Physiol, 2003. **121**(1): p. 49-60.
52. Abiria, S.A., et al., *TRPM7 senses oxidative stress to release Zn2+ from unique intracellular vesicles.* Proc Natl Acad Sci U S A, 2017. **114**(30): p. E6079-E6088.
53. Inoue, K., D. Branigan, and Z.G. Xiong, *Zinc-induced neurotoxicity mediated by transient receptor potential melastatin 7 channels.* J Biol Chem, 2010. **285**(10): p. 7430-9.
54. Kim, Y., et al., *Stress hormone potentiates Zn(2+)-induced neurotoxicity via TRPM7 channel in dopaminergic neuron.* Biochem Biophys Res Commun, 2016. **470**(2): p. 362-367.
55. Li, M., et al., *Molecular determinants of Mg2+ and Ca2+ permeability and pH sensitivity in TRPM6 and TRPM7.* J Biol Chem, 2007. **282**(35): p. 25817-30.
56. Romani, A.M. and A. Scarpa, *Regulation of cellular magnesium.* Front Biosci, 2000. **5**: p. D720-34.
57. Beis, I. and E.A. Newsholme, *The contents of adenine nucleotides, phosphagens and some glycolytic intermediates in resting muscles from vertebrates and invertebrates.* Biochem J, 1975. **152**(1): p. 23-32.
58. Schumacher, M.A., et al., *The structural mechanism of GTP stabilized oligomerization and catalytic activation of the Toxoplasma gondii uracil phosphoribosyltransferase.* Proc Natl Acad Sci U S A, 2002. **99**(1): p. 78-83.
59. Demeuse, P., R. Penner, and A. Fleig, *TRPM7 channel is regulated by magnesium nucleotides via its kinase domain.* J Gen Physiol, 2006. **127**(4): p. 421-34.
60. Prakriya, M. and R.S. Lewis, *CRAC channels: activation, permeation, and the search for a molecular identity.* Cell Calcium, 2003. **33**(5-6): p. 311-21.
61. Zhang, Z., et al., *The TRPM6 kinase domain determines the Mg.ATP sensitivity of TRPM7/M6 heteromeric ion channels.* J Biol Chem, 2014. **289**(8): p. 5217-27.
62. Chubanov, V., et al., *Hypomagnesemia with secondary hypocalcemia due to a missense mutation in the putative pore-forming region of TRPM6.* J Biol Chem, 2007. **282**(10): p. 7656-67.
63. Yu, H., et al., *TRPM7 is regulated by halides through its kinase domain.* Cell Mol Life Sci, 2013. **70**(15): p. 2757-71.

64. Kozak, J.A., et al., *Charge screening by internal pH and polyvalent cations as a mechanism for activation, inhibition, and rundown of TRPM7/MIC channels.* J Gen Physiol, 2005. **126**(5): p. 499-514.
65. Runnels, L.W., L. Yue, and D.E. Clapham, *The TRPM7 channel is inactivated by PIP(2) hydrolysis.* Nat Cell Biol, 2002. **4**(5): p. 329-36.
66. Ryazanov, A.G., K.S. Pavur, and M.V. Dorovkov, *Alpha-kinases: a new class of protein kinases with a novel catalytic domain.* Curr Biol, 1999. **9**(2): p. R43-5.
67. Pinna, L.A. and M. Ruzzene, *How do protein kinases recognize their substrates?* Biochim Biophys Acta, 1996. **1314**(3): p. 191-225.
68. Runnels, L.W., *TRPM6 and TRPM7: A Mul-TRP-PLIK-cation of channel functions.* Curr Pharm Biotechnol, 2011. **12**(1): p. 42-53.
69. Riazanova, L.V., et al., *[Novel type of signaling molecules: protein kinases covalently linked to ion channels].* Mol Biol (Mosk), 2001. **35**(2): p. 321-32.
70. Yamaguchi, H., et al., *Crystal structure of the atypical protein kinase domain of a TRP channel with phosphotransferase activity.* Mol Cell, 2001. **7**(5): p. 1047-57.
71. Li, M., J. Jiang, and L. Yue, *Functional characterization of homo- and heteromeric channel kinases TRPM6 and TRPM7.* J Gen Physiol, 2006. **127**(5): p. 525-37.
72. Drennan, D. and A.G. Ryazanov, *Alpha-kinases: analysis of the family and comparison with conventional protein kinases.* Prog Biophys Mol Biol, 2004. **85**(1): p. 1-32.
73. Ryazanova, L.V., et al., *Characterization of the protein kinase activity of TRPM7/ChaK1, a protein kinase fused to the transient receptor potential ion channel.* J Biol Chem, 2004. **279**(5): p. 3708-16.
74. Kim, T.Y., et al., *Identification of the phosphorylation sites on intact TRPM7 channels from mammalian cells.* Biochem Biophys Res Commun, 2012. **417**(3): p. 1030-4.
75. Clark, K., et al., *Massive autophosphorylation of the Ser/Thr-rich domain controls protein kinase activity of TRPM6 and TRPM7.* PLoS One, 2008. **3**(3): p. e1876.
76. Brandao, K., et al., *TRPM6 kinase activity regulates TRPM7 trafficking and inhibits cellular growth under hypomagnesic conditions.* Cell Mol Life Sci, 2014. **71**(24): p. 4853-67.
77. Cai, N., et al., *Mass Spectrometric Analysis of TRPM6 and TRPM7 Phosphorylation Reveals Regulatory Mechanisms of the Channel-Kinases.* Sci Rep, 2017. **7**: p. 42739.
78. Zhang, J., et al., *Conformational preference of ChaK1 binding peptides: a molecular dynamics study.* PMC Biophys, 2010. **3**(1): p. 2.
79. Dorovkov, M.V. and A.G. Ryazanov, *Phosphorylation of annexin I by TRPM7 channel-kinase.* J Biol Chem, 2004. **279**(49): p. 50643-6.
80. Deason-Towne, F., A.L. Perraud, and C. Schmitz, *Identification of Ser/Thr phosphorylation sites in the C2-domain of phospholipase C gamma2 (PLCgamma2) using TRPM7-kinase.* Cell Signal, 2012. **24**(11): p. 2070-5.
81. Clark, K., et al., *The alpha-kinases TRPM6 and TRPM7, but not eEF-2 kinase, phosphorylate the assembly domain of myosin IIA, IIB and IIC.* FEBS Lett, 2008. **582**(20): p. 2993-7.
82. Clark, K., et al., *TRPM7 regulates myosin IIA filament stability and protein localization by heavy chain phosphorylation.* J Mol Biol, 2008. **378**(4): p. 790-803.
83. Romagnani, A., et al., *TRPM7 kinase activity is essential for T cell colonization and alloreactivity in the gut.* Nat Commun, 2017. **8**(1): p. 1917.
84. Krapivinsky, G., et al., *The TRPM7 chanzyme is cleaved to release a chromatin-modifying kinase.* Cell, 2014. **157**(5): p. 1061-72.
85. Gerke, V., C.E. Creutz, and S.E. Moss, *Annexins: linking Ca2+ signalling to membrane dynamics.* Nat Rev Mol Cell Biol, 2005. **6**(6): p. 449-61.

86. Morand, E.F., et al., *Detection of intracellular lipocortin 1 in human leukocyte subsets.* Clin Immunol Immunopathol, 1995. **76**(2): p. 195-202.
87. Mulla, A., et al., *Correlation between the antiinflammatory protein annexin 1 (lipocortin 1) and serum cortisol in subjects with normal and dysregulated adrenal function.* J Clin Endocrinol Metab, 2005. **90**(1): p. 557-62.
88. Rhen, T. and J.A. Cidlowski, *Antiinflammatory action of glucocorticoids--new mechanisms for old drugs.* N Engl J Med, 2005. **353**(16): p. 1711-23.
89. Wein, S., et al., *Mediation of annexin 1 secretion by a probenecid-sensitive ABC-transporter in rat inflamed mucosa.* Biochem Pharmacol, 2004. **67**(6): p. 1195-202.
90. Perretti, M., et al., *Annexin I is stored within gelatinase granules of human neutrophil and mobilized on the cell surface upon adhesion but not phagocytosis.* Cell Biol Int, 2000. **24**(3): p. 163-74.
91. Yogi, A., et al., *Aldosterone signaling through transient receptor potential melastatin 7 cation channel (TRPM7) and its alpha-kinase domain.* Cell Signal, 2013. **25**(11): p. 2163-75.
92. Dorovkov, M.V., A.S. Kostyukova, and A.G. Ryazanov, *Phosphorylation of annexin A1 by TRPM7 kinase: a switch regulating the induction of an alpha-helix.* Biochemistry, 2011. **50**(12): p. 2187-93.
93. Zhao, Y., et al., *Following OGD/R, annexin 1 nuclear translocation and subsequent induction of apoptosis in neurons are assisted by myosin IIA in a TRPM7 kinase-dependent manner.* Mol Neurobiol, 2015. **51**(2): p. 729-42.
94. Krendel, M. and M.S. Mooseker, *Myosins: tails (and heads) of functional diversity.* Physiology (Bethesda), 2005. **20**: p. 239-51.
95. Clark, K., et al., *TRPM7, a novel regulator of actomyosin contractility and cell adhesion.* EMBO J, 2006. **25**(2): p. 290-301.
96. Guilbert, A., et al., *Transient receptor potential melastatin 7 is involved in oestrogen receptor-negative metastatic breast cancer cells migration through its kinase domain.* Eur J Cancer, 2013. **49**(17): p. 3694-707.
97. Vines, C.M., *Phospholipase C.* Adv Exp Med Biol, 2012. **740**: p. 235-54.
98. Desai, B.N., et al., *Cleavage of TRPM7 releases the kinase domain from the ion channel and regulates its participation in Fas-induced apoptosis.* Dev Cell, 2012. **22**(6): p. 1149-62.
99. Bilmen, J.G. and F. Michelangeli, *Inhibition of the type 1 inositol 1,4,5-trisphosphate receptor by 2-aminoethoxydiphenylborate.* Cell Signal, 2002. **14**(11): p. 955-60.
100. Chokshi, R., P. Fruasaha, and J.A. Kozak, *2-aminoethyl diphenyl borinate (2-APB) inhibits TRPM7 channels through an intracellular acidification mechanism.* Channels (Austin), 2012. **6**(5): p. 362-9.
101. Chubanov, V., et al., *Natural and Synthetic Modulators of the TRPM7 Channel.* Cells, 2014. **3**(4): p. 1089-101.
102. Bilmen, J.G., et al., *Inhibition of SERCA Ca2+ pumps by 2-aminoethoxydiphenyl borate (2-APB). 2-APB reduces both Ca2+ binding and phosphoryl transfer from ATP, by interfering with the pathway leading to the Ca2+-binding sites.* Eur J Biochem, 2002. **269**(15): p. 3678-87.
103. Gregory, R.B., G. Rychkov, and G.J. Barritt, *Evidence that 2-aminoethyl diphenylborate is a novel inhibitor of store-operated Ca2+ channels in liver cells, and acts through a mechanism which does not involve inositol trisphosphate receptors.* Biochem J, 2001. **354**(Pt 2): p. 285-90.
104. Iwasaki, H., et al., *2-Aminoethoxydiphenyl borate (2-APB) inhibits capacitative calcium entry independently of the function of inositol 1,4,5-trisphosphate receptors.* Receptors Channels, 2001. **7**(6): p. 429-39.

105. Togashi, K., H. Inada, and M. Tominaga, *Inhibition of the transient receptor potential cation channel TRPM2 by 2-aminoethoxydiphenyl borate (2-APB).* Br J Pharmacol, 2008. **153**(6): p. 1324-30.
106. Xu, S.Z., et al., *Block of TRPC5 channels by 2-aminoethoxydiphenyl borate: a differential, extracellular and voltage-dependent effect.* Br J Pharmacol, 2005. **145**(4): p. 405-14.
107. Prakriya, M. and R.S. Lewis, *Separation and characterization of currents through store-operated CRAC channels and Mg2+-inhibited cation (MIC) channels.* J Gen Physiol, 2002. **119**(5): p. 487-507.
108. Lievremont, J.P., G.S. Bird, and J.W. Putney, Jr., *Mechanism of inhibition of TRPC cation channels by 2-aminoethoxydiphenylborane.* Mol Pharmacol, 2005. **68**(3): p. 758-62.
109. Pena, F. and B. Ordaz, *Non-selective cation channel blockers: potential use in nervous system basic research and therapeutics.* Mini Rev Med Chem, 2008. **8**(8): p. 812-9.
110. Ma, K.T., et al., *2-Aminoethoxydiphenyl borate blocks electrical coupling and inhibits voltage-gated K+ channels in guinea pig arteriole cells.* Am J Physiol Heart Circ Physiol, 2011. **300**(1): p. H335-46.
111. Strobaek, D., et al., *Inhibitory gating modulation of small conductance Ca2+-activated K+ channels by the synthetic compound (R)-N-(benzimidazol-2-yl)-1,2,3,4-tetrahydro-1-naphtylamine (NS8593) reduces afterhyperpolarizing current in hippocampal CA1 neurons.* Mol Pharmacol, 2006. **70**(5): p. 1771-82.
112. Chubanov, V., et al., *Natural and synthetic modulators of SK (K(ca)2) potassium channels inhibit magnesium-dependent activity of the kinase-coupled cation channel TRPM7.* Br J Pharmacol, 2012. **166**(4): p. 1357-76.
113. Zierler, S., et al., *Waixenicin A inhibits cell proliferation through magnesium-dependent block of transient receptor potential melastatin 7 (TRPM7) channels.* J Biol Chem, 2011. **286**(45): p. 39328-35.
114. Qin, X., et al., *Sphingosine and FTY720 are potent inhibitors of the transient receptor potential melastatin 7 (TRPM7) channels.* Br J Pharmacol, 2013. **168**(6): p. 1294-312.
115. Song, C., et al., *Identification of TG100-115 as a new and potent TRPM7 kinase inhibitor, which suppresses breast cancer cell migration and invasion.* Biochim Biophys Acta, 2017. **1861**(4): p. 947-957.
116. Matsushita, M., et al., *Channel function is dissociated from the intrinsic kinase activity and autophosphorylation of TRPM7/ChaK1.* J Biol Chem, 2005. **280**(21): p. 20793-803.
117. Ryazanova, L.V., et al., *Elucidating the role of the TRPM7 alpha-kinase: TRPM7 kinase inactivation leads to magnesium deprivation resistance phenotype in mice.* Sci Rep, 2014. **4**: p. 7599.
118. Kaitsuka, T., et al., *Inactivation of TRPM7 kinase activity does not impair its channel function in mice.* Sci Rep, 2014. **4**: p. 5718.
119. Faouzi, M., et al., *The TRPM7 channel kinase regulates store-operated calcium entry.* J Physiol, 2017. **595**(10): p. 3165-3180.
120. Yee, N.S., *Role of TRPM7 in Cancer: Potential as Molecular Biomarker and Therapeutic Target.* Pharmaceuticals (Basel), 2017. **10**(2).
121. Park, H.S., et al., *The Pathophysiologic Roles of TRPM7 Channel.* Korean J Physiol Pharmacol, 2014. **18**(1): p. 15-23.
122. Gao, S.L., et al., *TRPM7 is overexpressed in bladder cancer and promotes proliferation, migration, invasion and tumor growth.* Oncol Rep, 2017. **38**(4): p. 1967-1976.
123. Chen, L., et al., *Downregulation of TRPM7 suppressed migration and invasion by regulating epithelial-mesenchymal transition in prostate cancer cells.* Med Oncol, 2017. **34**(7): p. 127.

124. Kim, B.J. and C. Hong, *Role of transient receptor potential melastatin type 7 channel in gastric cancer.* Integr Med Res, 2016. **5**(2): p. 124-130.
125. Greenman, C., et al., *Patterns of somatic mutation in human cancer genomes.* Nature, 2007. **446**(7132): p. 153-8.
126. Dai, Q., et al., *The relation of magnesium and calcium intakes and a genetic polymorphism in the magnesium transporter to colorectal neoplasia risk.* Am J Clin Nutr, 2007. **86**(3): p. 743-51.
127. Shen, B., et al., *The association between single-nucleotide polymorphisms of TRPM7 gene and breast cancer in Han Population of Northeast China.* Med Oncol, 2014. **31**(7): p. 51.
128. Hermosura, M.C., et al., *A TRPM7 variant shows altered sensitivity to magnesium that may contribute to the pathogenesis of two Guamanian neurodegenerative disorders.* Proc Natl Acad Sci U S A, 2005. **102**(32): p. 11510-5.
129. Jin, J., et al., *The channel kinase, TRPM7, is required for early embryonic development.* Proc Natl Acad Sci U S A, 2012. **109**(5): p. E225-33.
130. Brauchi, S., et al., *TRPM7 facilitates cholinergic vesicle fusion with the plasma membrane.* Proc Natl Acad Sci U S A, 2008. **105**(24): p. 8304-8.
131. Krapivinsky, G., et al., *The TRPM7 ion channel functions in cholinergic synaptic vesicles and affects transmitter release.* Neuron, 2006. **52**(3): p. 485-96.
132. Low, S.E., et al., *TRPM7 is required within zebrafish sensory neurons for the activation of touch-evoked escape behaviors.* J Neurosci, 2011. **31**(32): p. 11633-44.
133. Decker, A.R., et al., *Abnormal differentiation of dopaminergic neurons in zebrafish trpm7 mutant larvae impairs development of the motor pattern.* Dev Biol, 2014. **386**(2): p. 428-39.
134. Turlova, E., et al., *TRPM7 Regulates Axonal Outgrowth and Maturation of Primary Hippocampal Neurons.* Mol Neurobiol, 2016. **53**(1): p. 595-610.
135. Aarts, M., et al., *A key role for TRPM7 channels in anoxic neuronal death.* Cell, 2003. **115**(7): p. 863-77.
136. Sun, H.S., et al., *Suppression of hippocampal TRPM7 protein prevents delayed neuronal death in brain ischemia.* Nat Neurosci, 2009. **12**(10): p. 1300-7.
137. Chen, W., et al., *TRPM7 inhibitor carvacrol protects brain from neonatal hypoxic-ischemic injury.* Mol Brain, 2015. **8**: p. 11.
138. Gotru, S.K., et al., *TRPM7 (Transient Receptor Potential Melastatin-Like 7 Channel) Kinase Controls Calcium Responses in Arterial Thrombosis and Stroke in Mice.* Arterioscler Thromb Vasc Biol, 2017.
139. Touyz, R.M., et al., *Differential regulation of transient receptor potential melastatin 6 and 7 cation channels by ANG II in vascular smooth muscle cells from spontaneously hypertensive rats.* Am J Physiol Regul Integr Comp Physiol, 2006. **290**(1): p. R73-8.
140. He, Y., et al., *Transient receptor potential melastatin 7 ion channels regulate magnesium homeostasis in vascular smooth muscle cells: role of angiotensin II.* Circ Res, 2005. **96**(2): p. 207-15.
141. Yu, Y., et al., *TRPM7 is involved in angiotensin II induced cardiac fibrosis development by mediating calcium and magnesium influx.* Cell Calcium, 2014. **55**(5): p. 252-60.
142. Sah, R., et al., *Timing of myocardial trpm7 deletion during cardiogenesis variably disrupts adult ventricular function, conduction, and repolarization.* Circulation, 2013. **128**(2): p. 101-14.
143. Sah, R., et al., *Ion channel-kinase TRPM7 is required for maintaining cardiac automaticity.* Proc Natl Acad Sci U S A, 2013. **110**(32): p. E3037-46.

144. Antunes, T.T., et al., *Transient Receptor Potential Melastatin 7 Cation Channel Kinase: New Player in Angiotensin II-Induced Hypertension.* Hypertension, 2016. **67**(4): p. 763-73.
145. Zhang, K., et al., *Interleukin-18 Enhances Vascular Calcification and Osteogenic Differentiation of Vascular Smooth Muscle Cells Through TRPM7 Activation.* Arterioscler Thromb Vasc Biol, 2017. **37**(10): p. 1933-1943.
146. Guo, J.L., et al., *Transient receptor potential melastatin 7 (TRPM7) contributes to H2O2-induced cardiac fibrosis via mediating Ca(2+) influx and extracellular signal-regulated kinase 1/2 (ERK1/2) activation in cardiac fibroblasts.* J Pharmacol Sci, 2014. **125**(2): p. 184-92.
147. Du, J., et al., *TRPM7-mediated Ca2+ signals confer fibrogenesis in human atrial fibrillation.* Circ Res, 2010. **106**(5): p. 992-1003.
148. Fresno Vara, J.A., et al., *PI3K/Akt signalling pathway and cancer.* Cancer Treat Rev, 2004. **30**(2): p. 193-204.
149. Vrenken, K.S., et al., *Beyond ion-conduction: Channel-dependent and -independent roles of TRP channels during development and tissue homeostasis.* Biochim Biophys Acta, 2016. **1863**(6 Pt B): p. 1436-46.
150. Chang, F., et al., *Involvement of PI3K/Akt pathway in cell cycle progression, apoptosis, and neoplastic transformation: a target for cancer chemotherapy.* Leukemia, 2003. **17**(3): p. 590-603.
151. Sahni, J. and A.M. Scharenberg, *TRPM7 ion channels are required for sustained phosphoinositide 3-kinase signaling in lymphocytes.* Cell Metab, 2008. **8**(1): p. 84-93.
152. Zhang, X., et al., *Ion channel functional protein kinase TRPM7 regulates Mg ions to promote the osteoinduction of human osteoblast via PI3K pathway: In vitro simulation of the bone-repairing effect of Mg-based alloy implant.* Acta Biomater, 2017. **63**: p. 369-382.
153. Lu, D., et al., *Ca2+/Mg2+ homeostasisrelated TRPM7 channel mediates chondrocyte hypertrophy via regulation of the PI3KAkt signaling pathway.* Mol Med Rep, 2017. **16**(4): p. 5699-5705.
154. Fang, L., et al., *TRPM7 channel regulates PDGF-BB-induced proliferation of hepatic stellate cells via PI3K and ERK pathways.* Toxicol Appl Pharmacol, 2013. **272**(3): p. 713-25.
155. Chen, W.L., et al., *Xyloketal B suppresses glioblastoma cell proliferation and migration in vitro through inhibiting TRPM7-regulated PI3K/Akt and MEK/ERK signaling pathways.* Mar Drugs, 2015. **13**(4): p. 2505-25.
156. Chen, W.L., et al., *Inhibition of TRPM7 by carvacrol suppresses glioblastoma cell proliferation, migration and invasion.* Oncotarget, 2015. **6**(18): p. 16321-40.
157. Luo, Y., et al., *Carvacrol Alleviates Prostate Cancer Cell Proliferation, Migration, and Invasion through Regulation of PI3K/Akt and MAPK Signaling Pathways.* Oxid Med Cell Longev, 2016. **2016**: p. 1469693.
158. Cao, R., et al., *Decreased TRPM7 inhibits activities and induces apoptosis of bladder cancer cells via ERK1/2 pathway.* Oncotarget, 2016. **7**(45): p. 72941-72960.
159. Wang, J., et al., *TRPM7 is required for ovarian cancer cell growth, migration and invasion.* Biochem Biophys Res Commun, 2014. **454**(4): p. 547-53.
160. Meng, X., et al., *TRPM7 mediates breast cancer cell migration and invasion through the MAPK pathway.* Cancer Lett, 2013. **333**(1): p. 96-102.
161. Zhang, W. and H.T. Liu, *MAPK signal pathways in the regulation of cell proliferation in mammalian cells.* Cell Res, 2002. **12**(1): p. 9-18.

162. Sun, Y., et al., *Signaling pathway of MAPK/ERK in cell proliferation, differentiation, migration, senescence and apoptosis.* J Recept Signal Transduct Res, 2015. **35**(6): p. 600-4.
163. Cox, J.A., *Calcium-calmodulin interaction and cellular function.* J Cardiovasc Pharmacol, 1986. **8 Suppl 8**: p. S48-51.
164. Lodish H, B.A., Zipursky SL, et al., *Molecular Cell Biology. 4th edition. Chapter 20, Cell-to-Cell Signaling: Hormones and Receptors*. 2000, New York: W.H. Freeman.
165. Nairn, A.C. and M.R. Picciotto, *Calcium/calmodulin-dependent protein kinases.* Semin Cancer Biol, 1994. **5**(4): p. 295-303.
166. Tanaka, T., *Calmodulin-dependent calcium signal transduction.* Jpn J Pharmacol, 1988. **46**(2): p. 101-7.
167. Schmitt, J.M., et al., *Calcium activation of ERK mediated by calmodulin kinase I.* J Biol Chem, 2004. **279**(23): p. 24064-72.
168. Cargnello, M. and P.P. Roux, *Activation and function of the MAPKs and their substrates, the MAPK-activated protein kinases.* Microbiol Mol Biol Rev, 2011. **75**(1): p. 50-83.
169. Inoue, K. and Z.G. Xiong, *Silencing TRPM7 promotes growth/proliferation and nitric oxide production of vascular endothelial cells via the ERK pathway.* Cardiovasc Res, 2009. **83**(3): p. 547-57.
170. Lin, J., et al., *TRPM7 channel regulates ox-LDL-induced proliferation and migration of vascular smooth muscle cells via MEK-ERK pathways.* FEBS Lett, 2016. **590**(4): p. 520-32.
171. Zeng, Z., et al., *Silencing TRPM7 in mouse cortical astrocytes impairs cell proliferation and migration via ERK and JNK signaling pathways.* PLoS One, 2015. **10**(3): p. e0119912.
172. Sun, Y., et al., *Cholesterol-induced activation of TRPM7 regulates cell proliferation, migration, and viability of human prostate cells.* Biochim Biophys Acta, 2014. **1843**(9): p. 1839-50.
173. Wang, L., et al., *'Tuning' of type I interferon-induced Jak-STAT1 signaling by calcium-dependent kinases in macrophages.* Nat Immunol, 2008. **9**(2): p. 186-93.
174. Davis, F.M., et al., *Induction of epithelial-mesenchymal transition (EMT) in breast cancer cells is calcium signal dependent.* Oncogene, 2014. **33**(18): p. 2307-16.
175. Ihle, J.N., *The Stat family in cytokine signaling.* Curr Opin Cell Biol, 2001. **13**(2): p. 211-7.
176. Williams, J.G., *STAT signalling in cell proliferation and in development.* Curr Opin Genet Dev, 2000. **10**(5): p. 503-7.
177. Liu, M., et al., *TRPM7 channels regulate glioma stem cell through STAT3 and Notch signaling pathways.* Cell Signal, 2014. **26**(12): p. 2773-81.
178. Qin, Y., et al., *Functional characterization of TRPM7 in nasopharyngeal carcinoma and its knockdown effects on tumorigenesis.* Tumour Biol, 2016. **37**(7): p. 9273-83.
179. Liu, A., et al., *Regulation of TRPM7 Function by IL-6 through the JAK2-STAT3 Signaling Pathway.* PLoS One, 2016. **11**(3): p. e0152120.
180. Kretzschmar, M. and J. Massague, *SMADs: mediators and regulators of TGF-beta signaling.* Curr Opin Genet Dev, 1998. **8**(1): p. 103-11.
181. Yan, X., X. Xiong, and Y.G. Chen, *Feedback regulation of TGF-beta signaling.* Acta Biochim Biophys Sin (Shanghai), 2018. **50**(1): p. 37-50.
182. Weiss, A. and L. Attisano, *The TGFbeta superfamily signaling pathway.* Wiley Interdiscip Rev Dev Biol, 2013. **2**(1): p. 47-63.
183. Li, M.O., et al., *Transforming growth factor-beta regulation of immune responses.* Annu Rev Immunol, 2006. **24**: p. 99-146.

184. Fang, L., et al., *TGF-beta1-elevated TRPM7 channel regulates collagen expression in hepatic stellate cells via TGF-beta1/Smad pathway.* Toxicol Appl Pharmacol, 2014. **280**(2): p. 335-44.
185. Krapivinsky, G., et al., *Histone phosphorylation by TRPM6's cleaved kinase attenuates adjacent arginine methylation to regulate gene expression.* Proc Natl Acad Sci U S A, 2017. **114**(34): p. E7092-E7100.
186. Sandberg, A.A., et al., *Chromosomes and causation of human cancer and leukemia. L. Cytogenetics of leukemias complicating other diseases.* Cancer Genet Cytogenet, 1982. **7**(2): p. 95-136.
187. Kotecki, M., P.S. Reddy, and B.H. Cochran, *Isolation and characterization of a near-haploid human cell line.* Exp Cell Res, 1999. **252**(2): p. 273-80.
188. Li, Y. and L. Shuai, *A versatile genetic tool: haploid cells.* Stem Cell Res Ther, 2017. **8**(1): p. 197.
189. Wutz, A., *Haploid animal cells.* Development, 2014. **141**(7): p. 1423-6.
190. Jinek, M., et al., *A programmable dual-RNA-guided DNA endonuclease in adaptive bacterial immunity.* Science, 2012. **337**(6096): p. 816-21.
191. Doudna, J.A. and E. Charpentier, *Genome editing. The new frontier of genome engineering with CRISPR-Cas9.* Science, 2014. **346**(6213): p. 1258096.
192. Carette, J.E., et al., *Ebola virus entry requires the cholesterol transporter Niemann-Pick C1.* Nature, 2011. **477**(7364): p. 340-3.
193. Essletzbichler, P., et al., *Megabase-scale deletion using CRISPR/Cas9 to generate a fully haploid human cell line.* Genome Res, 2014. **24**(12): p. 2059-65.
194. Chubanov, V., L. Mittermeier, and T. Gudermann, *Role of kinase-coupled TRP channels in mineral homeostasis.* Pharmacol Ther, 2017.
195. Chubanov, V., et al., *Epithelial magnesium transport by TRPM6 is essential for prenatal development and adult survival.* Elife, 2016. **5**.
196. Baubet, V., et al., *Chimeric green fluorescent protein-aequorin as bioluminescent Ca2+ reporters at the single-cell level.* Proc Natl Acad Sci U S A, 2000. **97**(13): p. 7260-5.
197. Hofmann, T., et al., *Activation of TRPM7 channels by small molecules under physiological conditions.* Pflugers Arch, 2014. **466**(12): p. 2177-89.
198. Nurmio, M., et al., *Peritubular myoid cells have a role in postnatal testicular growth.* Spermatogenesis, 2012. **2**(2): p. 79-87.
199. Shelton, L. and J.S. Rada, *Effects of cyclic mechanical stretch on extracellular matrix synthesis by human scleral fibroblasts.* Exp Eye Res, 2007. **84**(2): p. 314-22.
200. Chen, Y.C., et al., *Norcantharidin reduced cyclins and cytokines production in human peripheral blood mononuclear cells.* Life Sci, 2009. **84**(7-8): p. 218-26.
201. Sztiller-Sikorska, M., et al., *Natural compounds' activity against cancer stem-like or fast-cycling melanoma cells.* PLoS One, 2014. **9**(3): p. e90783.
202. Solinski, H.J., et al., *Human Mas-related G protein-coupled receptors-X1 induce chemokine receptor 2 expression in rat dorsal root ganglia neurons and release of chemokine ligand 2 from the human LAD-2 mast cell line.* PLoS One, 2013. **8**(3): p. e58756.
203. Graham, F.L., et al., *Characteristics of a human cell line transformed by DNA from human adenovirus type 5.* J Gen Virol, 1977. **36**(1): p. 59-74.
204. Lin, Y.C., et al., *Genome dynamics of the human embryonic kidney 293 lineage in response to cell biology manipulations.* Nat Commun, 2014. **5**: p. 4767.
205. Janeway CA Jr, T.P., Walport M, et al., *Immunobiology: The Immune System in Health and Disease. 5th edition. The components of the immune system.* . 5th edition ed. 2001, New York: Garland Science.

206. Strober, W., *Trypan blue exclusion test of cell viability.* Curr Protoc Immunol, 2001. **Appendix 3**: p. Appendix 3B.
207. Gstraunthaler, G., *Alternatives to the use of fetal bovine serum: serum-free cell culture.* ALTEX, 2003. **20**(4): p. 275-81.
208. Riley, L.K. and J. Rupert, *Evaluation of Patients with Leukocytosis.* Am Fam Physician, 2015. **92**(11): p. 1004-11.
209. Perez-de-Heredia, F., et al., *Influence of sex, age, pubertal maturation and body mass index on circulating white blood cell counts in healthy European adolescents-the HELENA study.* Eur J Pediatr, 2015. **174**(8): p. 999-1014.
210. Kuhns, D.B., et al., *Isolation and Functional Analysis of Human Neutrophils.* Curr Protoc Immunol, 2015. **111**: p. 7 23 1-16.
211. Doukas, J., et al., *Aerosolized phosphoinositide 3-kinase gamma/delta inhibitor TG100-115 [3-[2,4-diamino-6-(3-hydroxyphenyl)pteridin-7-yl]phenol] as a therapeutic candidate for asthma and chronic obstructive pulmonary disease.* J Pharmacol Exp Ther, 2009. **328**(3): p. 758-65.
212. Doukas, J., et al., *Phosphoinositide 3-kinase gamma/delta inhibition limits infarct size after myocardial ischemia/reperfusion injury.* Proc Natl Acad Sci U S A, 2006. **103**(52): p. 19866-71.
213. Maloney, C.G., et al., *Inflammatory agonists induce cyclooxygenase type 2 expression by human neutrophils.* J Immunol, 1998. **160**(3): p. 1402-10.
214. Cadieux, J.S., et al., *Potentiation of neutrophil cyclooxygenase-2 by adenosine: an early anti-inflammatory signal.* J Cell Sci, 2005. **118**(Pt 7): p. 1437-47.
215. Mazia, D., G. Schatten, and W. Sale, *Adhesion of cells to surfaces coated with polylysine. Applications to electron microscopy.* J Cell Biol, 1975. **66**(1): p. 198-200.
216. Neher, E., *Correction for liquid junction potentials in patch clamp experiments.* Methods Enzymol, 1992. **207**: p. 123-31.
217. Grynkiewicz, G., M. Poenie, and R.Y. Tsien, *A new generation of Ca2+ indicators with greatly improved fluorescence properties.* J Biol Chem, 1985. **260**(6): p. 3440-50.
218. Rio, D.C., et al., *Purification of RNA using TRIzol (TRI reagent).* Cold Spring Harb Protoc, 2010. **2010**(6): p. pdb prot5439.
219. Simms D., C.P., Chomczynski P., *TRIzol: a new reagent for optimal single-step isolation of RNA.* Focus, 1993. **15**(4).
220. Barbas, C.F., 3rd, et al., *Quantitation of DNA and RNA.* CSH Protoc, 2007. **2007**: p. pdb ip47.
221. Bustin, S.A., *Absolute quantification of mRNA using real-time reverse transcription polymerase chain reaction assays.* J Mol Endocrinol, 2000. **25**(2): p. 169-93.
222. https://www.horizondiscovery.com/media/datasheets/HZGHC002483c004_DataSheet.pdf.
223. Taylor, A.L., *What we talk about when we talk about capacitance measured with the voltage-clamp step method.* J Comput Neurosci, 2012. **32**(1): p. 167-75.
224. Golowasch, J., et al., *Membrane capacitance measurements revisited: dependence of capacitance value on measurement method in nonisopotential neurons.* J Neurophysiol, 2009. **102**(4): p. 2161-75.
225. Sutton, K.L. and J.A. Caruso, *Liquid chromatography-inductively coupled plasma mass spectrometry.* J Chromatogr A, 1999. **856**(1-2): p. 243-58.
226. Figueroa, J.A., et al., *Metal ion transport quantified by ICP-MS in intact cells.* Sci Rep, 2016. **6**: p. 20551.
227. Maret, W., *Zinc biochemistry: from a single zinc enzyme to a key element of life.* Adv Nutr, 2013. **4**(1): p. 82-91.
228. Baker, Z.N., P.A. Cobine, and S.C. Leary, *The mitochondrion: a central architect of copper homeostasis.* Metallomics, 2017. **9**(11): p. 1501-1512.

229. Jomova, K. and M. Valko, *Advances in metal-induced oxidative stress and human disease.* Toxicology, 2011. **283**(2-3): p. 65-87.
230. Clapham, D.E., *Calcium signaling.* Cell, 2007. **131**(6): p. 1047-58.
231. Alessi, D.R., et al., *Mechanism of activation of protein kinase B by insulin and IGF-1.* EMBO J, 1996. **15**(23): p. 6541-51.
232. Chen, K.H., et al., *TRPM7 channels regulate proliferation and adipogenesis in 3T3-L1 preadipocytes.* J Cell Physiol, 2014. **229**(1): p. 60-7.
233. Sutherland, C., I.A. Leighton, and P. Cohen, *Inactivation of glycogen synthase kinase-3 beta by phosphorylation: new kinase connections in insulin and growth-factor signalling.* Biochem J, 1993. **296 (Pt 1)**: p. 15-9.
234. Beals, C.R., et al., *Nuclear export of NF-ATc enhanced by glycogen synthase kinase-3.* Science, 1997. **275**(5308): p. 1930-4.
235. Chow, W., G. Hou, and M.P. Bendeck, *Glycogen synthase kinase 3beta regulation of nuclear factor of activated T-cells isoform c1 in the vascular smooth muscle cell response to injury.* Exp Cell Res, 2008. **314**(16): p. 2919-29.
236. Yang, T.T., et al., *Phosphorylation of NFATc4 by p38 mitogen-activated protein kinases.* Mol Cell Biol, 2002. **22**(11): p. 3892-904.
237. Chow, C.W. and R.J. Davis, *Integration of calcium and cyclic AMP signaling pathways by 14-3-3.* Mol Cell Biol, 2000. **20**(2): p. 702-12.
238. Serfling, E., et al., *NFATc1/alphaA: The other Face of NFAT Factors in Lymphocytes.* Cell Commun Signal, 2012. **10**(1): p. 16.
239. Serfling, E., et al., *NFATc1 autoregulation: a crucial step for cell-fate determination.* Trends Immunol, 2006. **27**(10): p. 461-9.
240. Nayak, A., et al., *Sumoylation of the transcription factor NFATc1 leads to its subnuclear relocalization and interleukin-2 repression by histone deacetylase.* J Biol Chem, 2009. **284**(16): p. 10935-46.
241. Terui, Y., et al., *Dual role of sumoylation in the nuclear localization and transcriptional activation of NFAT1.* J Biol Chem, 2004. **279**(27): p. 28257-65.
242. Yoeli-Lerner, M., et al., *Akt/protein kinase b and glycogen synthase kinase-3beta signaling pathway regulates cell migration through the NFAT1 transcription factor.* Mol Cancer Res, 2009. **7**(3): p. 425-32.
243. Valdor, R., et al., *Regulation of NFAT by poly(ADP-ribose) polymerase activity in T cells.* Mol Immunol, 2008. **45**(7): p. 1863-71.
244. Fan, Y., et al., *Regulation of the stability and transcriptional activity of NFATc4 by ubiquitination.* FEBS Lett, 2008. **582**(29): p. 4008-14.
245. Deluca, M., *Firefly luciferase.* Adv Enzymol Relat Areas Mol Biol, 1976. **44**: p. 37-68.
246. Baldwin, T.O., *Firefly luciferase: the structure is known, but the mystery remains.* Structure, 1996. **4**(3): p. 223-8.
247. Jiwaji, M., et al., *The Renilla luciferase gene as a reference gene for normalization of gene expression in transiently transfected cells.* BMC Mol Biol, 2010. **11**: p. 103.
248. *pRL Renilla Luciferase Reporter Vectors.* , in *Technical Bulletin No. TB550*. 2008, Promega Cooperation: Madison WI USA
249. Bruce A. Sherf, S.L.N., Rita R. Hannah and Keith V. Wood, *Dual-LuciferaseTM Reporter Assay: An Advanced Co-Reporter*

Technology Integrating Firefly and Renilla Luciferase Assays, in *Promega Notes Magazine*. 1996, Promega Cooperation

250. Matthews, J.C., K. Hori, and M.J. Cormier, *Purification and properties of Renilla reniformis luciferase.* Biochemistry, 1977. **16**(1): p. 85-91.
251. Shimomura, O. and F.H. Johnson, *Peroxidized coelenterazine, the active group in the photoprotein aequorin.* Proc Natl Acad Sci U S A, 1978. **75**(6): p. 2611-5.

252. Furman, J.L., I.A. Artiushin, and C.M. Norris, *Disparate effects of serum on basal and evoked NFAT activity in primary astrocyte cultures.* Neurosci Lett, 2010. **469**(3): p. 365-9.
253. Runnels, L.W., L. Yue, and D.E. Clapham, *TRP-PLIK, a bifunctional protein with kinase and ion channel activities.* Science, 2001. **291**(5506): p. 1043-7.
254. Tsuji, F.I., et al., *Site-specific mutagenesis of the calcium-binding photoprotein aequorin.* Proc Natl Acad Sci U S A, 1986. **83**(21): p. 8107-11.
255. Ginzinger, D.G., *Gene quantification using real-time quantitative PCR: an emerging technology hits the mainstream.* Exp Hematol, 2002. **30**(6): p. 503-12.
256. Heid, C.A., et al., *Real time quantitative PCR.* Genome Res, 1996. **6**(10): p. 986-94.
257. Cikos, S., A. Bukovska, and J. Koppel, *Relative quantification of mRNA: comparison of methods currently used for real-time PCR data analysis.* BMC Mol Biol, 2007. **8**: p. 113.
258. Mognol, G.P., et al., *Transcriptional regulation of the c-Myc promoter by NFAT1 involves negative and positive NFAT-responsive elements.* Cell Cycle, 2012. **11**(5): p. 1014-28.
259. Buchholz, M., et al., *Overexpression of c-myc in pancreatic cancer caused by ectopic activation of NFATc1 and the Ca2+/calcineurin signaling pathway.* EMBO J, 2006. **25**(15): p. 3714-24.
260. Iniguez, M.A., et al., *An essential role of the nuclear factor of activated T cells in the regulation of the expression of the cyclooxygenase-2 gene in human T lymphocytes.* J Biol Chem, 2000. **275**(31): p. 23627-35.
261. Wang, L., et al., *NFATc1 activation promotes the invasion of U251 human glioblastoma multiforme cells through COX-2.* Int J Mol Med, 2015. **35**(5): p. 1333-40.
262. Graef, I.A., et al., *L-type calcium channels and GSK-3 regulate the activity of NF-ATc4 in hippocampal neurons.* Nature, 1999. **401**(6754): p. 703-8.
263. Groth, R.D. and P.G. Mermelstein, *Brain-derived neurotrophic factor activation of NFAT (nuclear factor of activated T-cells)-dependent transcription: a role for the transcription factor NFATc4 in neurotrophin-mediated gene expression.* J Neurosci, 2003. **23**(22): p. 8125-34.
264. Chow, C.W., M. Rincon, and R.J. Davis, *Requirement for transcription factor NFAT in interleukin-2 expression.* Mol Cell Biol, 1999. **19**(3): p. 2300-7.
265. Hamberg, M. and B. Samuelsson, *Detection and isolation of an endoperoxide intermediate in prostaglandin biosynthesis.* Proc Natl Acad Sci U S A, 1973. **70**(3): p. 899-903.
266. Needleman, P., et al., *Arachidonic acid metabolism.* Annu Rev Biochem, 1986. **55**: p. 69-102.
267. Hinman, J.W., *Prostaglandins.* Annu Rev Biochem, 1972. **41**: p. 161-78.
268. Bakhle, Y.S. and R.M. Botting, *Cyclooxygenase-2 and its regulation in inflammation.* Mediators Inflamm, 1996. **5**(5): p. 305-23.
269. Yagami, T., H. Koma, and Y. Yamamoto, *Pathophysiological Roles of Cyclooxygenases and Prostaglandins in the Central Nervous System.* Mol Neurobiol, 2016. **53**(7): p. 4754-71.
270. Misra, S. and K. Sharma, *COX-2 signaling and cancer: new players in old arena.* Curr Drug Targets, 2014. **15**(3): p. 347-59.
271. Gakis, G., *The role of inflammation in bladder cancer.* Adv Exp Med Biol, 2014. **816**: p. 183-96.
272. Maru, G.B., et al., *The role of inflammation in skin cancer.* Adv Exp Med Biol, 2014. **816**: p. 437-69.
273. Fouad, T.M., et al., *The role of inflammation in inflammatory breast cancer.* Adv Exp Med Biol, 2014. **816**: p. 53-73.

274. Bingham, S., et al., *The role of the cylooxygenase pathway in nociception and pain.* Semin Cell Dev Biol, 2006. **17**(5): p. 544-54.
275. Edfors, F., et al., *Gene-specific correlation of RNA and protein levels in human cells and tissues.* Mol Syst Biol, 2016. **12**(10): p. 883.
276. Takumi, O., et al., *[Correlation between enzymatic activity and gene expression of orotate phosphoribosyl transferase (OPRT) in colorectal cancer].* Gan To Kagaku Ryoho, 2002. **29**(13): p. 2515-9.
277. Miyamoto, S., et al., *Discrepancies between the gene expression, protein expression, and enzymatic activity of thymidylate synthase and dihydropyrimidine dehydrogenase in human gastrointestinal cancers and adjacent normal mucosa.* Int J Oncol, 2001. **18**(4): p. 705-13.
278. Penning, T.D., et al., *Synthesis and biological evaluation of the 1,5-diarylpyrazole class of cyclooxygenase-2 inhibitors: identification of 4-[5-(4-methylphenyl)-3-(trifluoromethyl)-1H-pyrazol-1-yl]benze nesulfonamide (SC-58635, celecoxib).* J Med Chem, 1997. **40**(9): p. 1347-65.
279. Smith, C.J., et al., *Pharmacological analysis of cyclooxygenase-1 in inflammation.* Proc Natl Acad Sci U S A, 1998. **95**(22): p. 13313-8.
280. Smith, W.L., R.M. Garavito, and D.L. DeWitt, *Prostaglandin endoperoxide H synthases (cyclooxygenases)-1 and -2.* J Biol Chem, 1996. **271**(52): p. 33157-60.
281. Smith, W.L., *Prostanoid biosynthesis and mechanisms of action.* Am J Physiol, 1992. **263**(2 Pt 2): p. F181-91.
282. Font-Nieves, M., et al., *Induction of COX-2 enzyme and down-regulation of COX-1 expression by lipopolysaccharide (LPS) control prostaglandin E2 production in astrocytes.* J Biol Chem, 2012. **287**(9): p. 6454-68.
283. Zidar, N., et al., *Cyclooxygenase in normal human tissues--is COX-1 really a constitutive isoform, and COX-2 an inducible isoform?* J Cell Mol Med, 2009. **13**(9B): p. 3753-63.
284. Lipsky, P.E., et al., *Unresolved issues in the role of cyclooxygenase-2 in normal physiologic processes and disease.* Arch Intern Med, 2000. **160**(7): p. 913-20.
285. Kirkby, N.S., et al., *Systematic study of constitutive cyclooxygenase-2 expression: Role of NF-kappaB and NFAT transcriptional pathways.* Proc Natl Acad Sci U S A, 2016. **113**(2): p. 434-9.
286. Beutler, B., *TLR4 as the mammalian endotoxin sensor.* Curr Top Microbiol Immunol, 2002. **270**: p. 109-20.
287. Seamon, K.B., W. Padgett, and J.W. Daly, *Forskolin: unique diterpene activator of adenylate cyclase in membranes and in intact cells.* Proc Natl Acad Sci U S A, 1981. **78**(6): p. 3363-7.
288. Metzger, H. and E. Lindner, *The positive inotropic-acting forskolin, a potent adenylate cyclase activator.* Arzneimittelforschung, 1981. **31**(8): p. 1248-50.
289. Klein, T., et al., *Regulation of cyclooxygenase-2 expression by cyclic AMP.* Biochim Biophys Acta, 2007. **1773**(11): p. 1605-18.
290. Mellgren, R.L., G.R. Slaughter, and J.A. Thomas, *Dephosphorylation of phosphoproteins by Escherichia coli alkaline phosphatase.* J Biol Chem, 1977. **252**(17): p. 6082-9.
291. Beesetty, P., et al., *Inactivation of TRPM7 kinase in mice results in enlarged spleens, reduced T-cell proliferation and diminished store-operated calcium entry.* Sci Rep, 2018. **8**(1): p. 3023.
292. Suzuki, S., et al., *The TRPM7 kinase limits receptor-induced calcium release by regulating heterotrimeric G-proteins.* Cell Mol Life Sci, 2018. **75**(16): p. 3069-3078.
293. Feng, L., et al., *Cloning two isoforms of rat cyclooxygenase: differential regulation of their expression.* Arch Biochem Biophys, 1993. **307**(2): p. 361-8.

294. Beurel, E., S.F. Grieco, and R.S. Jope, *Glycogen synthase kinase-3 (GSK3): regulation, actions, and diseases.* Pharmacol Ther, 2015. **148**: p. 114-31.
295. Goode, N., et al., *Differential regulation of glycogen synthase kinase-3 beta by protein kinase C isotypes.* J Biol Chem, 1992. **267**(24): p. 16878-82.
296. Fang, X., et al., *Phosphorylation and inactivation of glycogen synthase kinase 3 by protein kinase A.* Proc Natl Acad Sci U S A, 2000. **97**(22): p. 11960-5.
297. Evans, C.A., et al., *Discovery of a Selective Phosphoinositide-3-Kinase (PI3K)-gamma Inhibitor (IPI-549) as an Immuno-Oncology Clinical Candidate.* ACS Med Chem Lett, 2016. **7**(9): p. 862-7.
298. Down, K., et al., *Optimization of Novel Indazoles as Highly Potent and Selective Inhibitors of Phosphoinositide 3-Kinase delta for the Treatment of Respiratory Disease.* J Med Chem, 2015. **58**(18): p. 7381-99.
299. Visser, D., et al., *Function and regulation of the channel-kinase TRPM7 in health and disease.* Eur J Cell Biol, 2014. **93**(10-12): p. 455-65.
300. Chen, J.P., et al., *TRPM7 regulates the migration of human nasopharyngeal carcinoma cell by mediating Ca(2+) influx.* Cell Calcium, 2010. **47**(5): p. 425-32.
301. Wei, C., et al., *Calcium flickers steer cell migration.* Nature, 2009. **457**(7231): p. 901-5.
302. Mittermeier, L., et al., *TRPM7 is the central gatekeeper of intestinal mineral absorption essential for postnatal survival.* Proc Natl Acad Sci U S A, 2019.
303. Roohani, N., et al., *Zinc and its importance for human health: An integrative review.* J Res Med Sci, 2013. **18**(2): p. 144-57.
304. Prasad, A.S., *Zinc in human health: effect of zinc on immune cells.* Mol Med, 2008. **14**(5-6): p. 353-7.
305. Kambe, T., B.P. Weaver, and G.K. Andrews, *The genetics of essential metal homeostasis during development.* Genesis, 2008. **46**(4): p. 214-28.
306. Aust, S.D., L.A. Morehouse, and C.E. Thomas, *Role of metals in oxygen radical reactions.* J Free Radic Biol Med, 1985. **1**(1): p. 3-25.
307. Yu, Z.L., et al., *Excessive copper induces the production of reactive oxygen species, which is mediated by phospholipase D, nicotinamide adenine dinucleotide phosphate oxidase and antioxidant systems.* J Integr Plant Biol, 2008. **50**(2): p. 157-67.
308. Balamurugan, K. and W. Schaffner, *Copper homeostasis in eukaryotes: teetering on a tightrope.* Biochim Biophys Acta, 2006. **1763**(7): p. 737-46.
309. Tisato, F., et al., *Copper in diseases and treatments, and copper-based anticancer strategies.* Med Res Rev, 2010. **30**(4): p. 708-49.
310. Chen, H.C., et al., *A key role for Mg(2+) in TRPM7's control of ROS levels during cell stress.* Biochem J, 2012. **445**(3): p. 441-8.
311. Langenbach, R., et al., *Cyclooxygenase knockout mice: models for elucidating isoform-specific functions.* Biochem Pharmacol, 1999. **58**(8): p. 1237-46.
312. Adelizzi, R.A., *COX-1 and COX-2 in health and disease.* J Am Osteopath Assoc, 1999. **99**(11 Suppl): p. S7-12.
313. Yermakova, A. and M.K. O'Banion, *Cyclooxygenases in the central nervous system: implications for treatment of neurological disorders.* Curr Pharm Des, 2000. **6**(17): p. 1755-76.
314. Harris, R.C. and M.D. Breyer, *Physiological regulation of cyclooxygenase-2 in the kidney.* Am J Physiol Renal Physiol, 2001. **281**(1): p. F1-11.
315. Kim, J.W., et al., *Gene expression of cyclooxygenase in the aging heart.* J Gerontol A Biol Sci Med Sci, 2001. **56**(8): p. B350-5.
316. Surowiak, P., et al., *Increase in cyclooxygenase-2 (COX-2) expression in keratinocytes and dermal fibroblasts in photoaged skin.* J Cosmet Dermatol, 2014. **13**(3): p. 195-201.

317. Morham, S.G., et al., *Prostaglandin synthase 2 gene disruption causes severe renal pathology in the mouse.* Cell, 1995. **83**(3): p. 473-82.
318. Camitta, M.G., et al., *Cyclooxygenase-1 and -2 knockout mice demonstrate increased cardiac ischemia/reperfusion injury but are protected by acute preconditioning.* Circulation, 2001. **104**(20): p. 2453-8.
319. Dinchuk, J.E., et al., *Renal abnormalities and an altered inflammatory response in mice lacking cyclooxygenase II.* Nature, 1995. **378**(6555): p. 406-9.
320. Kim, S.H., et al., *Cyclooxygenase-2 Expression Is a Predictive Marker for Late Recurrence in Colorectal Cancer.* Gastroenterol Res Pract, 2018. **2018**: p. 7968149.
321. Li, Y.J., et al., *The prognostic value of COX-2 expression on circulating tumor cells in nasopharyngeal carcinoma: A prospective analysis.* Radiother Oncol, 2018.
322. Gao, S., et al., *EpCAM and COX2 expression are positively correlated in human breast cancer.* Mol Med Rep, 2017. **15**(6): p. 3755-3760.
323. Soares, C.D., et al., *Prognostic significance of cyclooxygenase 2 and phosphorylated Akt1 overexpression in primary nonmetastatic and metastatic cutaneous melanomas.* Melanoma Res, 2017. **27**(5): p. 448-456.
324. Sun, H., et al., *COX-2 expression in ovarian cancer: an updated meta-analysis.* Oncotarget, 2017. **8**(50): p. 88152-88162.
325. Ricciotti, E. and G.A. FitzGerald, *Prostaglandins and inflammation.* Arterioscler Thromb Vasc Biol, 2011. **31**(5): p. 986-1000.
326. Liu, B., L. Qu, and S. Yan, *Cyclooxygenase-2 promotes tumor growth and suppresses tumor immunity.* Cancer Cell Int, 2015. **15**: p. 106.
327. Wang, D. and R.N. Dubois, *Prostaglandins and cancer.* Gut, 2006. **55**(1): p. 115-22.
328. Sicking, I., et al., *Prognostic influence of cyclooxygenase-2 protein and mRNA expression in node-negative breast cancer patients.* BMC Cancer, 2014. **14**: p. 952.
329. Jiao, G., et al., *Prognostic significance of cyclooxygenase-2 in osteosarcoma: a meta-analysis.* Tumour Biol, 2013. **34**(5): p. 2489-95.
330. Yang, G., et al., *Cyclooxygenase-2 expression is positively associated with lymph node metastasis in nasopharyngeal carcinoma.* PLoS One, 2017. **12**(3): p. e0173641.
331. Tsujii, M., S. Kawano, and R.N. DuBois, *Cyclooxygenase-2 expression in human colon cancer cells increases metastatic potential.* Proc Natl Acad Sci U S A, 1997. **94**(7): p. 3336-40.
332. Parrett, M., et al., *Cyclooxygenase-2 gene expression in human breast cancer.* Int J Oncol, 1997. **10**(3): p. 503-7.
333. Hida, T., et al., *Increased expression of cyclooxygenase 2 occurs frequently in human lung cancers, specifically in adenocarcinomas.* Cancer Res, 1998. **58**(17): p. 3761-4.
334. Lo, C.Y., et al., *High prevalence of cyclooxygenase 2 expression in papillary thyroid carcinoma.* Eur J Endocrinol, 2005. **152**(4): p. 545-50.
335. Ferrer, M.D., et al., *Cyclooxygenase-2 inhibitors as a therapeutic target in inflammatory diseases.* Curr Med Chem, 2018.
336. Katori, M. and M. Majima, *Cyclooxygenase-2: its rich diversity of roles and possible application of its selective inhibitors.* Inflamm Res, 2000. **49**(8): p. 367-92.
337. Yogi, A., et al., *Bradykinin regulates calpain and proinflammatory signaling through TRPM7-sensitive pathways in vascular smooth muscle cells.* Am J Physiol Regul Integr Comp Physiol, 2009. **296**(2): p. R201-7.
338. Mercau, M.E., et al., *Involvement of PI3K/Akt and p38 MAPK in the induction of COX-2 expression by bacterial lipopolysaccharide in murine adrenocortical cells.* Mol Cell Endocrinol, 2014. **384**(1-2): p. 43-51.

339. Jang, B.C., et al., *Induction of cyclooxygenase-2 in macrophages by catalase: role of NF-kappaB and PI3K signaling pathways.* Biochem Biophys Res Commun, 2004. **316**(2): p. 398-406.
340. Wu, W., et al., *p38 and EGF receptor kinase-mediated activation of the phosphatidylinositol 3-kinase/Akt pathway is required for Zn2+-induced cyclooxygenase-2 expression.* Am J Physiol Lung Cell Mol Physiol, 2005. **289**(5): p. L883-9.
341. Bansal, K., et al., *Src homology 3-interacting domain of Rv1917c of Mycobacterium tuberculosis induces selective maturation of human dendritic cells by regulating PI3K-MAPK-NF-kappaB signaling and drives Th2 immune responses.* J Biol Chem, 2010. **285**(47): p. 36511-22.
342. Roskoski, R., Jr., *ERK1/2 MAP kinases: structure, function, and regulation.* Pharmacol Res, 2012. **66**(2): p. 105-43.
343. Cross, D.A., et al., *Inhibition of glycogen synthase kinase-3 by insulin mediated by protein kinase B.* Nature, 1995. **378**(6559): p. 785-9.
344. Fang, X., et al., *Convergence of multiple signaling cascades at glycogen synthase kinase 3: Edg receptor-mediated phosphorylation and inactivation by lysophosphatidic acid through a protein kinase C-dependent intracellular pathway.* Mol Cell Biol, 2002. **22**(7): p. 2099-110.
345. Klein, P.S. and D.A. Melton, *A molecular mechanism for the effect of lithium on development.* Proc Natl Acad Sci U S A, 1996. **93**(16): p. 8455-9.
346. Kirshenboim, N., et al., *Lithium-mediated phosphorylation of glycogen synthase kinase-3beta involves PI3 kinase-dependent activation of protein kinase C-alpha.* J Mol Neurosci, 2004. **24**(2): p. 237-45.
347. Clipstone, N.A. and G.R. Crabtree, *Identification of calcineurin as a key signalling enzyme in T-lymphocyte activation.* Nature, 1992. **357**(6380): p. 695-7.
348. Luo, C., et al., *Interaction of calcineurin with a domain of the transcription factor NFAT1 that controls nuclear import.* Proc Natl Acad Sci U S A, 1996. **93**(17): p. 8907-12.
349. Beals, C.R., et al., *Nuclear localization of NF-ATc by a calcineurin-dependent, cyclosporin-sensitive intramolecular interaction.* Genes Dev, 1997. **11**(7): p. 824-34.
350. Neal, J.W. and N.A. Clipstone, *Glycogen synthase kinase-3 inhibits the DNA binding activity of NFATc.* J Biol Chem, 2001. **276**(5): p. 3666-73.
351. Klemm, J.D., C.R. Beals, and G.R. Crabtree, *Rapid targeting of nuclear proteins to the cytoplasm.* Curr Biol, 1997. **7**(9): p. 638-44.
352. Putney, J.W., *Calcium signaling: deciphering the calcium-NFAT pathway.* Curr Biol, 2012. **22**(3): p. R87-9.
353. Song, S., et al., *COX-2 induction by unconjugated bile acids involves reactive oxygen species-mediated signalling pathways in Barrett's oesophagus and oesophageal adenocarcinoma.* Gut, 2007. **56**(11): p. 1512-21.
354. St-Germain, M.E., et al., *Regulation of COX-2 protein expression by Akt in endometrial cancer cells is mediated through NF-kappaB/IkappaB pathway.* Mol Cancer, 2004. **3**: p. 7.
355. von Knethen, A., D. Callsen, and B. Brune, *NF-kappaB and AP-1 activation by nitric oxide attenuated apoptotic cell death in RAW 264.7 macrophages.* Mol Biol Cell, 1999. **10**(2): p. 361-72.
356. Multhoff, G., M. Molls, and J. Radons, *Chronic inflammation in cancer development.* Front Immunol, 2011. **2**: p. 98.
357. Ghosh, R., et al., *Regulation of Cox-2 by cyclic AMP response element binding protein in prostate cancer: potential role for nexrutine.* Neoplasia, 2007. **9**(11): p. 893-9.

358. Kumar, A.P., et al., *Akt/cAMP-responsive element binding protein/cyclin D1 network: a novel target for prostate cancer inhibition in transgenic adenocarcinoma of mouse prostate model mediated by Nexrutine, a Phellodendron amurense bark extract.* Clin Cancer Res, 2007. **13**(9): p. 2784-94.
359. Chien, P.T., et al., *c-Src/Pyk2/EGFR/PI3K/Akt/CREB-activated pathway contributes to human cardiomyocyte hypertrophy: Role of COX-2 induction.* Mol Cell Endocrinol, 2015. **409**: p. 59-72.
360. Schappe, M.S., et al., *Chanzyme TRPM7 Mediates the Ca(2+) Influx Essential for Lipopolysaccharide-Induced Toll-Like Receptor 4 Endocytosis and Macrophage Activation.* Immunity, 2018. **48**(1): p. 59-74 e5.
361. Ogata, K., et al., *The crucial role of the TRPM7 kinase domain in the early stage of amelogenesis.* Sci Rep, 2017. **7**(1): p. 18099.
362. Vane, J.R., *Inhibition of prostaglandin synthesis as a mechanism of action for aspirin-like drugs.* Nat New Biol, 1971. **231**(25): p. 232-5.
363. Jones, R., et al., *Gastrointestinal and cardiovascular risks of nonsteroidal anti-inflammatory drugs.* Am J Med, 2008. **121**(6): p. 464-74.
364. Horl, W.H., *Nonsteroidal Anti-Inflammatory Drugs and the Kidney.* Pharmaceuticals (Basel), 2010. **3**(7): p. 2291-2321.
365. Rayar, A.M., et al., *Update on COX-2 Selective Inhibitors: Chemical Classification, Side Effects and their Use in Cancers and Neuronal Diseases.* Curr Top Med Chem, 2017. **17**(26): p. 2935-2956.
366. Walker, C. and L.M. Biasucci, *Cardiovascular safety of non-steroidal anti-inflammatory drugs revisited.* Postgrad Med, 2018. **130**(1): p. 55-71.
367. Aneja, A. and M.E. Farkouh, *Adverse cardiovascular effects of NSAIDs: driven by blood pressure, or edema?* Ther Adv Cardiovasc Dis, 2008. **2**(1): p. 53-66.
368. Wright, J.M., *The double-edged sword of COX-2 selective NSAIDs.* CMAJ, 2002. **167**(10): p. 1131-7.
369. Wakabayashi, K., *NSAIDs as Cancer Preventive Agents.* Asian Pac J Cancer Prev, 2000. **1**(2): p. 97-113.
370. Zierler, S., et al., *TRPM7 kinase activity regulates murine mast cell degranulation.* J Physiol, 2016. **594**(11): p. 2957-70.
371. Santamaria, D. and S. Ortega, *Cyclins and CDKS in development and cancer: lessons from genetically modified mice.* Front Biosci, 2006. **11**: p. 1164-88.
372. Doukas, J., et al., *Isoform-selective PI3K inhibitors as novel therapeutics for the treatment of acute myocardial infarction.* Biochem Soc Trans, 2007. **35**(Pt 2): p. 204-6.

I Abbreviations

2-ABP	2-aminoethyl diphenylborinate
AA	amino acid
ALS-G	guamanian form of amyotrophic lateral sclerosis
AM	acetoxymethyl
ANXA1	annexin A1 (lipocortin)
ATP	adenosine triphosphate
BCR	B cell receptor
BMDM	bone marrow derived macrophage
bp	base pairs
Br^-	bromide
BSA	bovine serum albumin (albumin fraction V)
CaM	calmodulin
CaMK	calmodulin-dependent kinase
cAMP	3',5'-cyclic adenosine monophosphate
CF	cardiac fibroblast
cGMP	3',5'-cyclic guanosine monophosphate
CMF	chronic myelogenous leukemia
Cl^-	chloride
Co^{2+}	cobalt
COX	cyclooxygenase
CPK	conventional protein kinase
CREB	cAMP response element-binding
CRET	chemiluminescence resonance energy transfer
DAG	diacylglycerol
DMEM	Dulbecco's modified eagle medium
DNA	deoxyribonucleic acid
	- c complementary
dNTP	deoxyribonucleotide triphosphates
DPBS	Dulbecco's phosphate buffered saline
DEPC	diethyl pyrocarbonate
ECL	enhanced chemiluminescence
EDTA	ethylenediaminetetraacetic acid
EGF	epidermal growth factor
eGFP	enhanced green fluorescent protein

EGTA	ethylene glycol-bis(β-aminoethyl ether)-N,N,N',N'-tetraacetic acid
ER	endoplasmatic reticulum
ERK	extracellular signal-regulated kinase
ESC	embryonic stem cell
EZH2	enhancer of zeste homolog 2
FBS	fetal bovine serum
GAPDH	glyceraldehyde 3-phosphatase dehydrogenase
GFP	green fluorescent protein
GPCR	G-protein coupled receptor
GSK	glycogen synthase kinase
h	hour(s)
HAP1	haploid chronic myeloid leukemia cell line
HBSS	Hanks' balanced salt solution
HPRT	hypoxanthine phosphoribosyltransferase
HRP	horse radish peroxidase
HSC	hepatic stellate cell
I^-	iodide
ICP-MS	inductively coupled plasma mass spectrometry
IL	interleukin
IMDM	Iscove's modified Dulbecco's medium
IP_3	inositol 1,4,5-triphosphate
IP_3R	inositol 1,4,5-triphosphate receptor
JAK	Janus kinase
JNK	c-Jun terminal kinase
K^+	potassium
KI	knock-in
KO	knockout
LC-MS/MS	liquid chromatography-mass spectrometry/mass spectrometry
Li^{2+}	lithium
MIIA	myosin II A
MagNuM	magnesium nucleotide-regulated metal ion
MAPK	mitogen-activated protein kinase
MAPKAPK	MAPK-activated protein kinase
mESC	mouse embryonic stem cells
Mg^{2+}	magnesium
Mg-ATP	Mg^{2+}-bound adenosine triphosphate

Mg-GTP	Mg^{2+}-bound guanosine triphosphate
MIC	magnesium-inhibitied cation
min	minute(s)
Mn^{2+}	manganese
MNK	mitogen-activated protein kinase interacting protein kinase
mTOR	mechanistic target of rapamycin
Na^{2+}	sodium
NES	nuclear export sequence
NFAT	nuclear factor of activated T cells
NFκB	nuclear factor kappa-light-chain-enhancer of activated B cells
Ni^{2+}	nickel
NSAID	non-steroidal anti-inflammatory drug
	- ns non-selective
P	permeability
PAM	point accepted mutation
PCR	polymerase chain reaction
PD	Parkinsonism dementia
PDK	phosphoinositide-dependent kinase
PDL	poly-D-lysine
PG	prostaglandin
PI3K	phosphoinositide-3-kinase
PIP_2	phosphatidylinositol-4,5-bisphosphate
PIP_3	phosphatidylinositol-3,4,5-trisphosphate
PKA, B, C	protein kinase A, B (Akt), C
PLC	phospholipase C
PMN	polymorphonuclear leucocyte
PTGS	prostaglandin-endoperoxidase synthase
ppm	parts per million
RNA	ribonucleic acid
	- m messenger
ROS	reactive oxygen species
RSK	ribosomal protein S6 kinase
R-SMAD	receptor-regulated SMAD
RT-qPCR	real-time quantitative PCR
RYBP	Ring1 and YY1 binding protein
s	second(s)

	- ms millisecond(s)
S	sulfur
SDS	sodium dodecyl sulfate
Ser	serine
SF	sector field
SMAD	Mothers against decapentaplegic homolog
SLC41A2	solute carrier family 41 member 2
SOCC	store-operated Ca^{2+} channels
SOCE	store-operated Ca^{2+} entry
STAT	signal transducer and activator of transcription
STIM	stromal interaction molecule
TGF-β	transforming growth factor β
Thr	threonine
TM	transmembrane
TLR	toll-like receptor
TRP	transient receptor potential
	- A ankyrin,
	- C canonical
	- M melastatin-like
	- ML mucolipin
	- N no mechanoreceptor potential C (nompC)
	- P polycystin
	- V vanilloid
TRPM7	transient receptor potential melastatin-like channel 7
TRPM6	transient receptor potential melastatin-like channel 6
VDCC	voltage-dependent Ca^{2+} channel
VOCC	voltage-operated Ca^{2+} channel
vs.	*versus*
VSMC	vascular smooth muscle cell
WT	wild-type
YY1	Yin Yang 1
Zn^{2+}	zinc
x	times

II Illustration Index

Figures

Tables

III Publications

Papers

Romagnani A., Vettore V., Rezzonico-Jost T., **Hampe S.**, Rottoli E., Nadolni W., Perotti M., Meier MA., Hermanns C., Geiger S., Wennemuth G., Recordati C., Matsushita M., Muehlich S., Proietti M., Chubanov V., Gudermann T., Grassi F., Zierler S. (2017) *TRPM7 kinase activity is essential for T cell colonization and alloreactivity in the gut.* Nat Commun. Dec4;8(1):1917

Zierler S., **Hampe S.**, Nadolni W. (2017) *TRPM channels as potential therapeutic targets against pro-inflammatory diseases.* Cell Calcium. Nov; 67:105-115

In preparation for Science Signaling:

Hampe S., Nadolni W., Fraticelli M., Zaborsky N., Sperandido M., Greil R., Chubanov V., Boekhoff I., Breit A., Gudermann T., Zierler S. *TRPM7 kinase regulates COX-2 expression in human myeloid leukemia cells and primary neutrophils.*

Abstract:
The enzyme-coupled melastatin-like transient-receptor-potential-7 channel, TRPM7, has been associated with carcinogenesis and immune function. It is essential for lymphocyte proliferation and development and has been implicated in the growth of numerous malignancies. However, its role in leukemia remains elusive. We recently demonstrated that TRPM7 regulates the differentiation of pro-inflammatory T lymphocytes. Moreover, it is required for activation and differentiation of macrophages. Thus, TRPM7 might represent a potent regulator of innate and adaptive immune homeostasis. Cyclooxygenase-2 (COX-2) inhibitors are commonly used for the treatment of both cancerous cell growth as well as acute and chronic inflammation. Here, we show that targeting TRPM7 in human myeloid leukemia cells and primary neutrophils results in reduced constitutive and inducible *COX-2* gene expression and activity. Using a human TRPM7-deficient leukemia cell line (HAP1), we were able to link this defect to impaired NFAT and Akt signaling. Genetic inactivation of the TRPM7 kinase activity in HAP1 cells revealed that the defect in Akt phosphorylation was kinase-dependent and that TRPM7 kinase activity was essential to control *COX-2* gene expression. By using pharmacological blockade of TRPM7 channel or kinase in primary human neutrophils we were able to confirm the inhibitory effect on *COX-2* gene expression and activity in both carcinogenic and inflammatory contexts. Our results indicate that TRPM7 might facilitate its broad carcinogenic and immune-regulatory effects via the regulation of COX-2 and therefore represents a valuable target for the treatment of chronic leukemia and pro-inflammatory diseases.

Conferences

Romagnani A., Vettore V., Rezzonico-Jost T., **Hampe S.**, Rottoli E., Nadolni W., Perotti M., Meier MA., Hermanns C., Geiger S., Wennemuth G., Recordati C., Matsushita M., Muehlich S., Proietti M., Chubanov V., Gudermann T., Grassi F., Zierler S. *The kinase activity of the TRPM7 channel-enzyme is essential for gut colonization and graft-versus-host reaction*. TRR 152 Symposium, Sept. 28th to Oct. 1st, 2016, Herrsching, Germany. Poster

Romagnani A., Vettore V., **Hampe S.**, Chubanov V., Gudermann T., Grassi F., Zierler S. *The channel-kinase TRPM7 regulates immune signaling via its kinase domain*. TRR 152 Meeting, Oct. 28th to 31st, Herrsching, Germany. Poster

Romagnani A., Vettore V., **Hampe S.** *The channel kinase regulates immune signaling via its kinase domain.* 2nd European Calcium Channel Conference (ECCC), May 13th to 16th, 2015, Alpbach, Austria. Oral presentation and Poster

IV Eidesstattliche Versicherung

Hampe, Sarah

Hiermit erkläre ich an Eides statt, dass ich die vorliegende Dissertation mit dem Titel

‚Domain-specific role of the channel-kinase TRPM7 in cell signaling'

selbständig und ohne unzulässige fremde Hilfe verfasst, mich außer der angegebenen keiner weiteren Hilfsmittel bedient und alle Erkenntnisse, die aus dem Schrifttum ganz oder annähernd übernommen sind, also solche kenntlich gemacht und nach ihrer Herkunft unter Bezeichnung der Fundstelle einzeln nachgewiesen habe.

Ich erkläre des Weiteren, dass die hier vorgelegte Dissertation nicht in gleicher oder in ähnlicher Form bei einer anderen Stelle zur Erlangung eines akademischen Grades eingereicht wurde.

München, den 28.01.2020 Sarah Hampe

V Acknowledgements

This thesis was completed in the Walther-Straub-Institute for Pharmacology and Toxicology, LMU Munich. The completion of my PhD would not have been possible without the enormous support from several people, who I would like to express my gratitude to in the following paragraph. In order to address everyone properly and with my own personal style, I will proceed in my native language german.

Als allererstes möchte ich mich bei **Prof. Dr. Thomas Gudermann** für die von Ihm erhaltene Möglichkeit danken, meine Dissertation am Walther-Straub-Institut der Pharmakologie und Toxikologie der LMU München anzufertigen zu können.

Ein sehr großes Dankeschön geht auch an meine Doktormutter bzw. Erstgutachterin **Prof. Dr. Ingrid Boekhoff**, die mir während der Erstellung dieser Arbeit mit Rat und Tat zur Seite stand und stets für die Klärung wichtiger Fragen und Probleme erreichbar war. Vielen lieben Dank Ingrid, ich weiß es wirklich sehr zu schätzen, dass du dir all diese Zeit genommen und mich so tatkräftig unterstützt hast! Ohne dich wäre diese Arbeit sicherlich nicht das, was sie ist ☺.

Auch bei **Dr. Andreas Breit** möchte ich mich herzlichst für die (zwischenzeitliche) Betreuung bedanken. Lieber Andreas, du hast mich nicht nur in neue Methoden eingeführt und mich diesbezüglich immer beraten, wenn ich mit Ergebnissen und/oder Fragen bei dir aufgetaucht bin, sondern hast mich zudem auch noch eine ganz andere, sehr kritische Sichtweise der eigenen bzw. auch der Experimente anderer gelehrt, welche mich bei der Etablierung unterschiedlicher Methoden sehr vorangebracht hat. Ferner habe ich im Laufe unserer gemeinsamen Zeit auch gelernt, meine Sätze immer zu Ende zu formulieren – eine Tatsache, die hauptsächlich dir zu verdanken ist und die dich sicherlich erfreut ;).

Es folgt die Danksagung an meine Betreuerin, **Dr. Susanna Zierler**: Liebe Susanna, ich bin wirklich unendlich dankbar dafür damals in deine Arbeitsgruppe gekommen zu sein und in deinen Laboratorien meine Doktorarbeit anfertigen zu dürfen. Ich habe so vieles unter deiner Obhut gelernt, was ich nicht missen möchte; von Laboraufbau über die Erlernung neuer Methoden, die Betreuung zahlreicher Studenten bis hin zu der Anfertigung von Präsentationen und Postern für Konferenzen oder die Erstellung von Stipendiumsanträgen war alles dabei. Dabei warst du stets zur Stelle, wenn ich um Unterstützung und weiterführende Gespräche gebeten habe, hast mich im Laufe der Zeit aber

auch ‚von der Leine gelassen' und mir den Freiraum gegeben, Eigenverantwortung zu zeigen und mich weiterzuentwickeln. In diesem Sinne nochmals vielen Dank für dein Vertrauen, ohne dies wäre das sicherlich nicht möglich gewesen. Des Weiteren habe ich mich sehr darüber gefreut, dass wir auch auf persönlicher Ebene so gut miteinander ausgekommen sind. Ich werde die herzlichen Geburtstagsfeiern oder Treffen bei dir in Starnberg schmerzlichst vermissen. Und letztendlich hätten wir ohne unsere gemeinsame Passion für Hawai'i sicherlich nie zueinander gefunden ;).

Ganz großer Dank geht auch sowohl an die aktuellen als auch an vergangene Mitglieder meines Labors: **Wiebke, Marco, Lynda, Sheila, Kilian** – ohne euch wäre die Zeit sicherlich nicht so strukturiert und aber auch unterhaltsam gewesen wie sie es war. Dabei danke ich dir, Wiebke, ganz besonders für gegenseitige Unterstützung und Stärkung in Susannas Ab- bzw. Valentinas Anwesenheit, für lustige Zeiten auf unserer Sonnenterasse, fürs erneute Beibringen von einmal bereits erlernten Techniken (aber bei Patch-Clamp zählt das ja quasi nicht, jede Zelle ist ja anders) und nicht zuletzt fürs Last Minute raussuchen von Kleinigkeiten (ja, da darf man auch mal meckern, ich weiß ;)). Ach ja, und für Bambi – für mich gehörte sie quasi schon zum Team, und insbesondere ihr Schnarchen hat mir am Ende gefehlt. Marco, dir danke ich für deinen Beitrag zu meinen Versuchen und natürlich für unsere zahlreichen Gespräche über HIIT und andere interessante Themen – dadurch wurde der Laboralltag immer etwas bunter als er eh schon war ☺. Lynda und Sheila, ihr seid die Besten wenn es um die Organisation und Aufrechterhaltung der täglichen Laborarbeit geht. Ohne eure Unterstützung durch die Anfertigungen von Lösungen oder anderen Dingen, das Ausführen von Bestellungen, das Auffüllen von Verbrauchsmaterialien und das Ausleeren entsprechender Abfälle wäre mein bzw. unser aller Laboralltag sicherlich nicht so reibungslos verlaufen! Ach ja, und besonderer Dank gebührt Lynda, nicht zuletzt auch wegen der Versorgung mit original-amerikanischen (bzw hawai'ianischen) Lebensmitteln: Ich sage nur , 'Kona Brewing Company'. Und Kilian, auch wenn unsere gemeinsame Zeit nur kurz war, ich danke dir für die medizinische ‚Unterstützung' im Labor - so mancher Versuch wäre sonst möglicherweise nicht so zustande gekommen. Danken möchte ich auch unserem Kurz- bzw. Langzeitintervalllaborzuwachs **Elli** und **Silvia**, über deren Anwesenheit ich mich immer gefreut habe und die mir auch bei Anliegen jedweder Art immer bereitwillig geholfen haben.

Dr. Vladimir Chubanov, auch dir möchte ich meinen Dank aussprechen. Zum einen für die Bereitstellung von einigen essentiellen Hilfsmitteln wie Antikörper und Vektoren, zum anderen aber auch für interessante wissenschaftliche Gespräche – meist zwischen Tür und Angel – die zum erneuten Nach- bzw. Überdenken meiner Versuche bzw. verschiedener Zusammenhänge anregten.

Nicht vergessen werde ich auch die entspannten Kaffeepausen mit **Prof. Dr. Harald Mückter**, wo nicht nur über die richtige Methode des Kaffeekochens, Knoblauch oder Monokel diskutiert wurde, sondern man auch stets IT-Probleme ansprechen konnte, die daraufhin auch immer zügig von ihm gelöst wurden. Danke, Harald!
Herrn Mann aus der Werkstatt des Walther-Straub-Instituts gilt besonderer Dank für das Basteln und Reparieren unterschiedlicher Laborgeräte.

Nicht in Worte zu fassen ist die unendlich große Dankbarkeit gegenüber meiner größten und besten Unterstützerin während dieser Zeit, meiner **Mutter**! Sie hatte immer ein offenes Ohr für meine Probleme und hat mich mit unermüdlicher Ausdauer immer wieder in meinem Vorhaben bestärkt. Hat mir den Frust genommen und mir die Geduld wiedergegeben, sodass ich dieses Werk nun letztendlich vor mir liegen habe. Liebe ‚Mami', auch wenn du fachlich nichts hierzu beitragen konntest, so steckt doch ein ganz großer Teil von dir in dieser Arbeit, und ohne dich würde es sie wohlmöglich gar nicht geben. Ohne wen es sie aber ganz sicherlich nicht geben würde, ist mein **Vater**, welchem ich letztendlich auch dieses Werk widme. ‚Paps', du hast mich von klein auf für die Naturwissenschaften begeistern können, hast durch immerwährendes Erklären von physikalischen, chemischen und mathematischen Zusammenhängen in mir die Neugier geweckt und somit dazu beigetragen, dass ich Biochemie studiert habe. Du warst es auch, der mich den Grundgedanken einer Doktorarbeit gelehrt hat. Und daher bin ich nun stolz darauf sagen zu können, diesen in deinem Sinne mit dieser Dissertation erfüllt zu haben. Danke. Ich liebe und vermisse dich!